FCP Report No. 44

FATIGUE OF GRAY IRON

by

D. F. Socie
J. W. Fash
S. D. Downing

Fatigue resistance of gray iron, compacted graphite and nodular iron are compared in Part I. Mean stress and strain effects in gray iron are discussed in Part II. Part III deals with stress strain simulation of gray iron. Finally, the effect of heat treating was investigated.

A Report of the

FRACTURE CONTROL PROGRAM

College of Engineering, University of Illinois at Urbana-Champaign
Urbana, Illinois 61801

October 1982

TABLE OF CONTENTS

Page

Part I "Fatigue Behavior and Crack Development in Cast Iron" by D. F. Socie and J. W. Fash----------1

Part II "Fatigue Behavior and Mean Effects in Gray Cast Iron" by J. W. Fash and D. F. Socie-------37

Part III "Stress-Strain Simulation Model for Gray Cast Iron" by S. D. Downing and D. F. Socie---------61

Part IV "Fatigue Behavior of As-Cast and Heat Treated Gray Iron" by D. F. Socie----------85

Part I: FATIGUE BEHAVIOR AND CRACK DEVELOPMENT IN CAST IRONS

D. F. Socie
J. W. Fash

Department of Mechanical and Industrial Engineering
University of Illinois at Urbana-Champaign
Urbana, IL 61801

ABSTRACT

The fatigue behavior of gray iron, compacted graphite iron, and nodular iron was investigated. Fatigue lives ranged from 10^2 to 10^6 cycles. Fatigue tests were conducted in both stress and strain control on smooth cylindrical specimens. In all three types of cast iron, the majority of the fatigue life was consumed in growing cracks. Nodular iron exhibits the best fatigue resistance in both stress and strain controlled tests while gray iron has the poorest fatigue resistance.

BACKGROUND

The effect of graphite configuration on the static and fatigue properties of cast irons has been the subject of numerous investigations. As a result of these studies, various trends have been established which relate the graphite morphology of these materials to their mechanical properties. In particular, the relationship of graphite structure to fatigue performance has been of considerable interest. The fatigue performance of a particular cast iron depends on the quantity, size, and shape of the free graphite constituent as well as its interaction with the matrix structure.

Cast irons, unlike mild steels, do not exhibit a characteristic yield point. Instead, the curve of plastic deformation merges into the "elastic" portion. Lack of a definite elastic-plastic transition in cast irons is due to the presence of free graphite which modifies the stress distribution within the matrix. These graphite formations can be regarded as inherent notches in which the stress concentration varies with effective notch geometry [1]. An increase in notch severity results in a decrease in the tangent modulus, indicating a corresponding increase in plastic deformation.

Fatigue behavior of various cast irons containing different graphite configurations were compared by Ikawa and Ohira [2]. Nodular (ductile) iron exhibited the best fatigue resistance while gray iron displayed relatively poor fatigue behavior. The superior performance of nodular iron over gray iron has been attributed to the dissimilarity in graphite morphology between the two materials. Graphite in gray iron is a highly branched and interconnected formation within a eutectic cell cluster. These cell structures are composed of sharp flake edges which provide paths of easy fracture in addition to regions of high stress concentration. Nodular iron, on the other hand, contains graphite particles of nearly spherical shape which

are non-interconnected, thus minimizing stress concentration effects and interrupting planes of easy fracture. Accordingly, nodular iron exhibits higher strength (both static and fatigue), ductility, and toughness than does gray iron.

In order to better predict the fatigue life of cast iron components in service, a more complete understanding of the mechanism of crack formation and growth in cast irons is required. Gilbert [3,4,5] studied the stress-strain response of these materials in tension and compression and reported the observed mechanism of failure. Under the assumption that the free graphite phase would not transmit a tensile stress, cast iron was modeled as a steel-like matrix containing effective notches of graphite. These graphite particles, when loaded in tension, separate from the matrix interface. Local stresses are produced which exceed the material's strength under the particular conditions of loading. Cracks were detected at these regions of highly localized stress indicating the significance of graphite in the process of crack initiation in cast irons. Many investigations have subsequently been undertaken to better explain and compare the mechanisms of crack initiation and propagation in both gray and nodular iron.

Fatigue cracks in gray iron have been observed to originate at the graphite flakes [2,6]. Increased graphite flake size results in an increase in notch severity and hence a decrease in the fatigue resistance [2,7]. Initiation of cracks have been detected at rather early stages in the life of gray iron specimens [6]. Under low to medium loading conditions, cracks have started at flakes most normally oriented to the loading axis, resulting in the extensive development of only a few major crack systems. At higher loading situations, cracks were observed to originate from flakes oriented randomly as well as normal to the direction of loading. The development of numerous crack

systems occurred in the latter case. On the basis of these observations, the actual crack growth process in gray iron appears to be dominated by the size and orientation of graphite flakes.

The controlling mechanism for crack initiation in nodular iron is not as well defined as that in gray iron. Graphite nodules, under a tensile load, have been observed to debond from the surrounding matrix [4]. The initiation of cracks from the resulting weak boundaries has been shown by Michell [8]. Other investigations found that fatigue cracks initiate not only from nodules but also from casting imperfections such as inclusions, microshrinkage pores, and irregularly shaped graphite clusters [9,10]. These irregularities have been determined to initiate cracks at an earlier stage in life than well formed nodules. This result is not surprising due to the irregular size and shape of these casting discontinuities which increase the severity of stress concentration. Regardless of the initiation process, these cracks have been detected rather early in the life of nodular iron specimens [10].

A type of cast iron with graphite configuration intermediate to that of gray and nodular iron has recently received increased attention for engineering use because of its fine mixture of mechanical, thermal, and casting properties. This intermediary form, referred to as compacted graphite iron, can be achieved by the variation of such factors as section size, rate of cooling, and chemical composition. Fatigue characteristics of compacted graphite have not been studied, particularly in the finite life range.

This paper compares the fatigue behavior of gray iron, compacted graphite and nodular iron. Emphasis is paced on the finite life range, i.e. less than 10^6 cycles to failure. Typical chemical compositions for each iron are investigated. No attempt has been made to investigate the wide range of chemical compositions for each type of cast iron. The purpose of this work is to compare the overall behavior of the three types of cast irons.

MATERIAL

Gray Iron

Test bars, 36 mm in diameter and 200 mm in length were cast in green sand molds to produce the pearlitic gray iron. Matrix microstructure and flake structure, classified by ASTM A247 as approximately 60 percent Type A, approximately 40 percent Type D, size 4 are shown in Fig. 1. Material compositions are given in Table 1 and mechanical properties are given in Table 2.

Compacted Graphite

In order to achieve a pearlitic matrix, test bars 30 mm in diameter by 200 mm in length were sand cast in green molds and then air cooled through the critical austenite transformation range (720 to 900°C). Compacted graphite configuration was accomplished by the simultaneous treatment of the molten iron with Mg (as a spheroidizing element) in addition to Ti and Al (as anti-spheroidizing elements). The microstructure of this iron is shown in Fig. 2. It contains 5 percent spheroidal shaped graphite. Note also that the flake tips have a much greater radius and hence lower stress concentration factor than found in gray iron. Material compositions are given in Table 1 and mechanical properties are given in Table 2.

Nodular Iron

Standard Y blocks with a test section 50 mm by 100 mm by 200 mm were cast in green sand molds. The melt was inoculated with Mg in the laddle before pouring into the mold. Matrix microstructure and graphite distribution is shown in Fig. 3. The matrix consists of both ferrite and pearlite. The graphite is ASTM Types 1 and 2. Material compositions are given in Table 1 and mechanical properties in Table 2.

TESTING PROCEDURE

Smooth, cylindrical specimens were machined from the as-cast test bars. The dimensions for these specimens are given in Fig. 4. A standard surface finish, as specified by ASTM E606, was attained for each test specimen. This degree of finish was sufficient for monotonic and base-line fatigue tests, however, a finer polish was required in order to obtain a clear resolution for crack growth observations. These specimens, while being rotated on a lathe, were mechanically polished with a pneumatic rotary polishing rod wrapped with separate strips of emery paper and felt. Initial rough polishing was accomplished with the emery paper, followed by a fine polishing procedure utilizing the felt saturated with a suspension of 0.3 micron alumina metallographic powder in water. An acceptable surface finish was obtained once machining and rough polishing marks were almost completely eliminated.

Material testing performed during the course of this investigation was accomplished in the Materials Engineering Research Laboratory at the University of Illinois at Urbana-Champaign. An MTS computer-based material test system was employed for the performance of all tests. This system consists of a $\pm$20-kip closed loop sevohydraulic test frame interfaced with a multiuser digital minicomputer, CRT graphic display terminal, and a hard copy unit. Function generation, data acquisition, and data analysis were implemented through MTS BASIC, a modified version of the interaction BASIC programming language.

RESULTS AND DISCUSSION

Gray Iron

Tests were conducted in fully reversed stress control. A typical hysteresis loop is shown in Fig. 5. Note that the stress strain response is not symmetric. The strain is not zero and the maximum tensile strain increases throughout the entire test.

Crack formation and growth was monitored in the pearlitic gray iron. A replicating procedure using standard metallographic acetyl cellulose film was used to record the surface of specimens during fatigue. By softening the film with acetone and placing it around the gauge section of the specimen, a "cast" of the surface is obtained. Observation of the replicas after the testing was completed was accomplished using an optical microscope by illuminating through the replica.

Crack growth data was obtained by taking replicas at approximately every 10 percent of the expected life. The replicating procedure allows qualitative observation of the amount and extent of crack development as well as quantitative observation of the crack system which grows to failure. Deformation occurs in the matrix material upon the first tensile loading and in critically oriented graphite structures, cracking or debonding from the matrix causes crack-like void formation. Cracks initiated within eutectic cells grow in a complex process consisting of crack propagation through the matrix material and incremental crack extension from the linking of crack systems. Crack arrest via a type of crack-tip blunting has been observed when cracks link with flake structures oriented parallel to the loading axis or with hemispherical surface discontinuities.

At larger stress amplitudes, cracks have been found within the first 5 percent of the specimen life. Microdiscontinuities with the largest stress

concentrations initiate cracks first, but damage, as evidence by the formation of cracks, occurs throughout the material. Damage accrues over the entire specimen surface and many cracks of similar magnitude are growing through the duration of the test. Near failure, several cracks have grown to 2 mm in length and failure occurs by the linking of some of these crack systems. Tests peformed at smaller stress amplitudes show initiated cracks within the first 10 percent of he specimen life. Fewer major crack systems developed at this amplitude but small cracks are found throughout the specimen at intermediate lives. Near failure, very few crack systems have developed to 2 mm in length in the lower stress amplitude tests.

Development of the crack system resulting in failure has been measured from the surface replicas. At a given life, the crack length, a, was taken as the length of the largest portion of the failure crack system distinguishable on the surface. When two or more crack systems were well developed and near joining, the sum of their lengths was considered as the crack length at the particular life. The initial flaw size is taken as the eutectic cell diameter.

Crack growth versus applied cycles, as shown in Fig. 6 for the pearlitic gray iron, indicates that most of the specimen life is spent growing a crack to a length of 1 to 2 mm. Once a crack reaches this length, growth occurs rapidly, resulting in failure in a relatively few numbers of cycles. The stress life curve for this iron is shown in Fig. 7. Failure is defined as separation of the specimen into two pieces.

Compacted Graphite

Similar tests were conducted for compacted graphite iron. A typical hysteresis loop is shown in Fig. 8. The maximum strain increases throughout the fatigue life.

Cracks originate at the graphite microdiscontinuities which induce the most severe stress concentrations. Graphite flakes, with their interconnected structure and sharp edges, were observed to initiate cracks in the pearlitic gray iron. The formation of cracks in compacted graphite iron generally appeared to start at the modified flake form, and shaped graphite particles were also seen to initiate cracks. Once initiated, these cracks develop via a combination of crack propagation through the matrix material and incremental crack extension brought about by the joining of crack systems.

The extent of crack development varied with the magnitude of applied stress. At large stress amplitudes, cracks were detected within the first 5 percent of the fatigue life. Cracks initiate at several graphite sites oriented both oblique and normal to the loading axis. Many cracks of similar size developed throughout the duration of these high stress-amplitude tests. Several of these cracks were observed to develop to a significant magnitude, 2 mm and above, near failure of the specimen. Conversely, at low stress amplitudes, cracks were observed to initiate only at graphite structures oriented normal to the loading direction. In this case, cracks were detected within the first 10 percent of the specimen life. Although small cracks were found throughout the specimen surface, very few major crack systems were developed near failure. This result is again consistent with gray iron observations.

Crack arrest occurs in gray irons when craks join with flake configurations oriented parallel to the loading axis. This sort of crack-tip blunting was also observed in compated graphite iron when cracks encounter spherically or irregularly shaped graphite forms. Since crack initiation was detected early in the lives of both compacted graphite and gray iron, this blunting phenomenon and its relative degree of effectiveness in these two

materials may very well influence the rate of crack growth and consequently the fatigue life obtained.

Crack length versus applied cycles curves determined from surface replicas are shown in Fig. 9. These curves indicate that 90 to 95 percent of the specimen life is spent in crack growth. Growth of cracks proceed steadily until they reach the significant size of 1 to 2 mm at which point rapid growth occurs. Failure ensues at a relatively short number of cycles thereafter. Fatigue test results are shown in Fig. 10.

Nodular Iron

Typical hysteresis loops for nodular iron are shown in Fig. 11. During these tests, the maximum strain decreased during the initial portion of the life and then increases. The initial strain decrease is due to cyclic hardening of the matrix material. During the latter stages of the life the strain increases due to macro cracking which increases the specimen compliance.

Cracks in nodular iron initiate at graphite nodules, microshrinkage cavities, and clusters of nodules. The failure crack initiated at the largest discontinuity, usually a microshrinkage cavity. At higher stress amplitides, multiple crack systems developed. Once initiated, cracks progress via crack growth through the matrix and incremental crack extension by the linking of several crack systems. Fewer crack systems were observed at lower stress levels.

Crack length versus applied cycles curves are shown in Fig. 12. As was the case with the other irons tested, the majority of the fatigue life was spent in crack growth. Stable crack growth occurs until the cracks reach a length of about 2 mm at which time rapid growth to failure occurs. Fatigue test results are shown in Fig. 13.

Strain Controlled Tests

Strain controlled tests were also conducted on the three types of cast irons. Results are summarized in Figs. 14, 15, and 16. The same qualitative behavior that was observed during stress controlled testing was also observed during strain controlled tests and will not be expanded upon further.

A summary plot for stress controlled tests of all three irons is shown in Fig. 17. Strain controlled tests are shown in Fig. 18. There is a large difference in materials when compared on the basis of stress controlled tests. This difference becomes much smaller when the comparisons are based on strain controlled tests.

Many service fatigue failures of castings originate at a geometric stress concentration that is part of the casting design. The local high stress area is undergoing strain controlled deformation.

For these situations, it would be better to compare materials on the basis of strain controlled tests. Stress controlled tests should be used to compare materials for those situations where failure occurs in a nominal stress area free from geometric stress concentrations.

SUMMARY

These tests show that the majority of the useful fatigue lives of cast iron materials in the low cycle fatigue regime is dominated crack growth. For practical purposes, crack initiation may be assumed to occur on the first cycle of loading. Accurate life prediction models for cast iron components should be based on crack growth phenomena not crack initiation.

ACKNOWLEDGEMENTS

Financial support was provided by the Fracture Control Program at the University of Illinois at Urbana-Champaign, College of Engineering.

Mssrs. P. Furman, C. Hua, and L. Molinaro and Miss C. Cleary all assisted in performing the tests reported in this paper.

The iron was cast by Deere and Company and International Harvester.

REFERENCES

1. Thun, A., and Ude, H., "Die Elastizitat und die Schwingungsfestigkeit des Gusseisens," Die Giesserei, Vol. 16, 1929, pp. 547-556.

2. Ikawa, K., and Ohira, G., "Fatigue Properties of Cast Iron in Relation to Graphite Structure," American Foundry Society, Cast Metals Res. J., Vol. 3, 1967, pp. 11-21.

3. Gilbert, G. N. J., "An Evaluation of the Stress/Strain Properties of Flake Graphite Cast Iron in Tension and Compression," J. of the British Cast Iron Res. Assn., Vol. 7, 1959, pp. 745-789.

4. Gilbert, G. N. J., "The Streas/Strain Properties of Nodular Cast Irons in Tension and Compression," J. of the British Cast Iron Res. Assn., Vol. 12, No. 2, 1965, pp. 170-193.

5. Gilbert, G. N. J., "Factors relating to the Stress/Strain Properties of Cast Iron," J. of the British Cast Iron Res. Assn., Vol. 6, No. 11, 1957, pp. 546-588.

6. Fash, J. W., Socie, D. F., and Russell, E. S., "Fatigue Crack Initiation and Growth in Gray Cast Iron," Proc. of Fatigue '81, Society of Environmental Engineers, Fatigue Group Conf., Warwick University, England, March 24-27, 1981, pp. 40-51.

7. Mitchell, M. R., "Effect of Graphite Morphology, Matrix Hardness and Structure on the Fatigue Resistance of Gray Cast Iron," Society of Automotive Engineers, Inc., Report No. 750198, 1975.

8. Mitchell, M. R., "A Unified Predictive Technique for the Fatigue Resistance fo Cast Ferrous-based Metals and High Hardness Wrought Steels," Society of Automotive Engineers, Inc., Report No. 790890, 1979.

9. Testin, R. A., "Characterization of the Cyclic Deformation and Fracture Behavior of Nodular Cast Iron," T&AM Report No. 371, Dept. of Theoretical and Applied Mechanics, University of Illinois at Urbana-Champaign, Urbana, Ill., 1973.

10. Starkey, M. S., and Irving, P. E., "The Influence of Microstructure on Fatigue Crack Initiation in Spheroidal Graphite Cast Iron," Proc. of Int. Symp. on Low Cycle Fatigue Strength and Elasto-Plastic Behavior of Materials, Stuttgart, 1979.

Table 1 Material Compositions

	Compacted Graphite	Nodular Iron	Pearlitic Gray Iron
C	3.60	3.57	3.30
Si	2.40	2.73	2.20
Mn	0.48	0.53	0.44
P	0.01	0.01	0.01
S	0.01	0.01	0.02
Cr	0.05	0.06	0.03
Ni	0.48	0.05	0.06
Mo	0.01	0.01	0.01
Cu	0.28	0.41	0.40
Mg	0.02	0.05	-
Ti	0.18	-	0.01
Sn	0.10	-	-
Al	0.01	-	0.01

Table 2 Mechanical Properties

	Compacted Graphite	Nodular Iron	Pearlitic Gray Iron
Modulus of Elasticity E (tension) GPa	134	152	84
Yield Strength 0.2% Sy MPa	345	440	185
Ultimate Strength True Fracture Strength, σ_f MPa	438	665	228
True Fracture Ductility ϵ_f	0.0153	0.0486	0.0122
Bulk Hardness (3000 kg)	195	235	180

List of Figures

Figure 1 Microstructure of Grey Iron

Figure 2 Microstructure of Compacted Graphite Iron

Figure 3 Microstructure of Nodular Iron

Figure 4 Test Specimen

Figure 5 Grey Iron Hysteresis Loops

Figure 6 Crack Development in Grey Iron

Figure 7 Stress-Life Curve for Grey Iron

Figure 8 Compacted Graphite Iron Hysteresis Loops

Figure 9 Crack Development in Compacted Graphite Iron

Figure 10 Stress-Life Curve for Compacted Graphite Iron

Figure 11 Nodular Iron Hysteresis Loops

Figure 12 Crack Development in Nodular Iron

Figure 13 Stress-Life Curve for Nodular Iron

Figure 14 Strain-Life Curve for Grey Iron

Figure 15 Strain-Life Curve for Compacted Graphite Iron

Figure 16 Strain-Life Curve for Nodular Iron

Figure 17 Summary of Stress-Life Curves

Figure 18 Summary of Strain-Life Curves

PEARLITIC GRAY IRON

TYPE A, ~60 %
TYPE D, ~40 %
SIZE 4

2 % NITAL

Figure 1 Microstructure of Grey Iron

COMPACTED GRAPHITE FLAKE - JDC

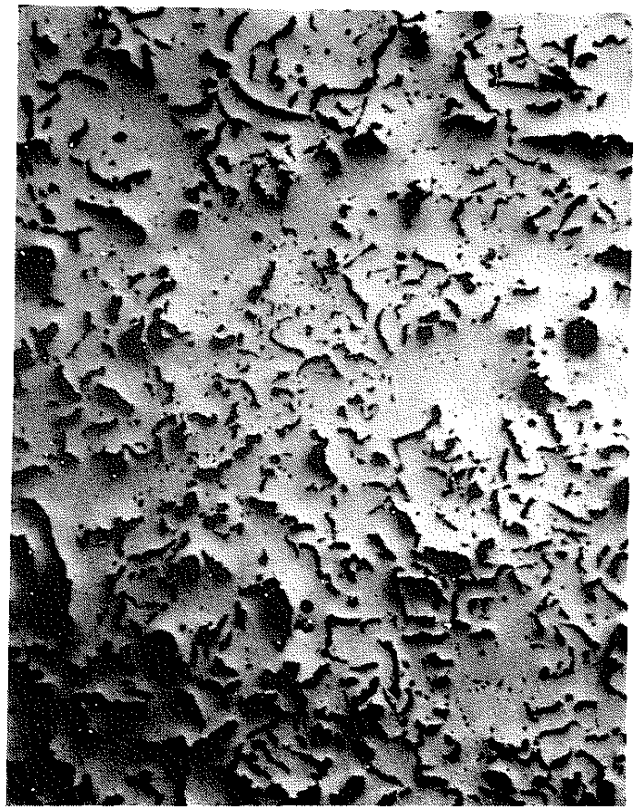

100X

PEARLITE 400X
ETCHED 2% NITAL

Figure 2 Microstructure of Compacted Graphite Iron

NODULAR IRON - SR3

100X

PEARLITE 400X
ETCHED 2% NITAL

Figure 3 Microstructure of Nodular Iron

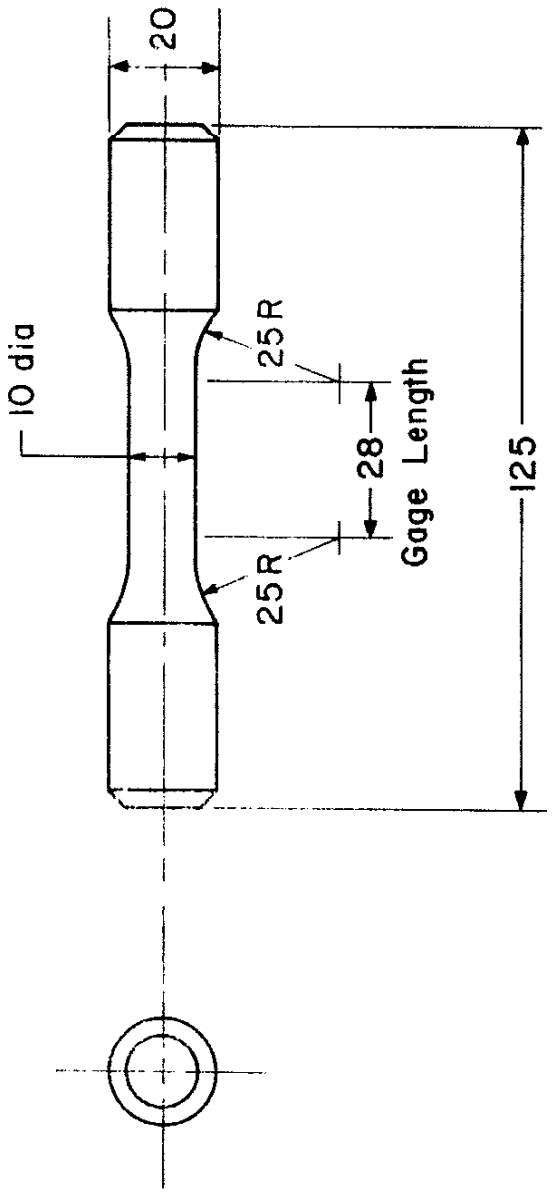

Figure 4 Test Specimen

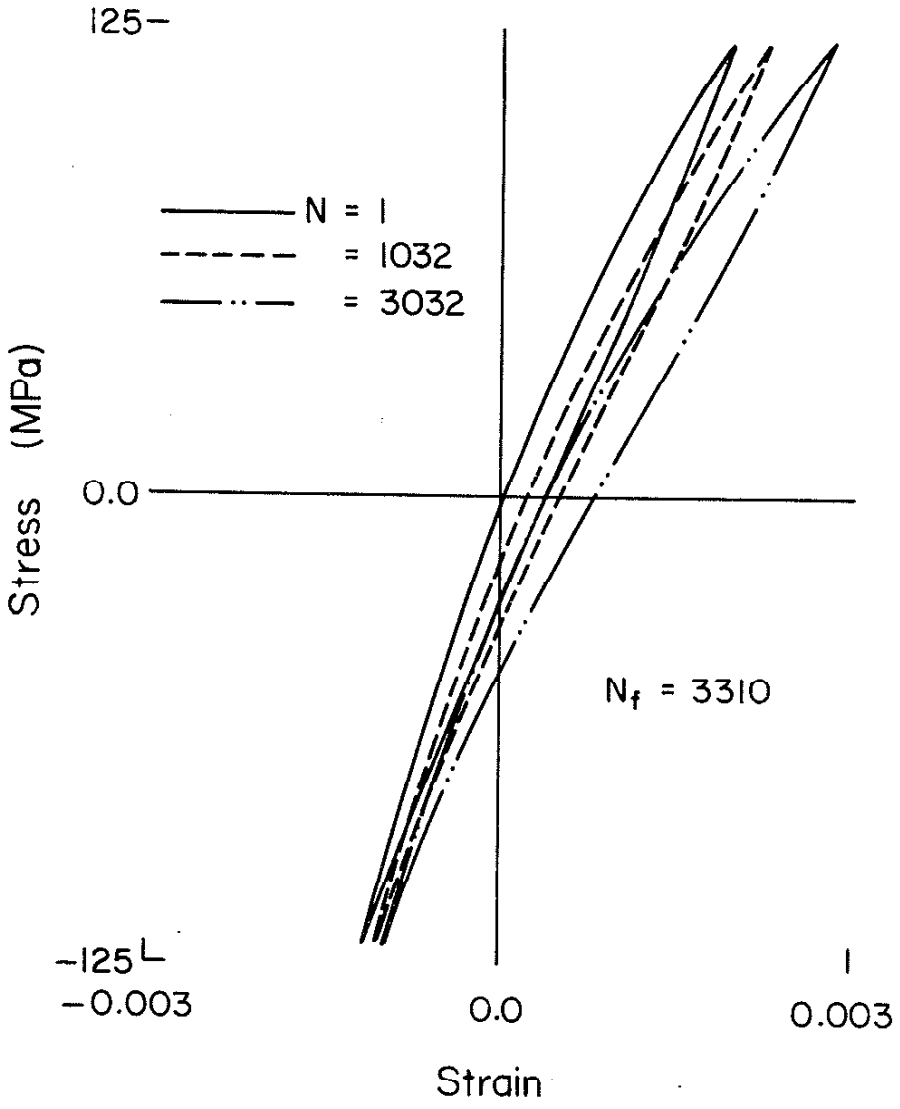

Figure 5 Grey Iron Hysteresis Loops

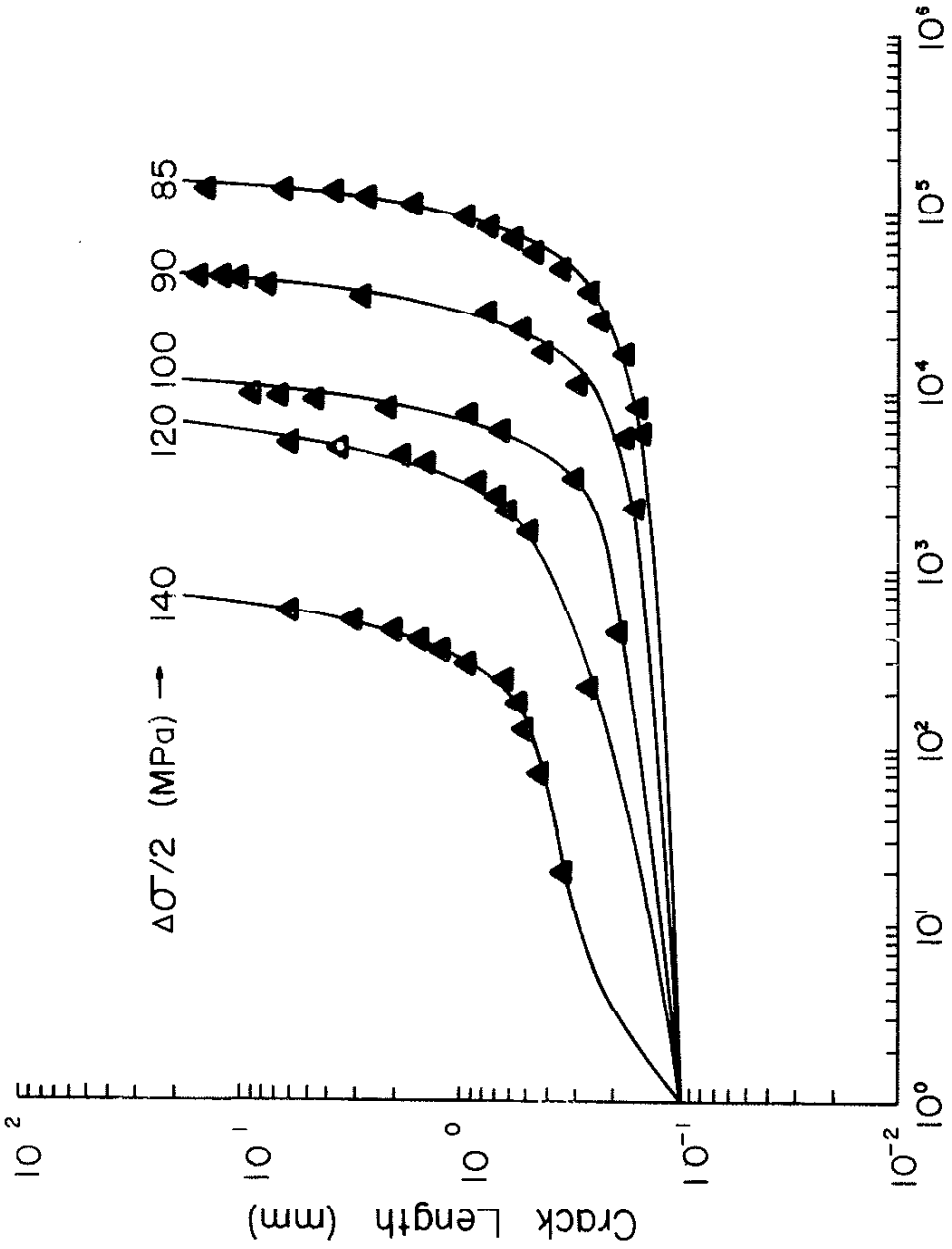

Figure 6 Crack Development in Grey Iron

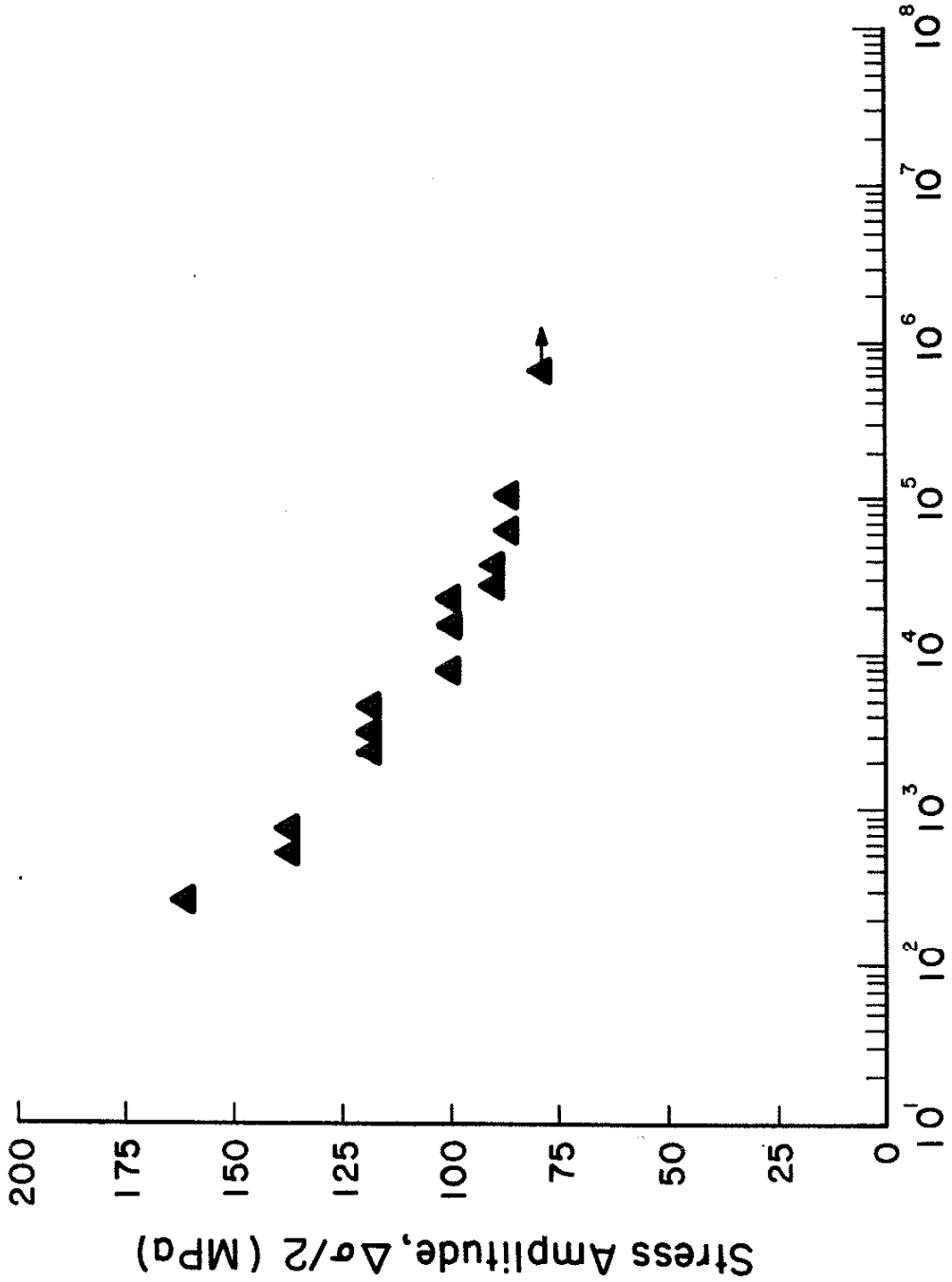

Figure 7 Stress-Life Curve for Grey Iron

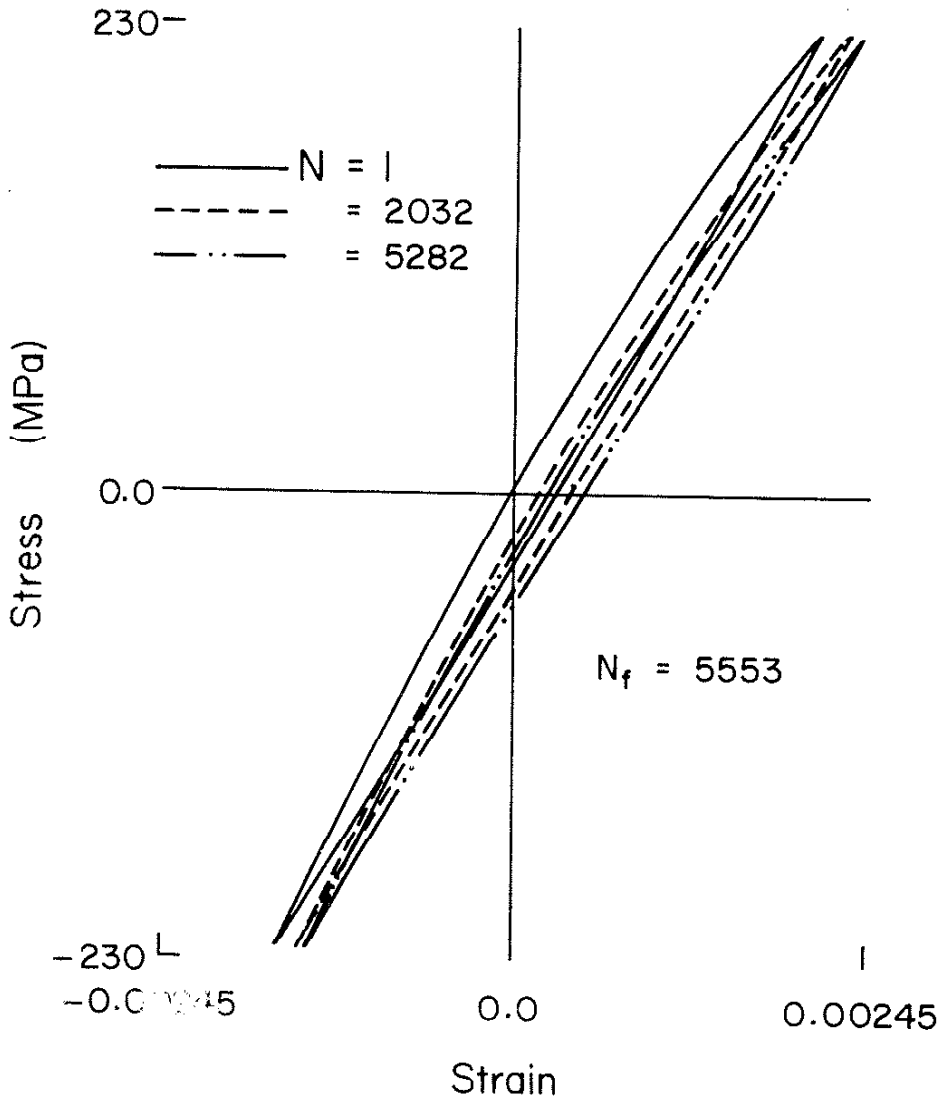

Figure 8 Compacted Graphite Iron
Hysteresis Loops

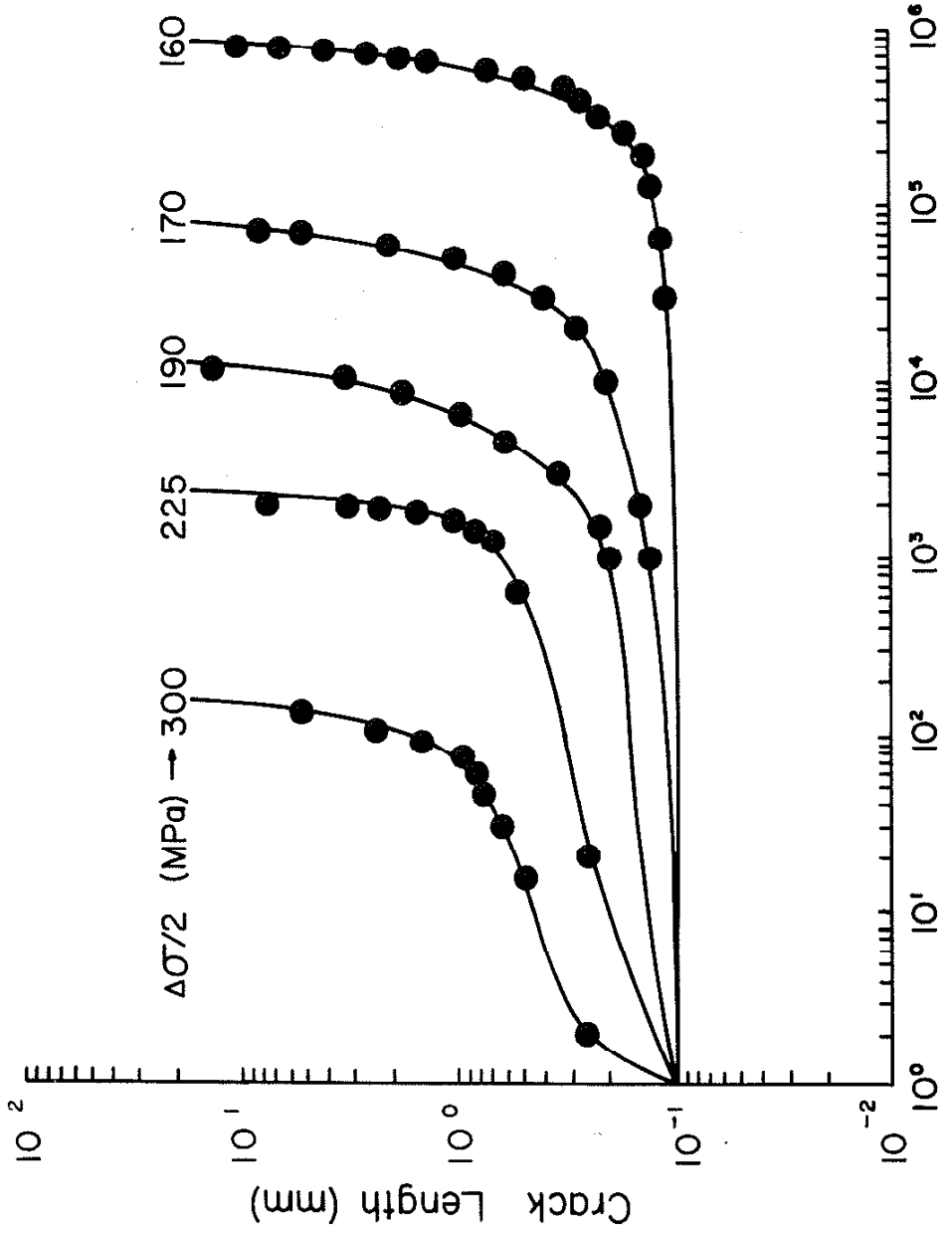

Figure 9 Crack Development in Compacted Graphite Iron

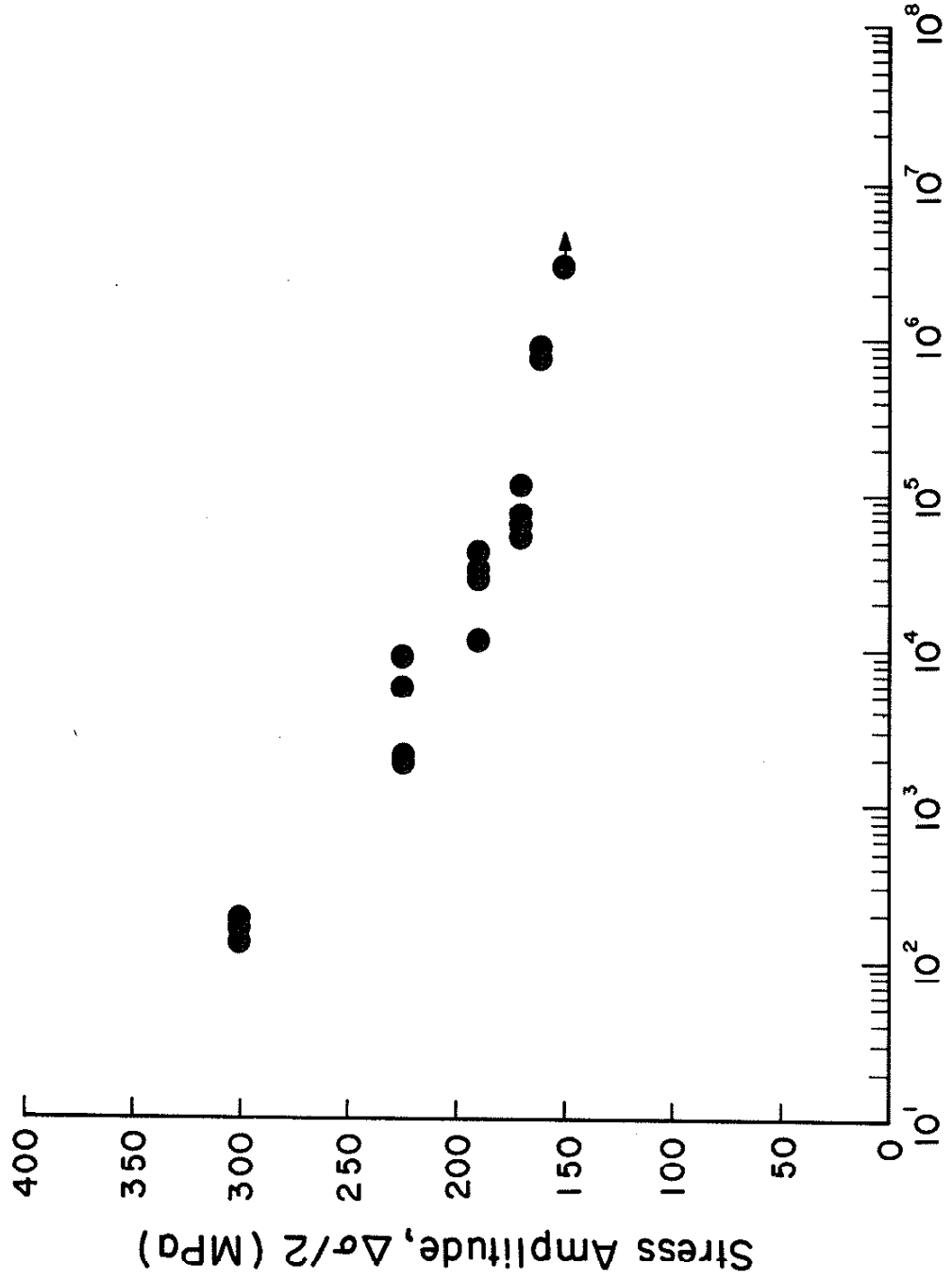

Figure 10 Stress-Life Curve for Compacted Graphite Iron

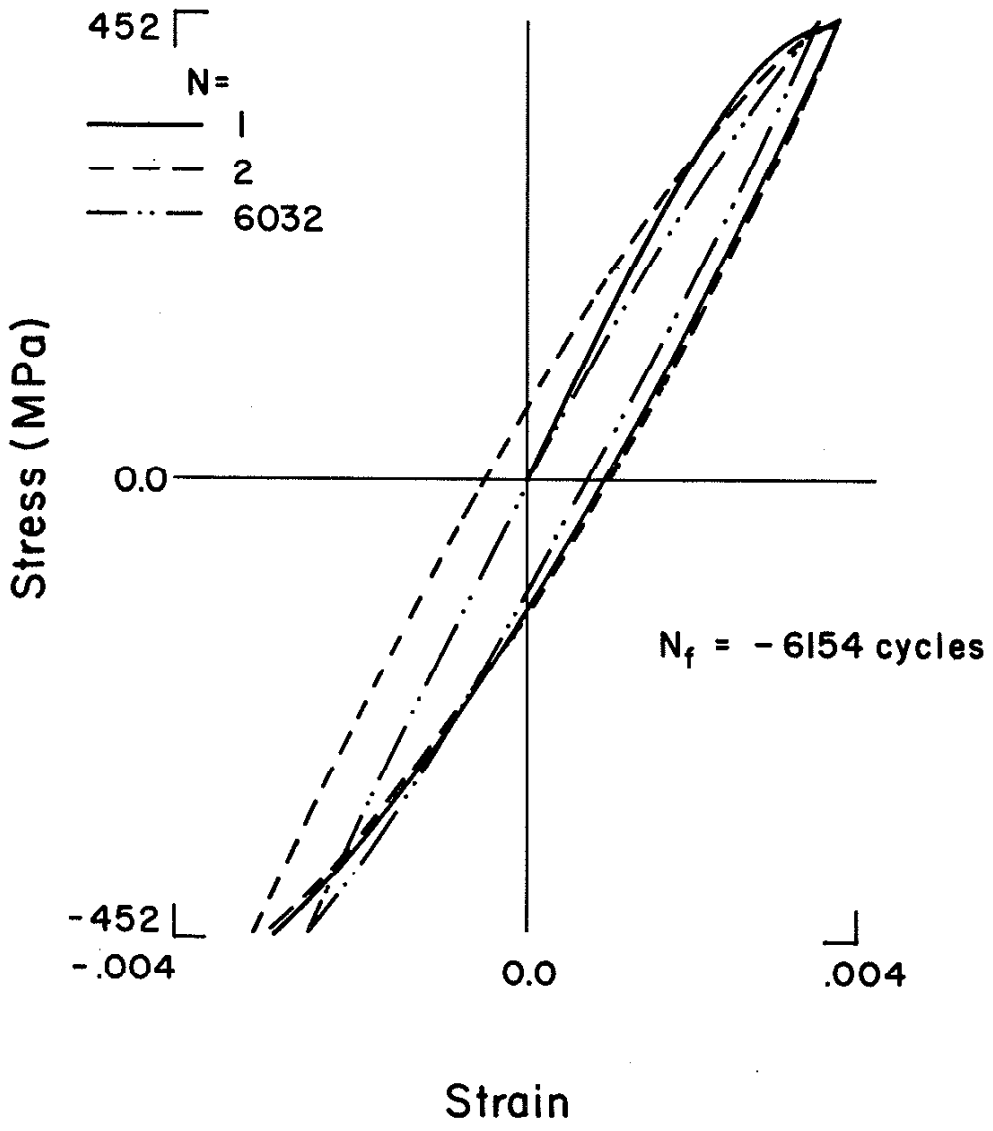

Figure 11 Nodular Iron Hysteresis Loops

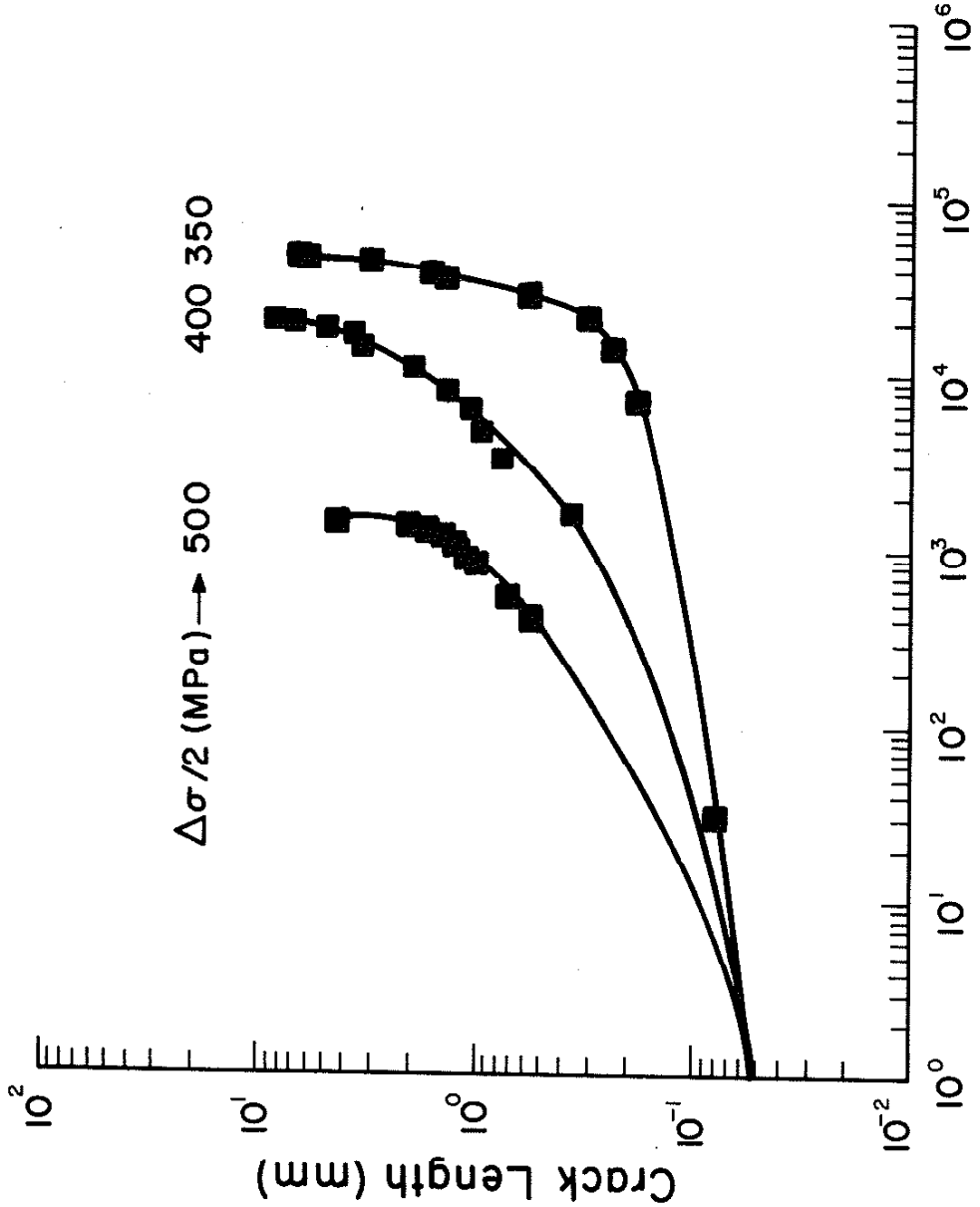

Figure 12 Crack Development in Nodular Iron

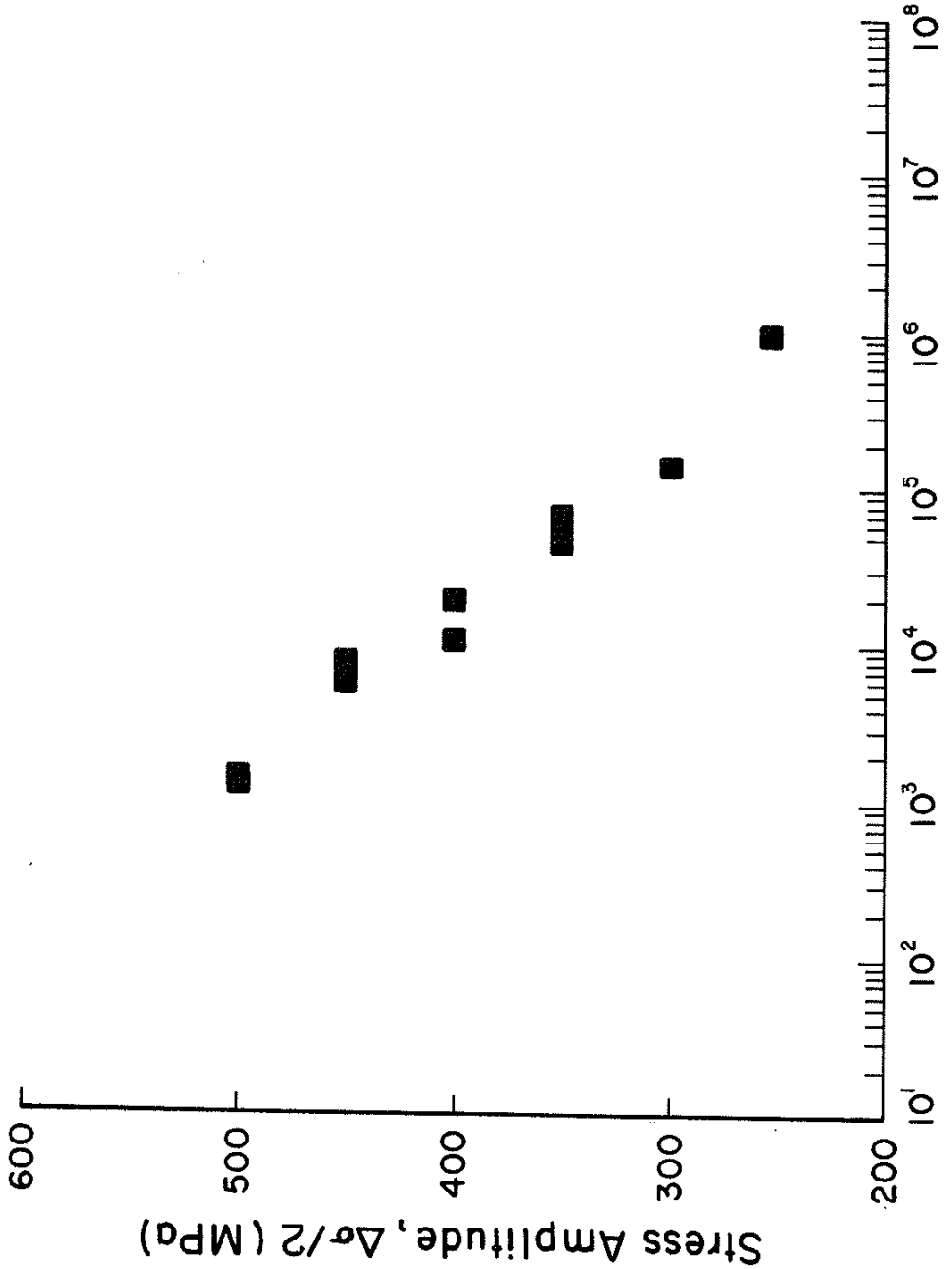

Figure 13 Stress-Life Curve for Nodular Iron

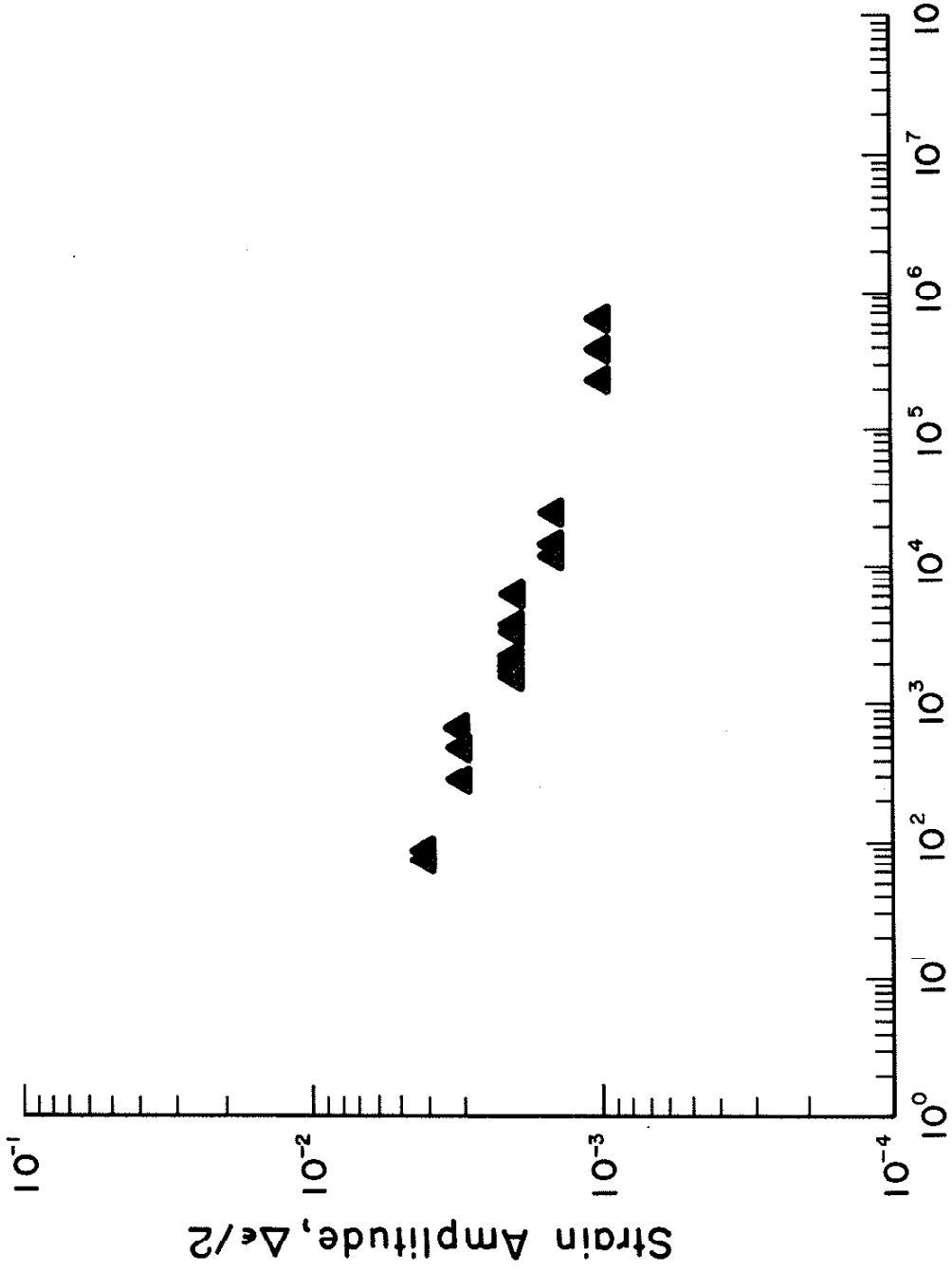

Figure 14 Strain-Life Curve for Grey Iron

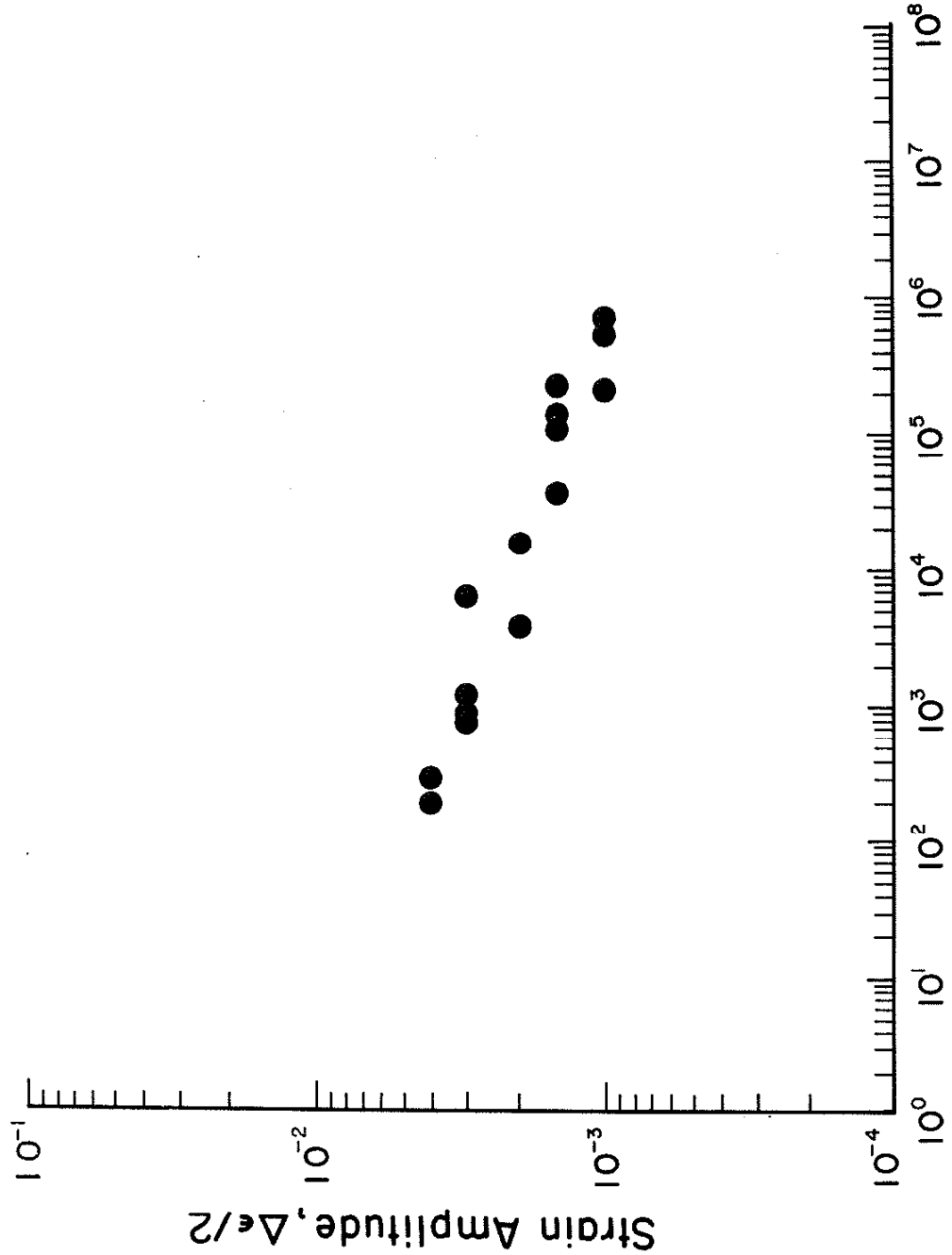

Figure 15 Strain-Life Curve for Compacted Graphite Iron

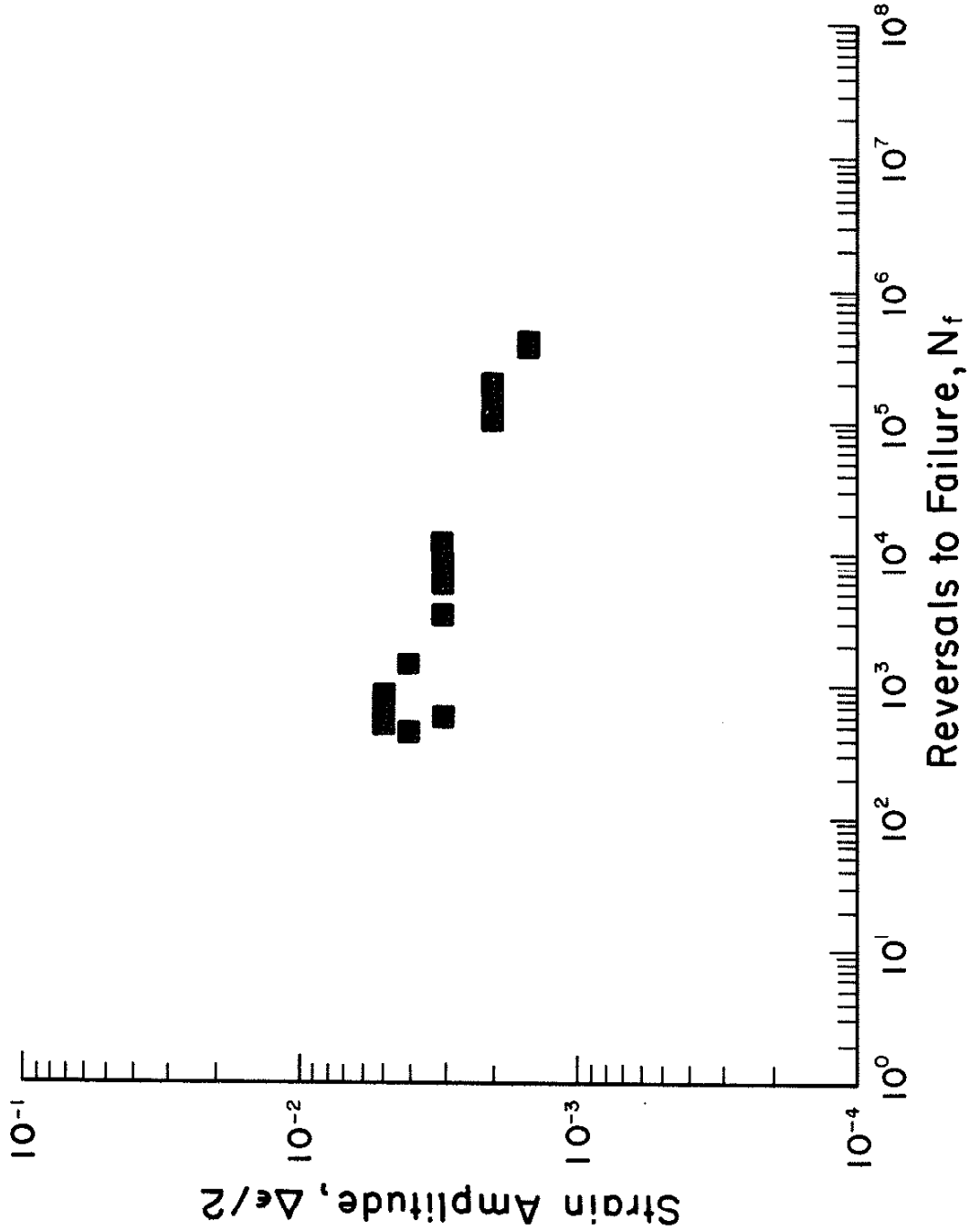

Figure 16 Strain-Life Curve for Nodular Iron

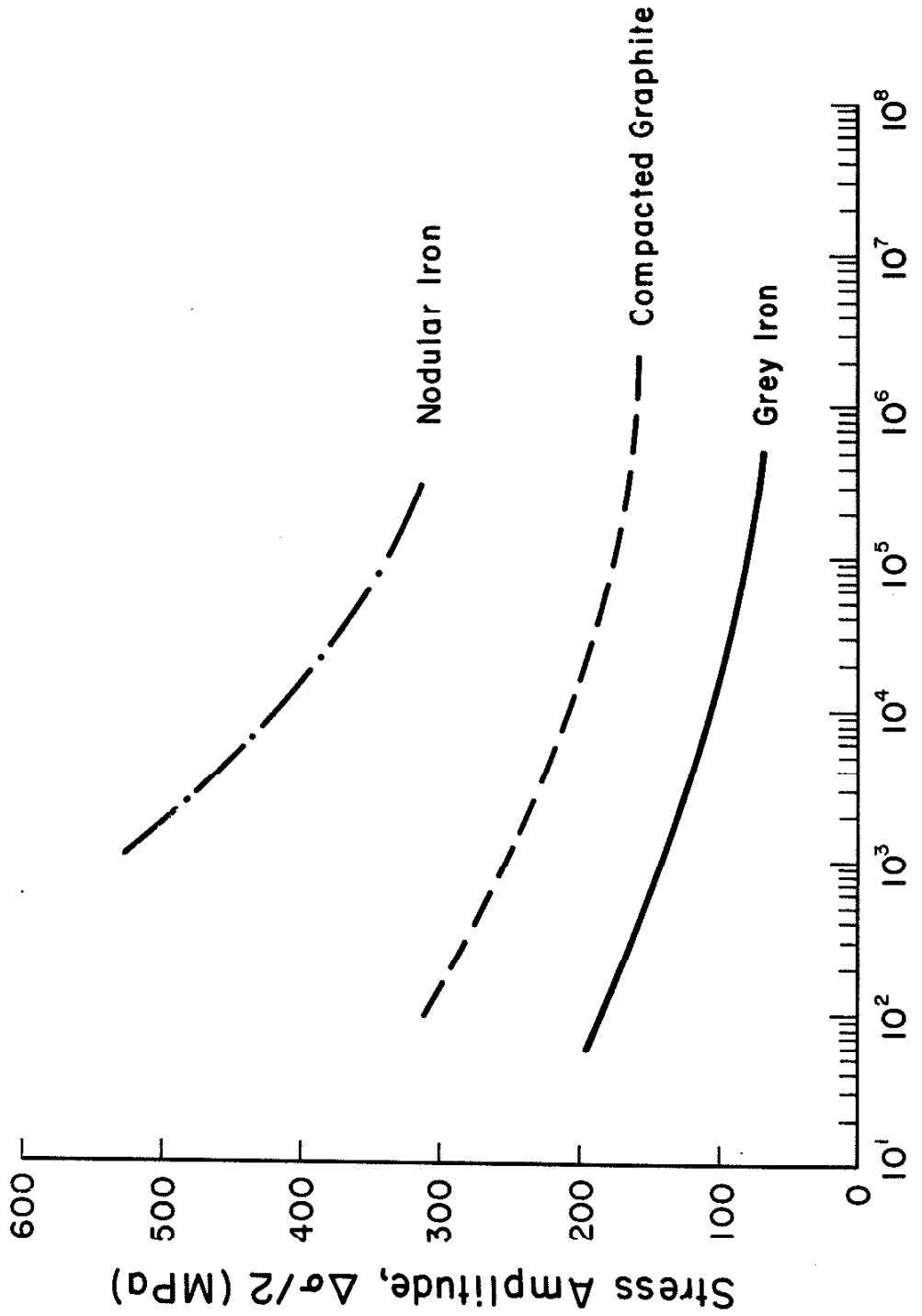

Figure 17 Summary of Stress-Life Curves

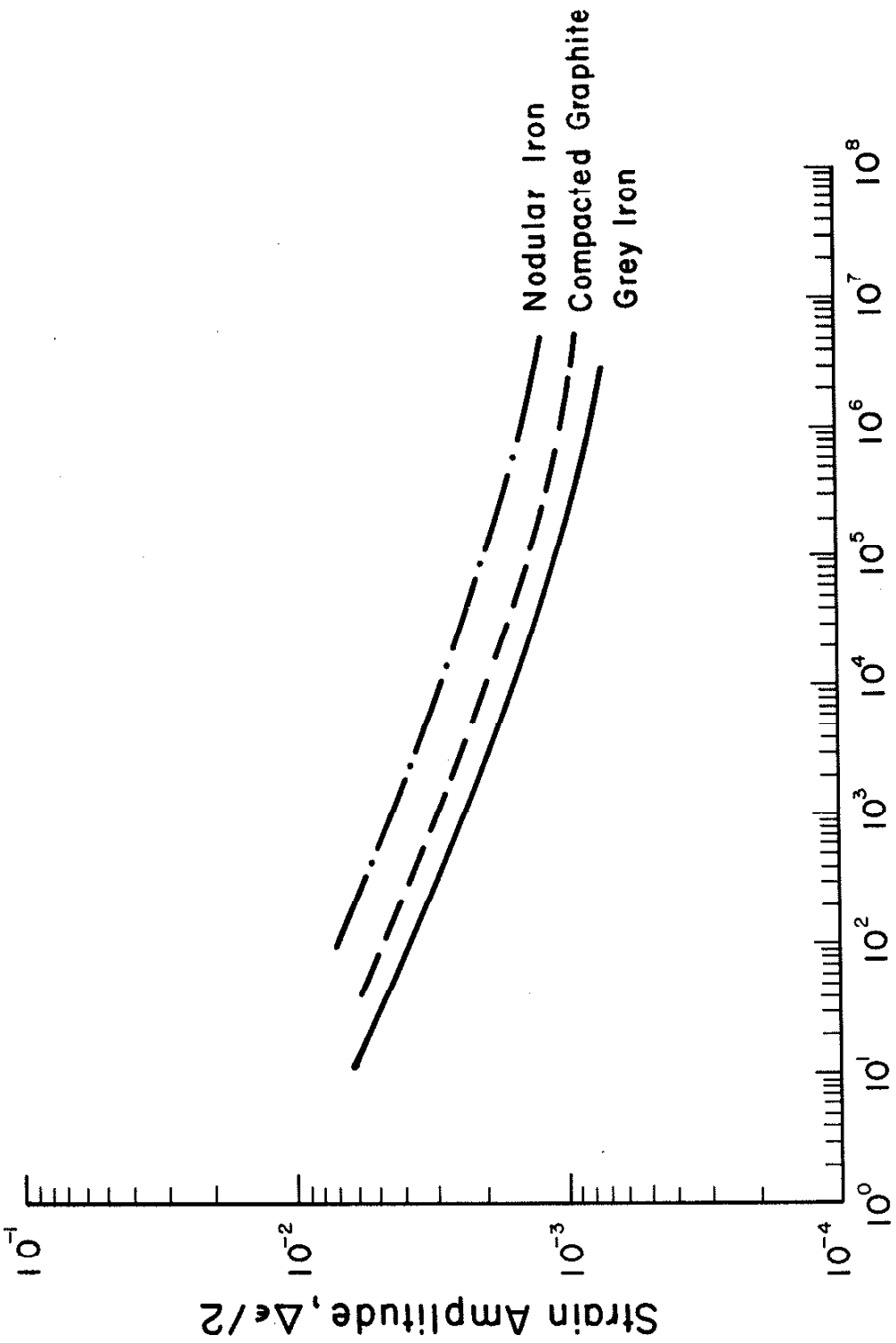

Figure 18 Summary of Strain-Life Curves

Part II: FATIGUE BEHAVIOR AND MEAN EFFECTS IN GRAY CAST IRON

J. W. Fash
D. F. Socie

Department of Mechanical and Industrial Engineering
University of Illinois at Urbana-Champaign
Urbana, IL 61801

ABSTRACT

Strain cycle fatigue concepts are well integrated into fatigue life prediction methodology for wrought components. Concepts developed for wrought materials can not be directly extended to cast materials due to differences in the fatigue mechanisms, but the framework of a life prediction method for cast iron components will be similar. Observations and results of constant amplitude completely reversed fatigue tests performed in strain and load control are reported for a pearlitic gray cast iron. Mean amplitude tests in both control modes have been conducted to evaluate the effects of mean stresses and strains. A parameter of the form (σ_{max} $\Delta\varepsilon$) gives good correlation of all the fatigue tests performed and provides a simple relationship to fatigue life.

Background

Design methodology to evaluate the fatigue resistance of components manufactured from wrought materials subjected to cyclic loads are in daily use by design engineers. Strain cycle fatigue and the local strain approach [1,2] are used extensively for predicting the crack initiation lifetime of components. Several variables such as material selection, component geometry and loading conditions, among others, must be understood for a successful design procedure. In order to be a useful design tool, the analytical techniques and experimentation required to complete the design procedure must be easily implemented. In the local strain approach, five major divisions can be made to describe the basic units of the fatigue analysis (Fig. 1). The following five areas must, in general, be considered. They are not totally independent and are by no means complete. In some situations, other factors will complicate the analysis.

(i) Laboratory characterization of the fatigue behavior of the material of interest provides the foundation of the analysis. Typically, completely reversed, strain cycle fatigue tests are performed on smooth, axial tension-compression specimens. The cyclic stress-strain curve is determined as representative of the materials behavior under cyclic loading. A relationship between cyclic strain amplitude and the number of cycles to failure is also determined. A Coffin-Manson type relationship is often fitted to this data.

(ii) Geometric discontinuities such as holes, fillet radii, and notches often initiate failure. To extend the laboratory materials characterization to the actual component, a stress strain simulation in the critical location where failure occures is required. Both material behavior and the local geometry must be considered.

Several stress analysis techniques are available to determine the local response to the applied loading conditions. Finite element analysis and Neuber notch analysis are techniques frequently employed.

(iii) Actual loading conditions vary considerably from the completely reversed, constant amplitude loading applied in the laboratory. A technique to reduce a complex load history into a series of events which can be incorporated into the fatigue analysis is required. Several methods are available for reducing the load sequence into damaging events. Of these methods, rainflow counting has been shown to give better life estimates. Typically, the damaging events are determined as closed hysteresis loops which have a strain range with a mean stress possibly present. To determine these values the cyclic response of the material must be modeled on a reversal by reversal basis through the complex history of either stress, strain, or load values.

(iv) Mean stresses, which are frequently present and can be determined by the material response model, influence the fatigue life. For a given strain range in a strain controlled fatigue test, increasing the mean stress causes a decrease in the fatigue life. Several parameters which characterise the effect of mean stresses on fatigue life have been proposed. Most of these are empirical relationships which best fit experimental data. The effects of mean strains are usually ignored.

(v) A damage model is necessary to accumulate the degradating effects of the closed hysteresis loops or damaging events. When the amount of damage accumulated equals some critical value, failure is

predicted. Miners linear damage rule is widely used in crack initiation analysis. For particular situations, variations of Miner's rule have been suggested. Damage models such as those based on continuum damage concepts are also available. This is usually the last step of the analysis and it includes all the previously mentioned interactions.

When the general areas described above are incorporated into a fatigue life analysis, the crack initiation life of a component can be estimated. Similar analytical techniques are not widely accepted for life predictions of cast iron components in which the effects of metallurgical notches such as free graphite, porosity and inclusions must be considered. The phenomena occuring during the fatigue of cast irons must be understood in order to develop the units of a life prediction technique which models the actual material behavior.

In order to develop fatigue design methodology for cast iron components, the fatigue behavior of gray iron has been observed during reserach conducted in the Materials Engineering Research Laboratory at the University of Illinois at Urbana-Champaign. Observations made during constant amplitude completely reversed fatigue tests performed in strain and load control have been reported previously [3,4] and will be reviewed below. Results from fatigue tests with mean values of the control parameter are reported. A previously proposed parameter for incorperating mean stress effects, is shown to give good correlation of the results of the completely reversed and mean amplitude tests for a pearlitic gray iron. Use of this parameter will satisfy section (iv) of the fatigue analysis procedure described above.

Material

Gray cast iron test bars 30 mm in diameter and 200 mm long were cast in green sand molds to give a pearlitic microstructure in the matrix steel. Chemical composition is given in Table 1. Classification of the size and distribution of the free graphite structure is given by ASTM standard A247 [5] as approximately 60 percent type A; and approximately 40 percent type D; size 4 (Fig. 2). Steads reagent was used to preferentially etch metallographic specimens to determine the eutectic cell size, which is approximately 0.14 mm. Mechanical and monotonic properties are given in Table 2.

Experimental Program

Low cycle fatigue specimens (Fig. 3) were machined from the as-cast test bars [6]. All fatigue tests were performed on 100 kN, closed loop servohydraulic materials testing equipment interfaced to a digital computer which in some tests recorded data and in other tests performed test control as well as data acquisition. Load-strain response versus applied cycles was monitored.

Deformation and crack initiation processes in cast irons have previously been reported in the literature [7-9]. Cracking occurs first in the free graphite structure. This structure is very brittle and weak in tension but will carry much larger compressive loads. Observations during fatigue loading [10,11] have shown that cracks grow from the graphite structure which causes large stress concentrations in the matrix steel. This crack growth behavior occurs very early in the life of the fatigue specimens.

Observations of the initiation and growth of cracks in the smooth specimens have been accomplished using a surface replication technique [3,4]. Standard metallographic actyl film which softens when moistened with

acetone is used. When it is soft, the tape is placed around the test section and it conforms to the surface topography. The tape rehardens and is then removed, giving a permanent replica of the surface. By taking a series of these replicas during a fatigue test, the development and growth of cracks can be observed. Results of these observations will be included below.

Results and Discussion

Strain Control

Strain controlled, completely reversed fatigue tests were performed. Tests were run to approximately 90 percent load drop from the initial maximum load. Cyclic stress strain response was observed during the tests but the typical stable hysteresis response found in wrought metals was not observed. A series of hysteresis loops from a strain control test are shown in Fig. 4. A continual decrease in the maximum tensile load occurs but the maximum compressive load remains constant throughout the test. This degredation in the load carrying capacity of the specimen is attributed to the formation and development of multiple crack systems. Development of the crack system causing failure was observed from the surface replicas taken throughout the test and it is found [3] that the crack system develops slowly to a size of about 1 to 2 mm. Once a crack reaches this size in the smooth specimen, failure occurs very quickly through a complex process of crack linking and crack growth. During completely reversed strain control tests, a compressive mean stress is present due to the anisotropy between tensile and compressive properties. This means stress decreases as the strain amplitude increases. The value of the compressive mean stress and the maximum stress decrease throughout the test as shown in Fig. 5 for the two test conditions. Strain life results are shown in Fig. 6 as well as the results of mean strain tests which will be discussed later.

Load Control

Constant amplitude load control tests were performed. As in the strain control tests, cyclic stability was not observed. In these tests, the cyclic strain amplitude continually increased (Fig. 7) due to the increased compliance of the specimen as crack systems developed. Maximum values of both the tensile and compressive strains increase but the tensile value increases much more than the compressive value. Crack initiation and growth similar to the behavior observed in the strain control tests was observed in the load control tests. Multiple crack systems were found very early in the fatigue life and were observed to grow slowly to about 1 to 2 mm [4]. Once a crack system reached this size, the crack became dominant and grew rapidly to instability and failure. In the completely reversed load control tests, the mean strain and strain amplitude both increase with cycles (Fig. 8). Stress versus life results are shown in Fig. 9. Mean stress data is also shown in this figure and will be discussed in the next section.

Mean Parameter

Ideally, mean parameters collapse all the results of fatigue tests into a single relationship which provides an interpretation of the effects of mean stresses and simplifies the fatigue life analysis. A simple relationship has been proposed by Smith, Watson and Topper [12]. This parameter (called the SWT parameter) was originally proposed by the authors to include crack growth and seems most appropriate for gray iron. Other parameters based on the reduction of static or fatigue strengths are inappropriate for fatigue problems that have been demonstrated to be crack growth.

Several forms of the SWT parameter are possible and a form which relates the product of the strain amplitude and the maximum stress to the fatigue life

for a given test condition will be used to correlate experimental results. The parameter is then of the form

$$(\sigma_{max} \quad \Delta \varepsilon/2)$$

where $\Delta\varepsilon/2$ = 1/2 total strain range, σ_{max} = stress at maximum strain.

A series of strain control fatigue tests were conducted in which a variety of strain amplitudes and mean strain combinations were imposed. These tests resulted in a wide range of mean stresses. Results are included in Fig. 6. Transient behavior, similar to that shown for the completely reversed tests in Fig. 5 was observed. In order to apply the SWT parameter a value of the maximum stress must be chosen at some point in the life. For convenience, the value at the half life of the specimen was used. The value of the maximum stress could be chosen at another point in the life but this would not change the results significantly since the change is small (see Fig. 5). Using the SWT parameter both the completely reversed and mean strain control data can be collapsed to a single scatter band as shown in Fig. 10.

Similar mean tests were conducted in load control. During these tests, the magnitude of the strain range increased throughout the test and the value at the half life was used in the SWT parameter. The data in Fig. 9 is collapsed into a single scatter band in Fig. 11 using this parameter.

Implementing this form of the SWT parameter allows a single graphical representation of both strain control and load control fatigue tests. For the approximately sixty test points shown in Fig. 12, a power law relationship can be fitted which takes the form

$$(\sigma_{max} \quad \Delta\varepsilon/2) = 1.82\ (N_f)^{-0.25}$$

The constants in this relationship were determined by a first order linear regression analysis.

Summary

In the finite life regime (less than 10^6 cycles to failure) the fatigue resistance of gray cast iron is dominated by crack growth. The SWT parameter provides an effective means for relating a wide range of loading conditions to the cyclic life and can easily be incorporated into a fatigue life prediction methodology. Further work must be done before this parameter can be extended into the life range of greater than 10^6 cycles where the mechanisms may differ.

Acknowledgements

Mr. Furman and Ms. Cleary are thanked for their assistance in conducting the tests. Tests were performed in the Materials Engineering Research Laboratory at the University of Illinois at Urbana-Champaign. Financial support was provided by the Fracture Control Program. Financial support for the second author was provided by the National Science Foundation Grant CME-78-23549. Test specimens were cast by Deere and Co.

References

1. Manual on Low Cycle Fatigue Testing, ASTM STP 465, American Society of Testing and Materials, Philadelphia, Pa., 1969.

2. Fatigue under Complex Loading, Society of Automotive Engineers, Warrendale, Pa., 1979.

3. Fash, J. W., D. F. Socie, and E. S. Russell, "Fatigue Crack Initiation and Growth in Gray Cast Iron," Proceedings of Fatigue '81, Society of Environmental Engineers, Fatigue Group Conference, Warwick University, England, March 24-27, 1981, pp. 40-51.

4. Molinaro, L., "Fatigue Behavior and Crack Development in Compacted Graphite Cast Iron," Fracture Control Program, Report No. 39, College of Engineering, University of Illinos at Urbana-Champaign, May 1981.

5. "Method of Evaluating the Microstructure of Graphite in Iron Castings," ASTM Designation: A247, Plate I (Graphite Form Types), Plate II (Graphite Flake Type Chart), and Plate III (Graphite Size), American Society for Testing and Materials, 1916 Race Street, Philadelphia, Pa., 19103.

6. "Constant Amplitude Low-Cycle Fatigue Testing," ASTM Designation: E606, American Society of Testing and Materials, Philadelphia, Pa.

7. Gilbert, G. N. J., "An Evaluation of the Stress/Strain Properties of Flake Graphite Cast Iron in Tension and Compression," J. of the British Cast Iron Research Association, Vol. 7, 1959, pp. 745-789.

8. Gilbert, G. N. J., "The Stress/Strain Properties of Nodular Cast Irons in Tension and Compression," J. of the British Cast Iron Research Association, Vol. 12, No. 2, 1964, pp. 170-193.

9. Gilbert, G. N. J., "Factors Relating to the Stress/Strain Properties of Cast Iron," J. of the British Cast Iron Research Association, Vol. 6, No. 11, 1957, pp. 546-588.

10. Ikawa, K., and G. Ohira, "Fatigue Properties of Cast Iron in Relation to Graphite Structure," American Foundry Society, Cast Metals Research J., Vol. 3, 1967, pp. 11-21.

11. Starkey, M. S., and P. E. Irving, "The Influence of Microstructure on Fatigue Crack Initiation in Spheroidal Graphite Cast Iron," Proc. of Int. Symp. on Low Cycle Fatigue Strength and Elasto-Plastic Behavior of Materials, Stuttgart, 1979.

12. Smith, K. N., P. Watson, and T. H. Topper, "A Stress-Strain Function for the Fatigue of Metals," J. of Materials, JMLSA, Vol. 5, No. 4, Dec. 1970, pp. 767-778.

LIST OF FIGURES

Fig. 1 Basic steps for applying local strain concepts to evaluate the fatigue performance of wrought components.

Fig. 2 Microstructure of pearlitic gray iron investigated.

Fig. 3 Low cycle fatigue specimen.

Fig. 4 Hysteresis response during completely reversed strain control fatigue test.

Fig. 5 Transient behavior of the maximum stress and mean stress during strain controlled fatigue tests.

Fig. 6 Cyclic life of strain controlled fatigue tests.

Fig. 7 Hysteresis response during completely reversed load control fatigue tests.

Fig. 8 Transient behavior of the strain amplitude and mean strain during load control fatigue tests.

Fig. 9 Cyclic life of load controlled fatigue tests.

Fig. 10 Results of strain control fatigue tests presented using the SWT parameter.

Fig. 11 Results of load control fatigue tests presented using the SWT parameter.

Fig. 12 Results of all fatigue tests presented using the SWT parameter.

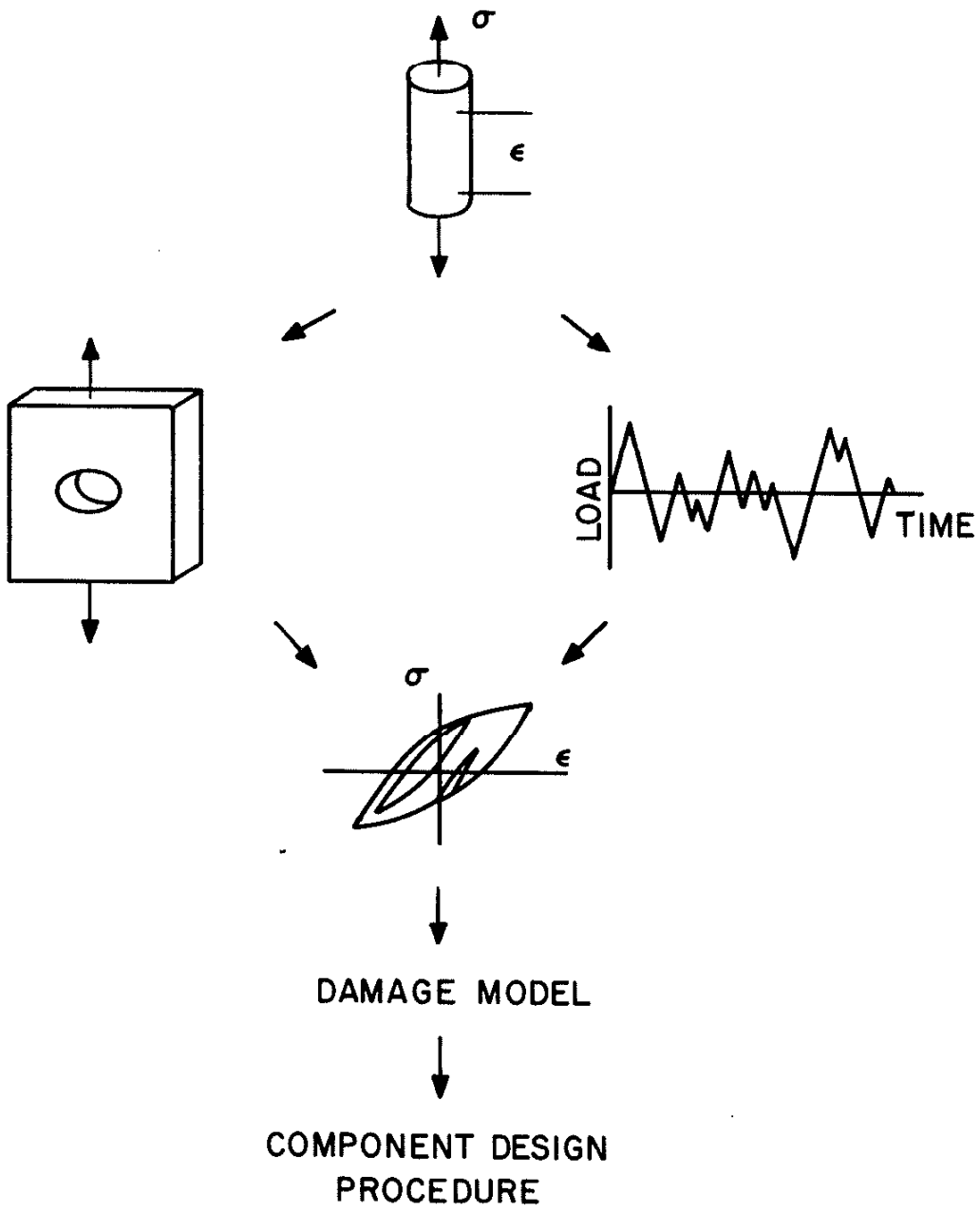

Fig. 1 Basic steps for applying local strain concepts to evaluate the fatigue performance of wrought components.

PEARLITIC GRAY IRON

TYPE A, ~60 %
TYPE D, ~40 %
SIZE 4

2 % NITAL

Fig. 2 Microstructure of pearlitic gray iron investigated.

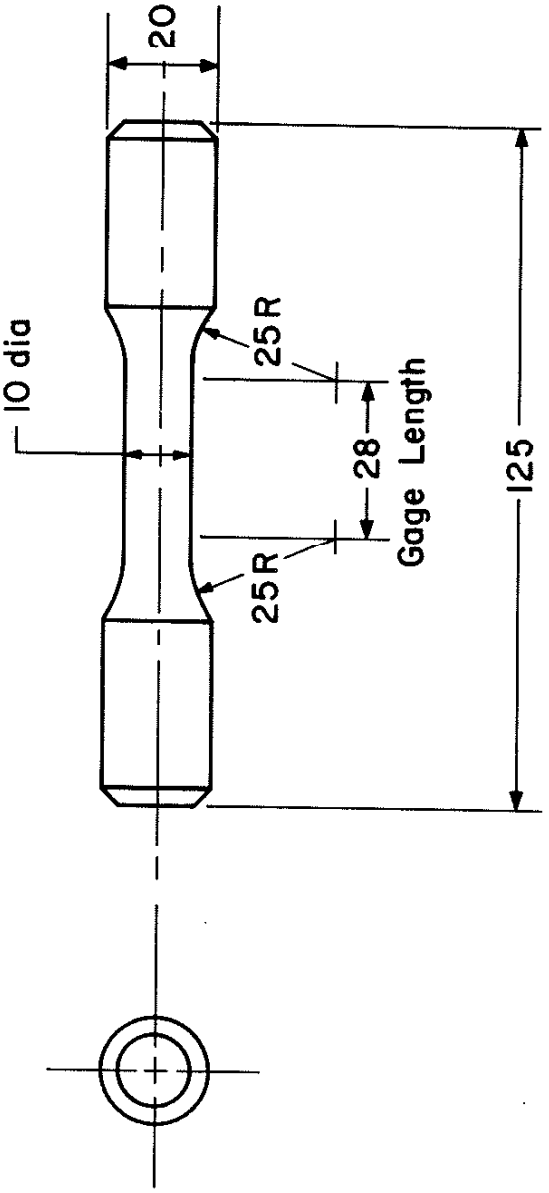

Fig. 3 Low cycle fatique specimen.

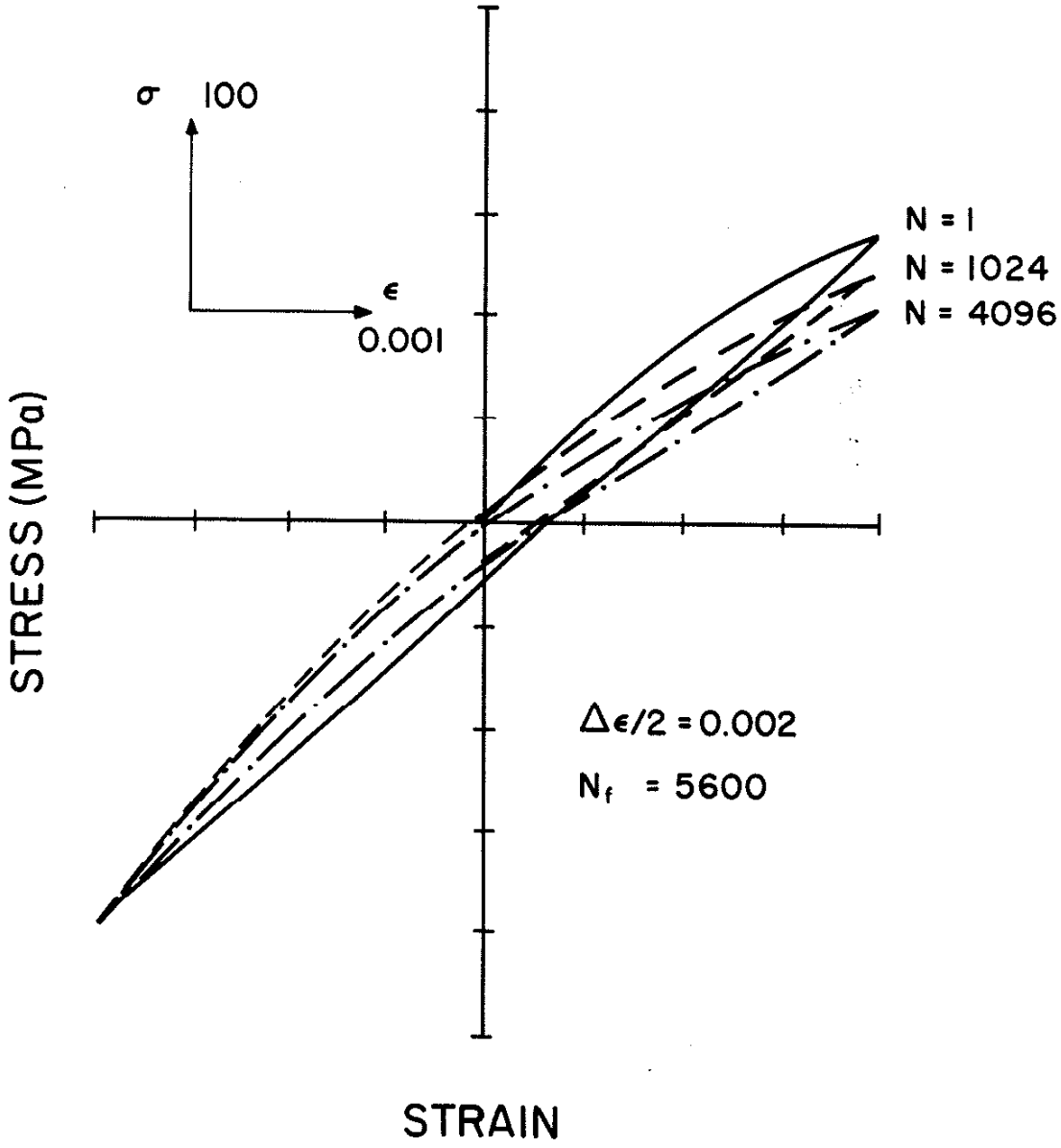

Figure 4 Hysteresis response during completely reversed strain control fatigue test.

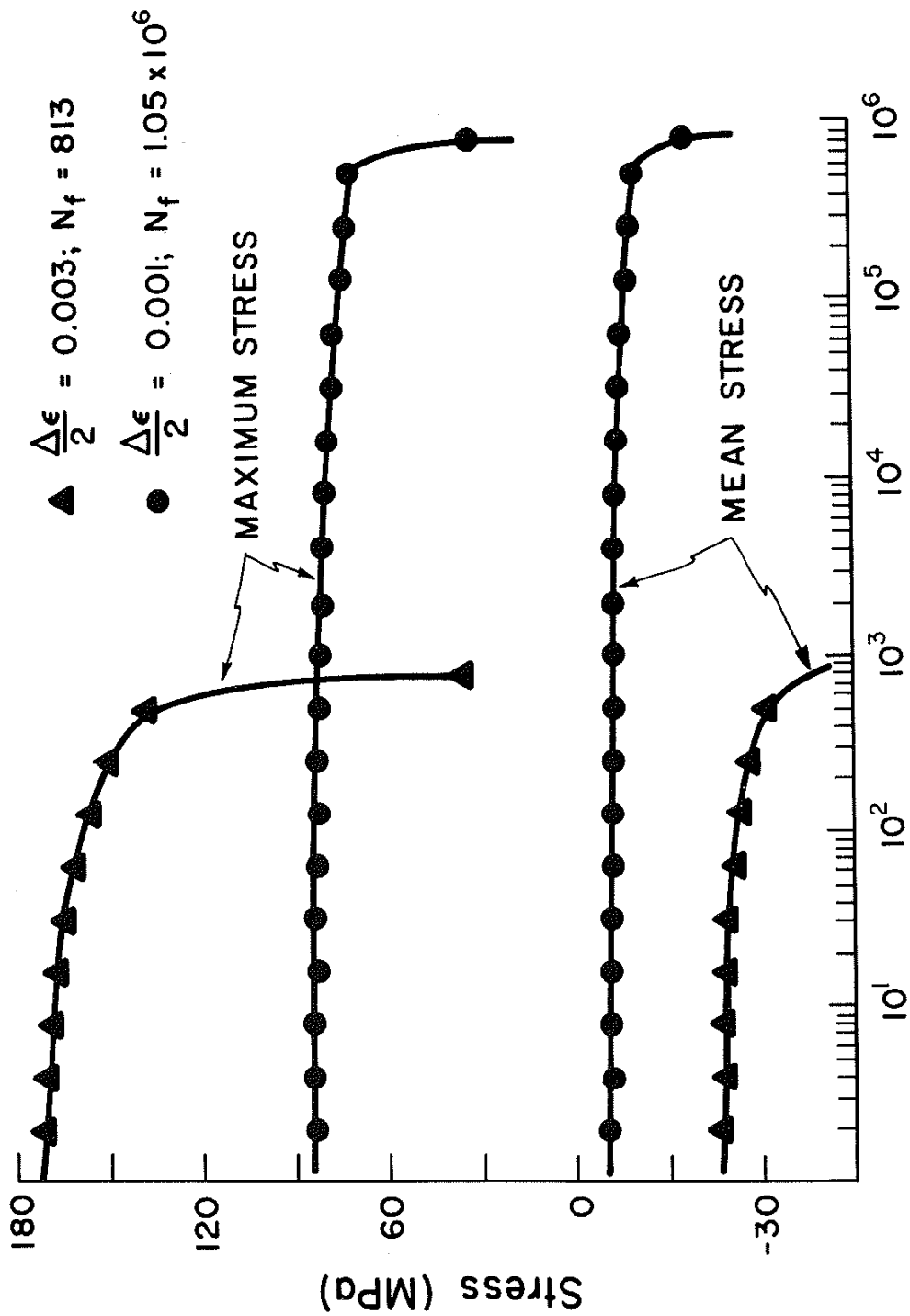

Figure 5 Transient Behavior of the Maximum Stress and Mean Strain during Strain Controlled Fatigue Tests

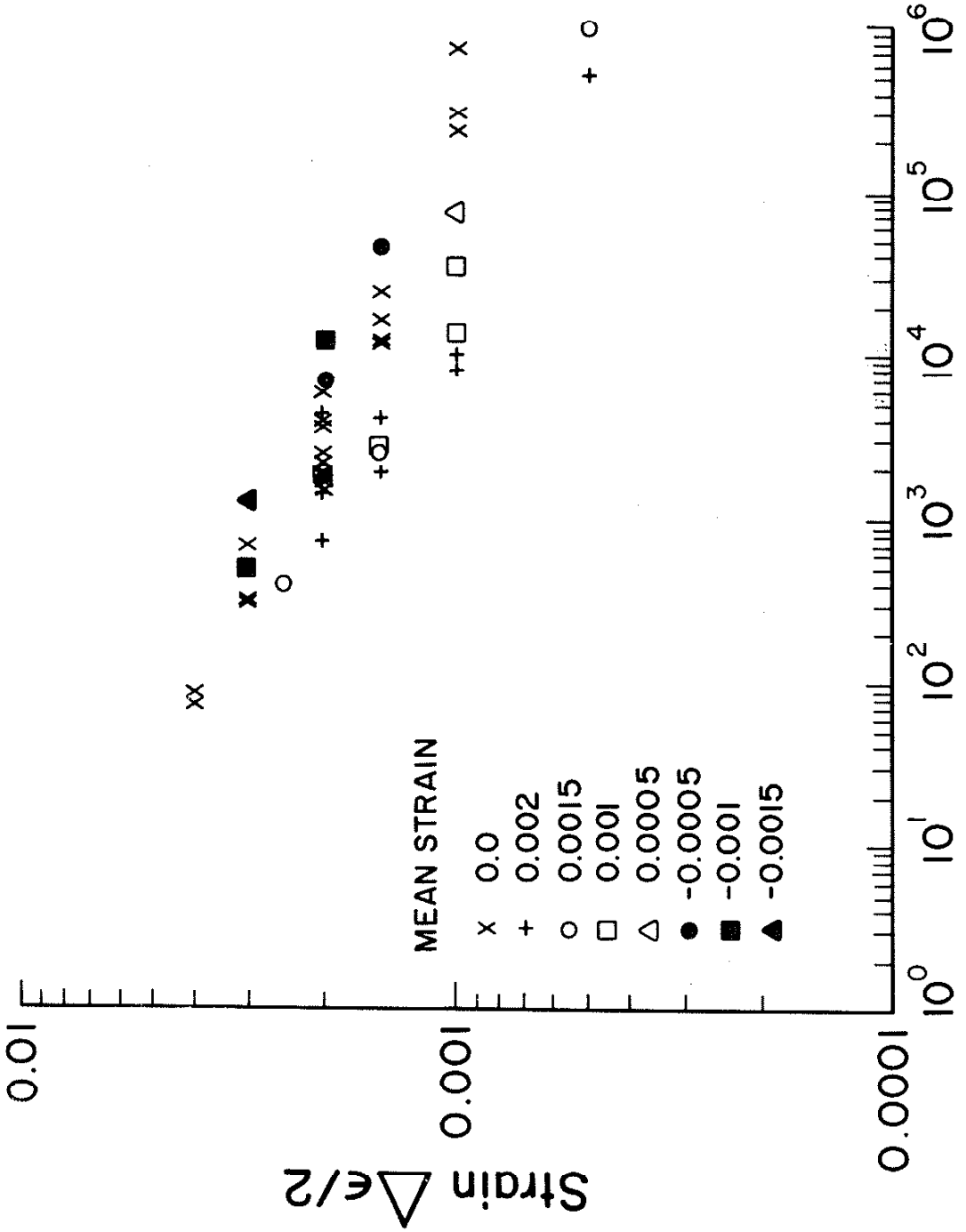

Figure 6 Cyclic life of strain controlled fatigue tests.

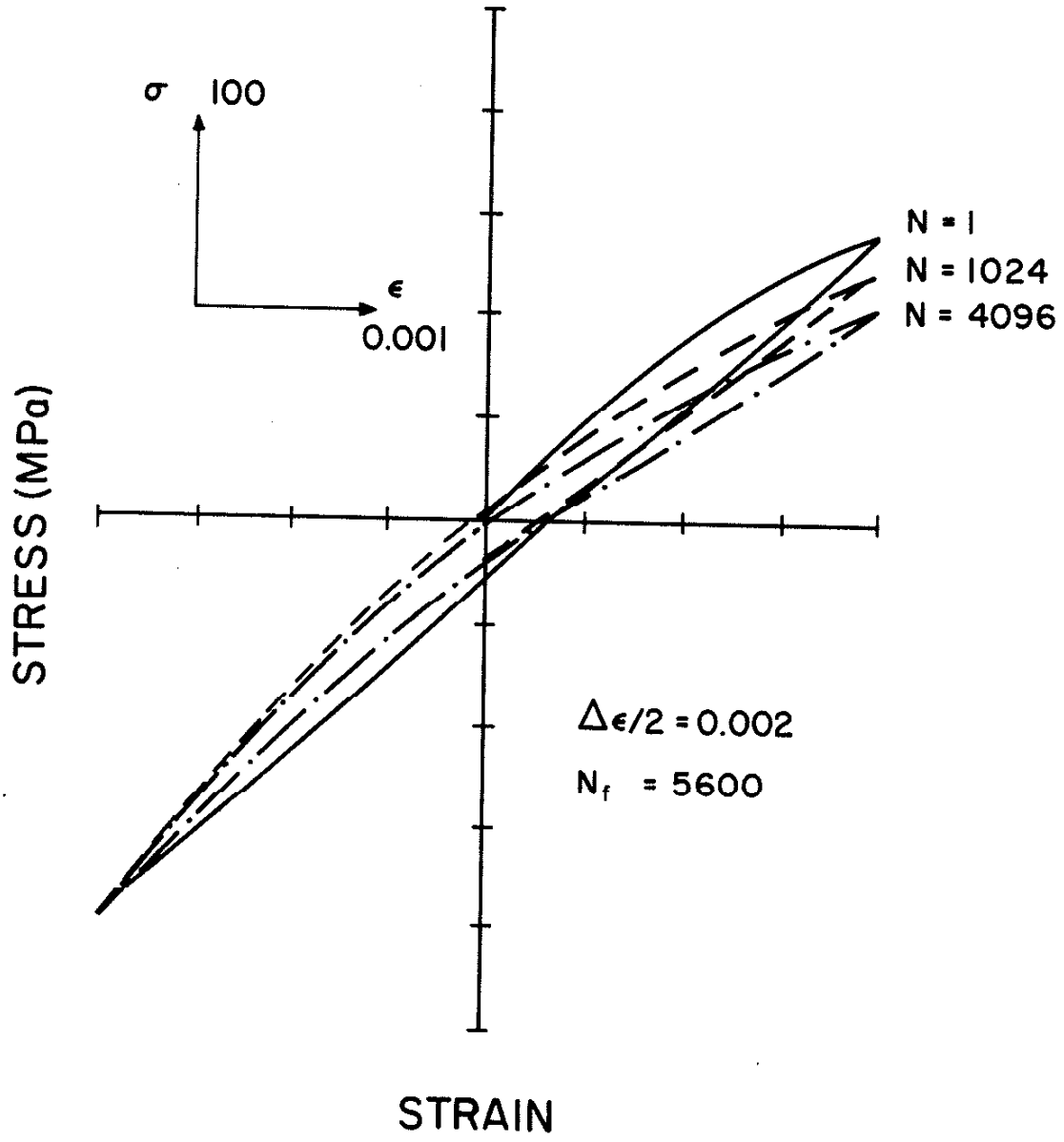

Figure 7 Hysteresis Response during Completely Reversed Load Control Fatigue Tests

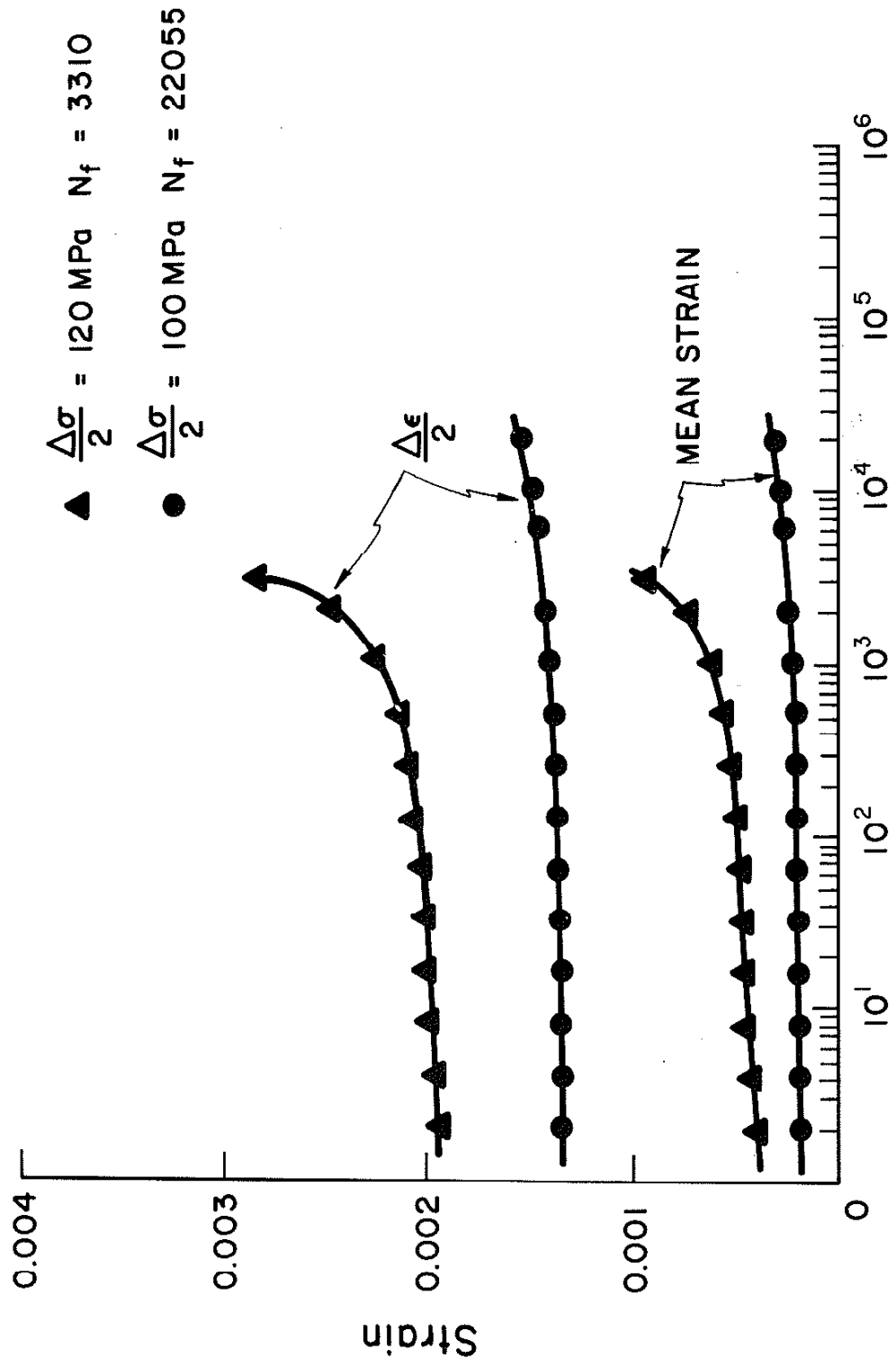

Figure 8 Transient Behavior of the Strain Amplitude and Mean Strain during Load Control Fatigue Tests

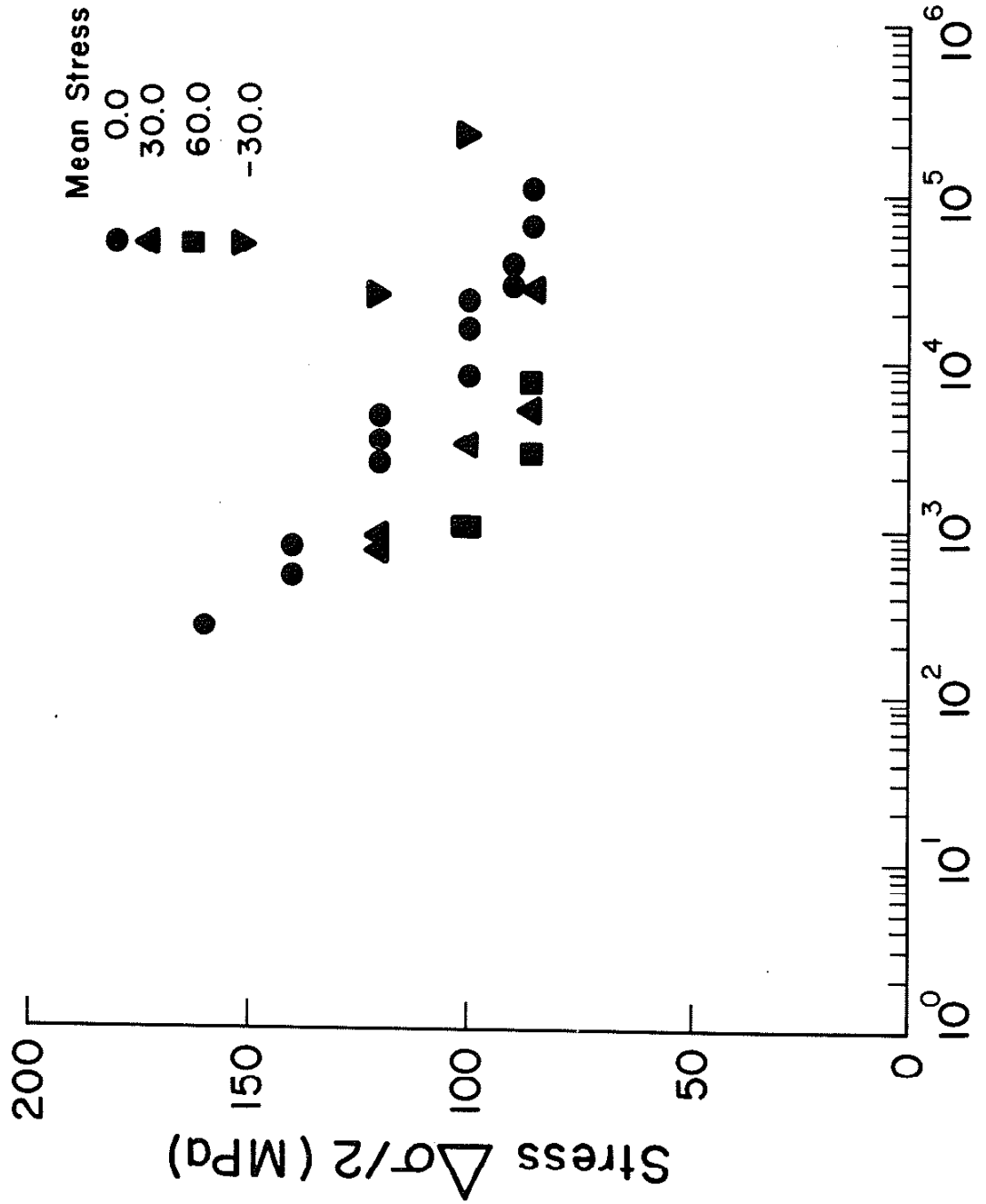

Figure 9 Cyclic Life of Load Controlled Fatigue Tests

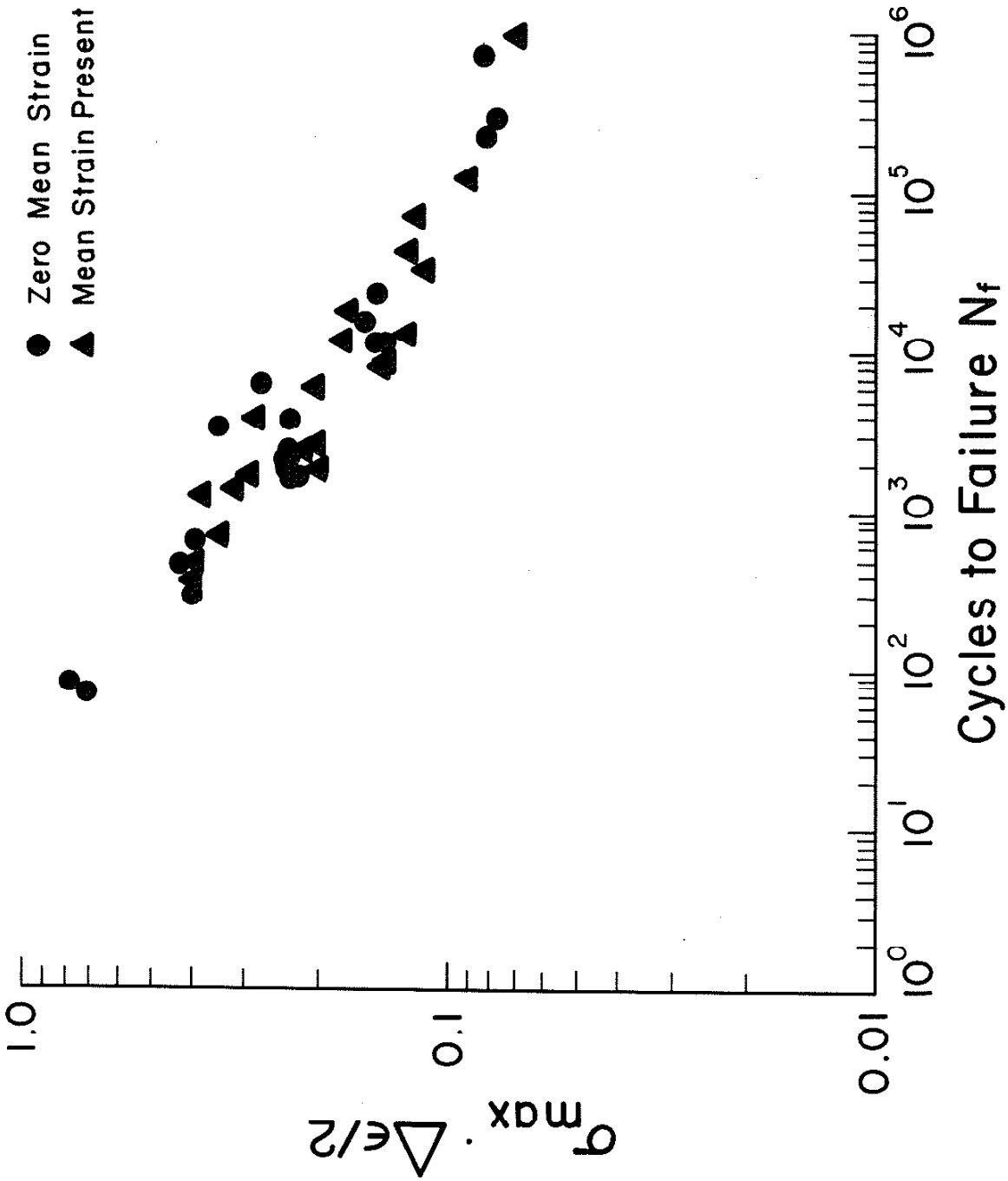

Figure 10 Results of Strain Control Fatigue presented using the SWT Parameter

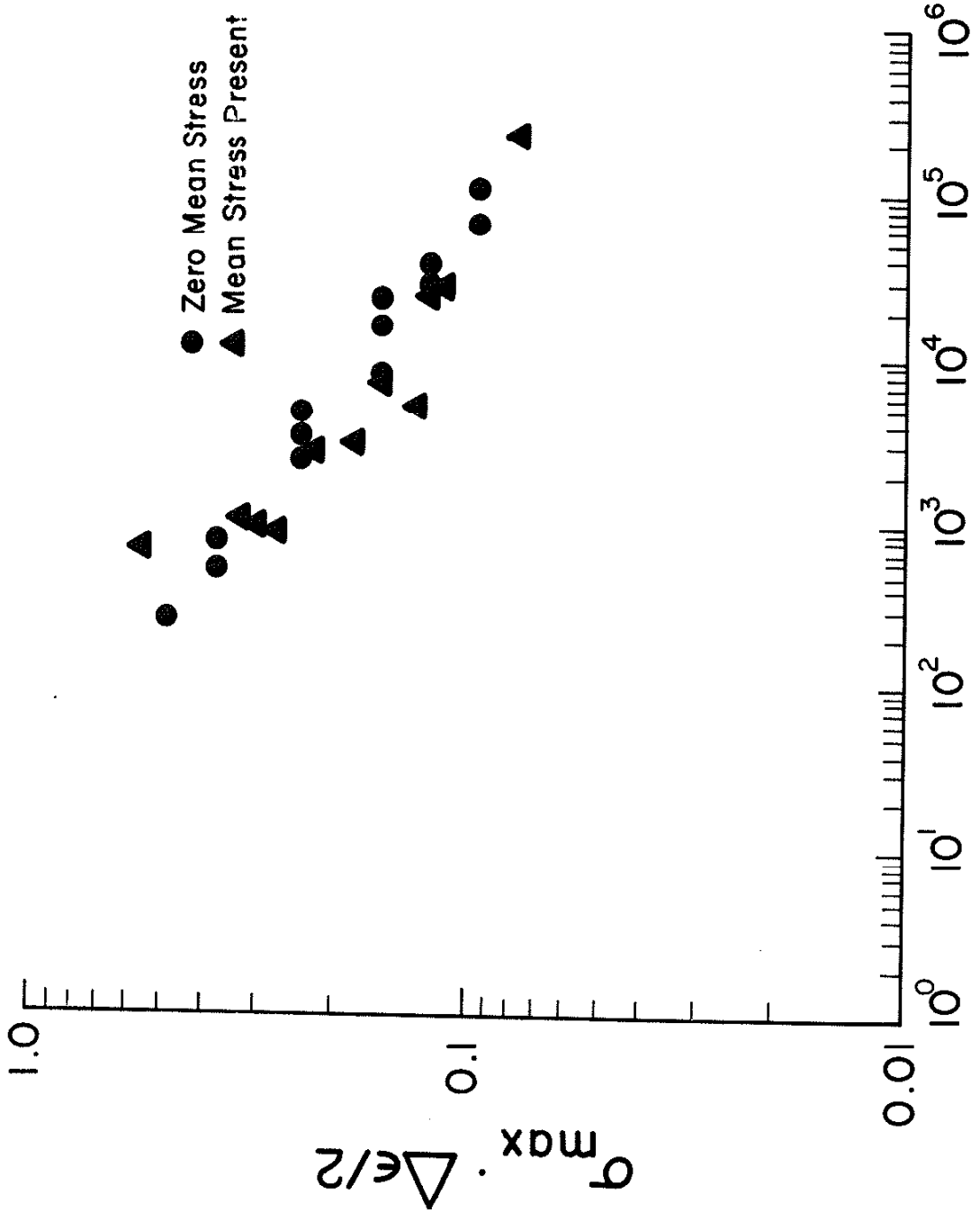

Figure 11 Results of Load Control Fatigue presented using the SWT Parameter

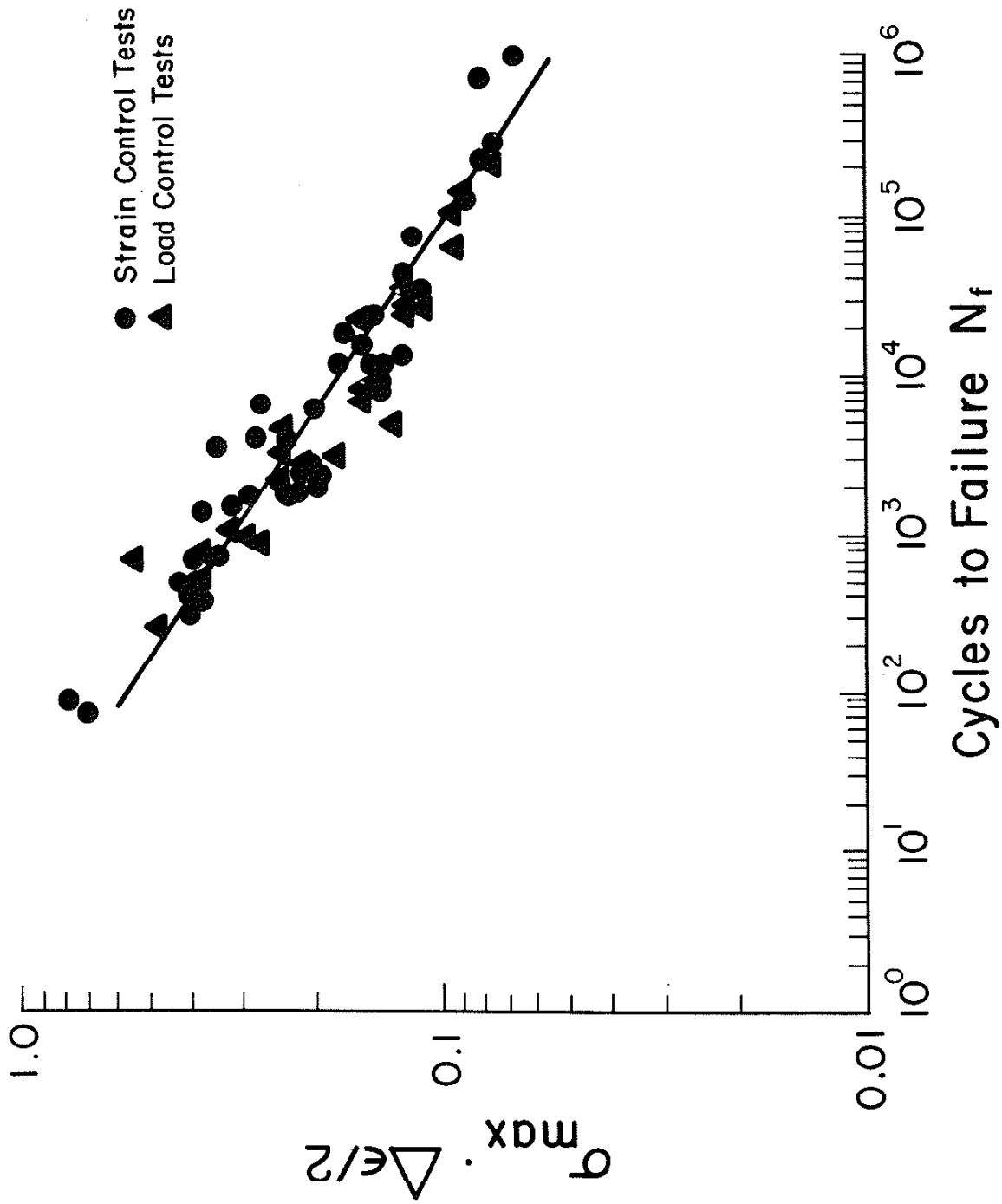

Figure 12 Results of all Fatigue Tests presented using the SWT Parameter

TABLE 1. MATERIAL CHEMISTRY

	C	Si	Mn	S	P	Ti	Ni	Cr	Mo	Cu	Sn
Pearlitic Iron	3.30	2.20	.44	.02	.01	.01	.06	.03	.01	.40	-

TABLE 2. MECHANICAL PROPERTIES

	Pearlitic
Modulus of Elasticity E (Tension/Compression) GPa	84/108
Yield Strength, .2% S_y MPa	185
Ultimate Strength (True Fracture Strength, σ_f) MPa	228
True Fracture Ductility (ϵ_f)	0.0122
Bulk Hardness	180 BHN (3000 kg)
Eutectic Cell size mm	0.14
ASTM A247 Flake Designation	∿60% Type A, ∿40% Type D
Size	4

Part III: STRESS-STRAIN SIMULATION MODEL FOR GRAY CAST IRON

S. D. Downing
D. F. Socie

Department of Mechanical and Industrial Engineering
University of Illinois at Urbana-Champaign
Urbana, IL 61801

ABSTRACT

A simple model for estimating the stress-strain response of gray cast iron subjected to variable amplitude cyclic loading is presented. Material properties for the model are readily determined from the tensile and compressive stress strain curve of the material.

the same as Martin [8], Wetzel [9], and Downing, et al [10], used to simulate the stress-strain response of wrought materials.

Extending this model to characterize a cracked body is simply a matter of adding broken bars as seen in Fig. 3. The stress-strain response of the broken elements is also elastic-perfectly plastic, except these bars cannot transmit tensile stress. Figure 4 shows the response of this system.

The model does not, however, account for the effects of graphite. These effects may be included by assuming that the unbroken elements describe the Massing part of the deformation and the broken elements describe both crack and graphite behavior. This is easily accomplished by giving the broken elements different material properties than the unbroken elements.

The properties of the unbroken elements are selected to match the tensile portion of the stress-strain curve given by Eq. (1). Properties of the broken elements are obtained by taking the difference between the absolute value of the tensile and compressive stress-strain curves and noting that these elements cannot transmit tensile stresses. This results in the following expressions for stress and strain using the subscripts u and b for unbroken and broken elements.

$$\sigma = \sigma_u + \sigma_b;$$

$$\sigma_u = E\,\varepsilon/(1 + \varepsilon);$$

$$\sigma_b = 0,\ \varepsilon \geq 0;$$

$$\sigma_b = (E\,\varepsilon/(1 - c\,\varepsilon) - (E\,\varepsilon/(1 - t\,\varepsilon),\ \varepsilon < 0 \qquad (4)$$

For cyclic deformation, the unbroken elements have all of the features normally associated with the cycle deformation of wrought materials such as material memory and Massing behavior. Broken elements are assumed to be nonlinear elastic. Computationally, the stresses are computed directly from these equations for each strain level i

$$\sigma_i = (\sigma_u)_i + (\sigma_b)_i \tag{5}$$

$$(\sigma_u)_i = (\sigma_u)_{i-1} + \Delta\sigma_u$$

$$\Delta\sigma_u = \frac{E\Delta\varepsilon}{1 + t\Delta\varepsilon/2} \cdot s$$

$$(\sigma_b)_i = 0 \text{ if } \varepsilon_i > 0$$

$$(\sigma_b)_i = \frac{E\varepsilon_i}{1 - cc_i} - \frac{E\varepsilon_i}{1 - te_i} \text{ if } \varepsilon_i < 0$$

where s is +1 for loading and -1 for unloading and $\Delta\varepsilon$ is always positive. Iterative techniques are required to solve these equations to determine the strains from a given stress history.

Material memory is implemented in a manner similar to that used in rainflow counting algorithms [11]. An example is given in the APPENDIX.

EXPERIMENTAL

Test bars, 36 mm in diameter and 200 mm in length, were cast in green sand molds to produce the pearlitic gray iron. Matrix microstructure and flake structure, classified by ASTM A247 as approximately 60 percent Type A, approximately 40 percent Type D, size 4. Test bars of the ferritic irons are cast in diameters of 36 mm and 50 mm to produce different eutectical structures. Flake structures were determined to be approximately 50 percent Type A, approximately 50 percent type D, size 5, for the iron designated "A"

and approximately 50 percent Type B, aprpoxiately 50 percent Type D, size 2, for the iron designated "B".

Material properties for Eq. 1 were detemined fom a simple tension and compression stress.

E = 120,000 MPa; t = 425; c = 120.

The modulus E is the tangent modulus through zero stress and strain. The constants t and c are the slopes of the secant modulus as a function of stress level for the tensile and comprssive stress-strain curves. See [3] for details in determining these constants.

Loading histories are shown in Fig. 5. All tests were conducted in strain control on a computer controlled servo-hydraulic testing system. A 10 mm diameter gage section specimen was used.

RESULTS AND DISCUSSION

Predicted and experimental data for the strain histories in Fig. 5 are shown in Figs. 6 through 9. Tabulated values for peak stress in MPa units are also shown in Fig. 5 . Agreement beween the experimental observations and predicted results is considered good. The maximum difference between experimental and predicted results is 40 MPa on small amplitude cycles near zero strain. Other strain histories and maximum strain amplitude were also investigated but are not reported here since the results were similar. Better agreement between prediction and experiment was found as the maximum strain amplitude decreased below 0.003 that is reported here.

The model tends to overestimate the hysteresis energy in all cases. Experimentally, the hysteresis loops are always narrower than predicted. This is due to neglecting the volume expansion of graphite during tensile loading. Including these effects would require additional material properties that are not easily determined from the tensile and compression stress-strain

curves.

An important feature not included in this model is the load drop observed during strain control cycling and strain increase observed during stress control cycling. These effects are caused by the growth of small cracks and can be included by a crack element in the bar model. Development is currently underway.

SUMMARY

A simple model for estimating the stress-strain response of gray cast iron has been presented. The model only requires that the tensile and compressive stess-strain curves of the material are known. Computational details have been peovided in the APPENDIX.

ACKNOWLEGEMENTS

Portions of this work will be submitted as part of Mr. Downing's Ph.D. thesis at the Univeristy of Illinois at Urbana-Champaign.

Financial support was provided by the Fracture Control Program. Testing was conducted in the Mateials Engineering Research Laboratory. Mr. Furman assisted in conducting the tests.

REFERENCES

1. Thum, A., and H. Ude, "Die Elastizitat und die Sahwingungsfestigkeit des Gusseinsens," Die Giesserei, Vol. 16, 1929, pp. 547-556.

2. Russell, E. S., "Finite Element Simulation of the Microstructure of Gray Cast Iron," Fracture Control Program No. 33, College of Engineering, University of Illinois at U-C, Urbana, Ill., 1979.

3. Gilbert, G. N. J., and S. D. Kemp, "Behavior of a Flake Graphite Cast Iron under Cyclic Loading in Tension," BCIRA Report 1352, 1978.

4. Gilbert, G. N. JK., "Mechanical Properties of Flake Graphite Cast Irons," Iron and Steel, Jan-Feb-March 1957.

5. Gilbert, G. N. J., and P. J. Richards, "Behavior of a Flake Graphite Cast Iron under Repeated Tensile Stress," BCIRA Report 948, 1969.

6. Gilbert, H. N. J., and S. D. Kemp, "The Cyclic Stress/Strain Properties of a Flake Graphite Cast Iron--A Progress Report," BCIRA Report 1384, 1980.

7. Newman, J. C., "Finite Element Analysis of Fatigue Crack Propagation including the Effect of Crack Closure," Ph.D. Thesis, Virginia Polytechnic Institute and State University, May 1974.

8. Martin, J. F., T. H. Topper, and G. M. Sinclair, "Computer Based Simulation of Cylic Stress-Strain Behavior with Applications to Fatigue," Materials Res. and Standards MTRSA, Vol 11, No. 2, Feb. 1971, pp. 23-29.

9. Wetzel, R. M., "A Method of Fatigue Damage Analysis," Ph.D. Thesis, Dept. of Civil Eng., University of Waterloo, Ontario, Canada, 1971.

10. Downing, S., D. Galliart, and T. Berenyi, "A Numbers Rule Fatigue Analysis Procedure for Use with a Mobile Computer," Fatigue under Complex Loading, AE6, Soc. of Automotive Engrs., 1977.

11. Downing, S., and D. F. Socie, "Simple Rainflow Counting Algorithms," Int. J. of Fatigue, Jan. 1982.

LIST OF FIGURES

Figure 1 Two-Bar Model

Figure 2 Load-Deflection Response of Two-Bar Model

Figure 3 Bar Model with Broken Elements

Figure 4 Load-Deflection Response of Bar Model with Broken Elements

Figure 5 Strain Histories A, B, C, and D

Figure 6 Experimental and Predicted Stress-Strain Response for History A

Figure 7 Experimental and Predicted Stress-Strain Response for History B

Figure 8 Experimental and Predicted Stress-Strain Response for History C

Figure 9 Experimental and Predicted Stress-Strain Response for History D

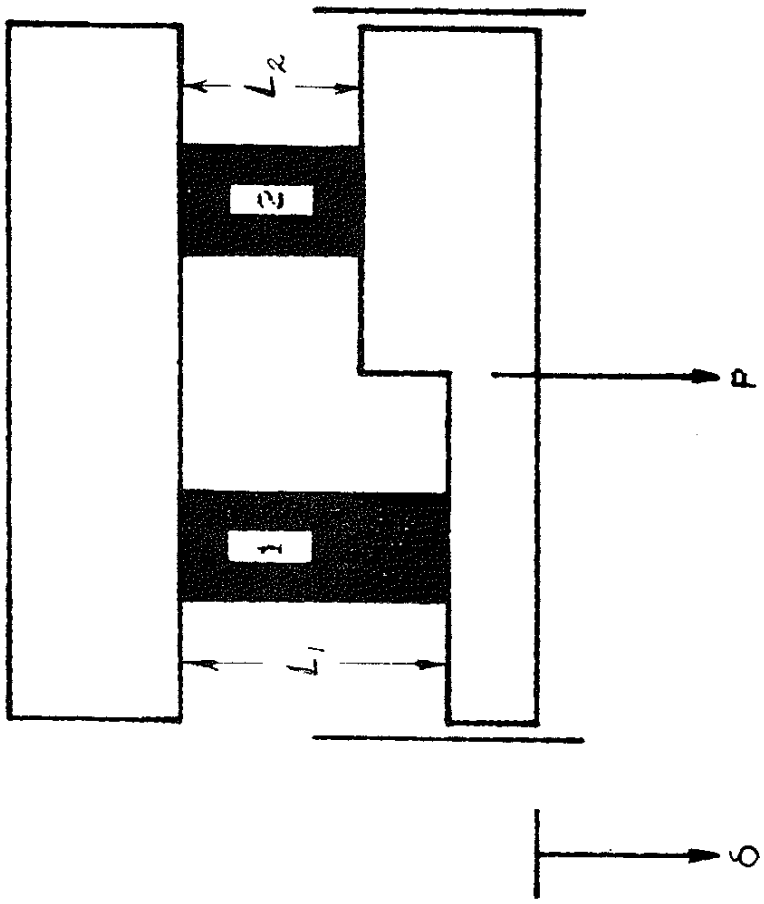

Figure 1 Two-Bar Model

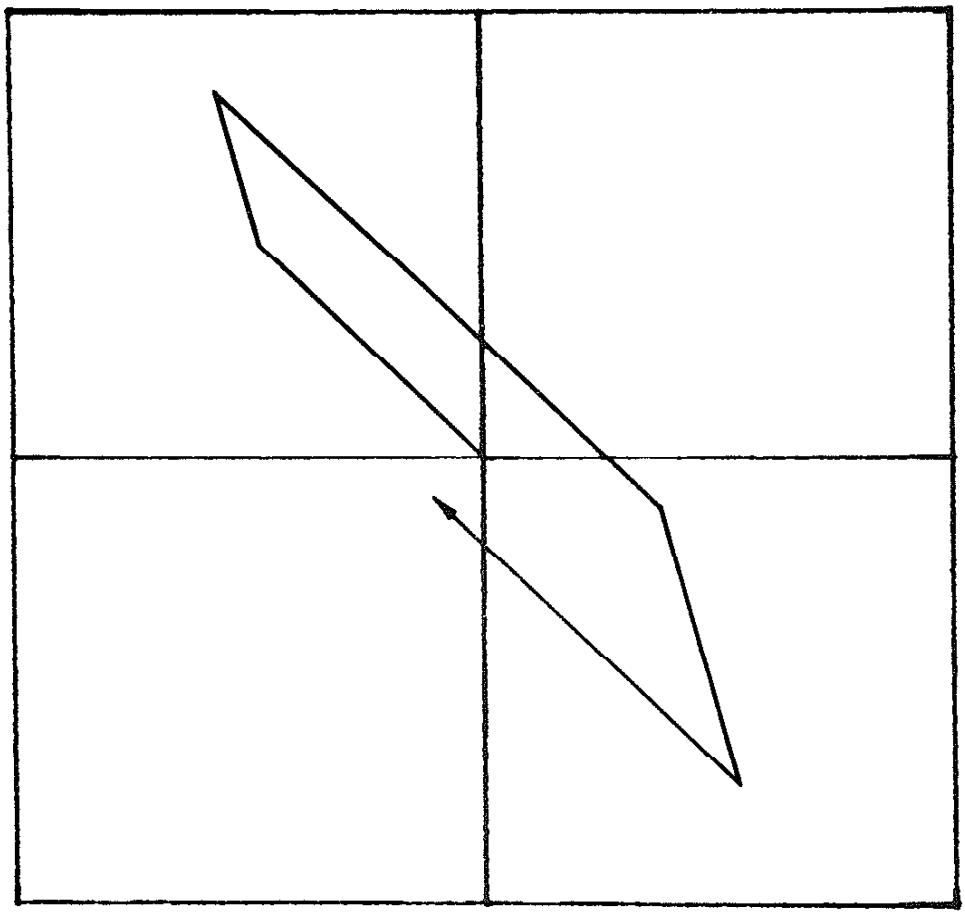

Figure 2 Load-Deflection Response of Two-Bar Model

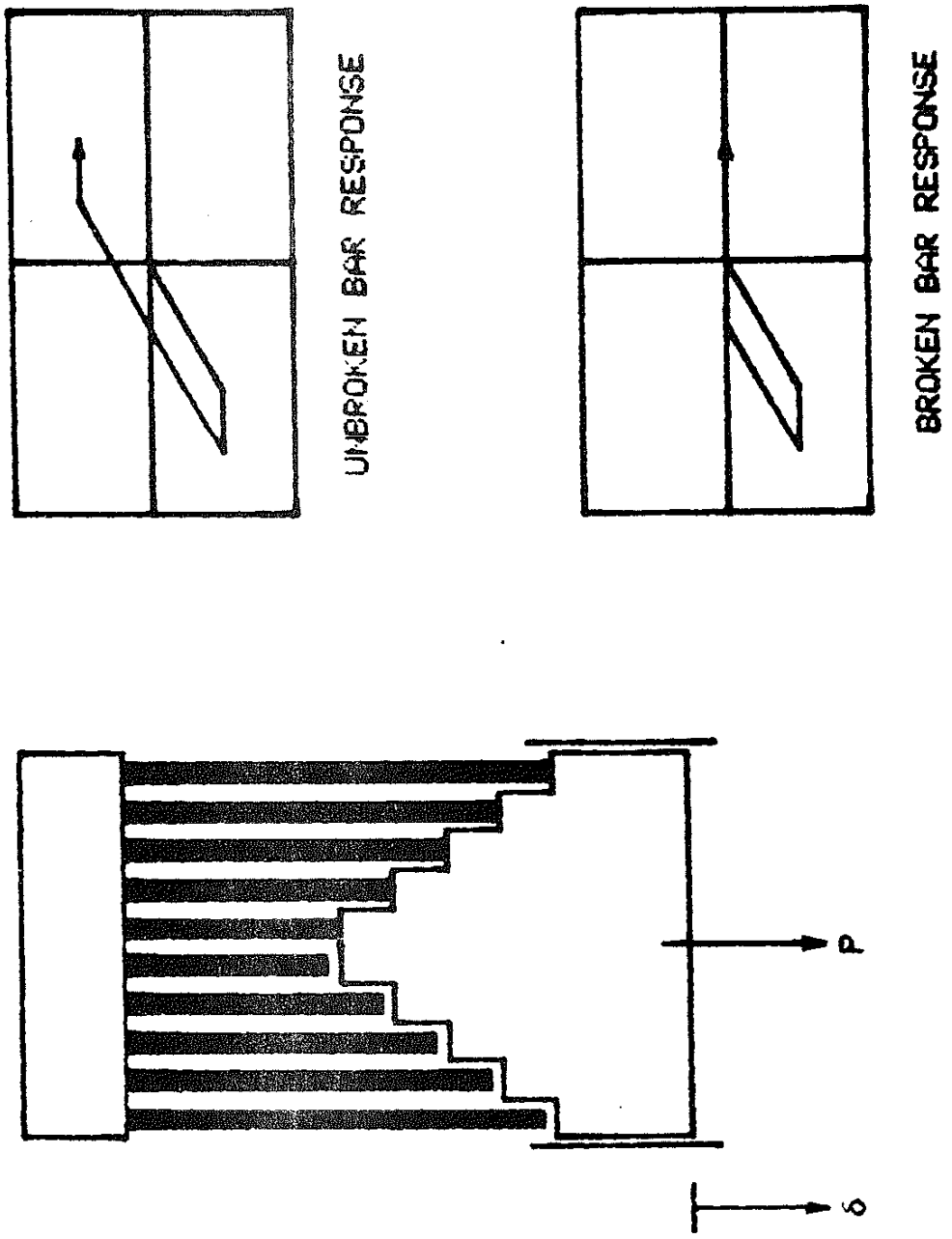

Figure 3 Bar Model with Broken Elements

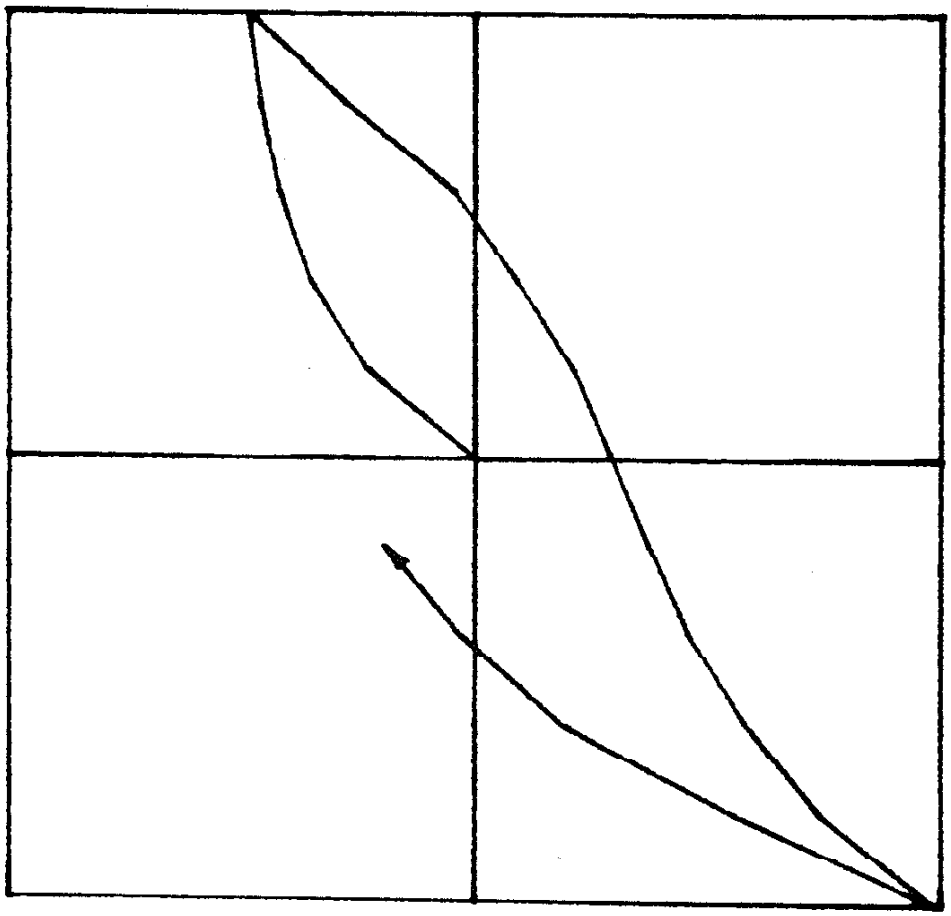

Figure 4 Load-Deflection Response of Bar Model with Broken Elements

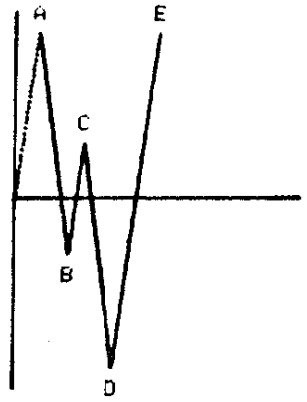

	STRAIN	ACTUAL STRESS	PRED STRESS
A	.0031	165	161
B	-.0010	-140	-125
C	.0010	59	66
D	-.0031	-275	-271
E	.0031	165	161

STRAIN HISTORY 'A'

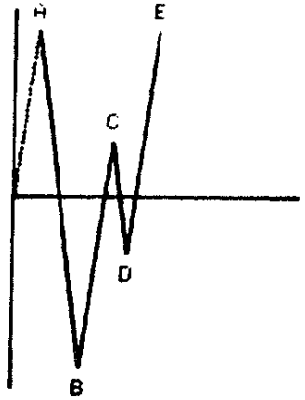

	STRAIN	ACTUAL STRESS	PRED STRESS
A	.0031	181	161
B	-.0031	-291	-271
C	.0010	97	102
D	-.0010	-91	-89
E	.0031	181	161

STRAIN HISTORY 'B'

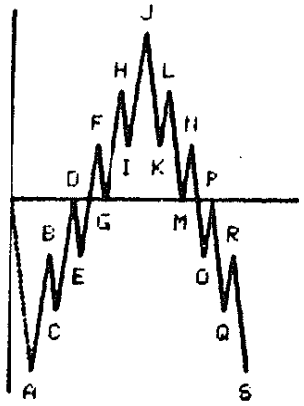

	STRAIN	ACTUAL STRESS	PRED STRESS
A	-.0031	-275	-271
B	-.0010	-49	-9
C	-.0020	-160	-149
D	.0	34	64
E	-.0010	-66	-58
F	.0010	93	102
G	.0	22	3
H	.0020	139	133
I	.0010	59	34
J	.0031	166	161
K	.0010	19	-14
L	.0020	97	85
M	.0	-45	-64
N	.0010	39	35
O	-.0010	-114	-125
P	.0	-15	-3
Q	-.0020	-196	-197
R	-.0010	-82	-57
S	-.0031	-275	-271

STRAIN HISTORY 'C'

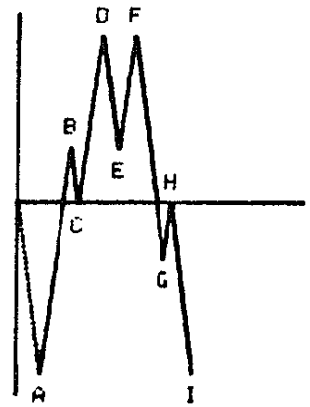

	STRAIN	ACTUAL STRESS	PRED STRESS
A	-.0031	-288	-271
B	.0010	102	102
C	.0	11	3
D	.0031	178	161
E	.0010	23	-14
F	.0031	178	161
G	-.0010	-123	-125
H	.0	-17	-3
I	-.0031	-288	-271

STRAIN HISTORY 'D'

Figure 5 Strain Histories A, B, C, and D

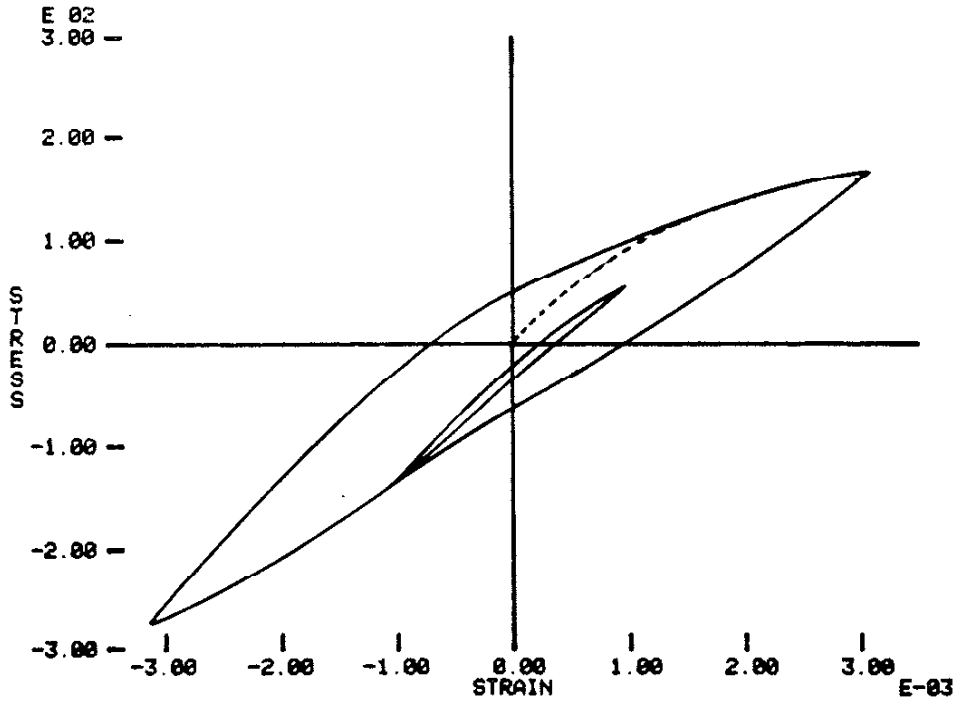

ACTUAL RESPONSE

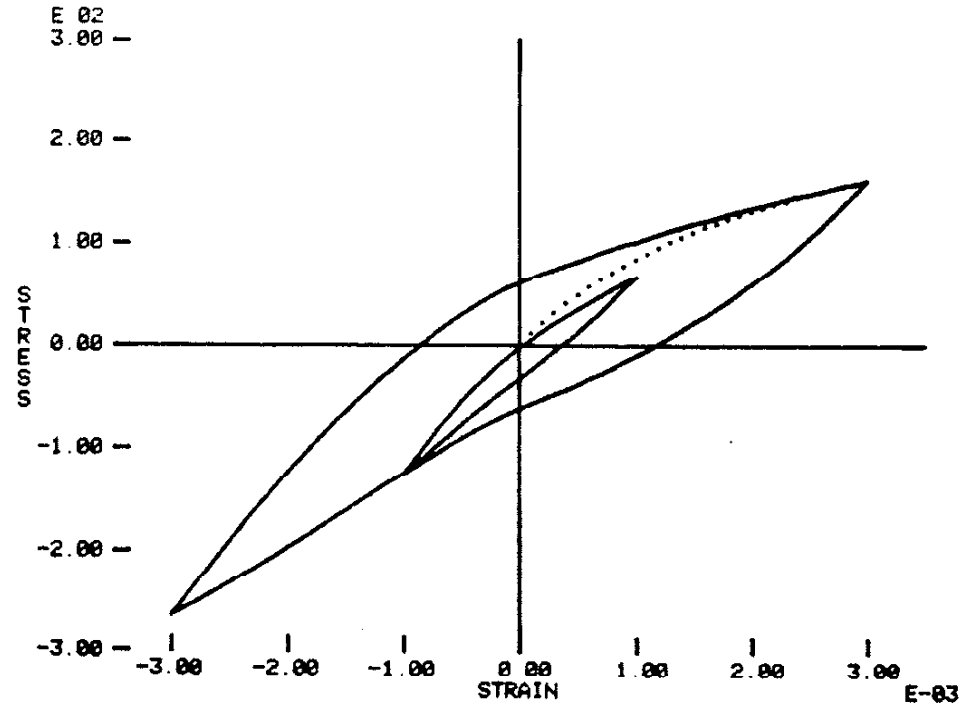

PREDICTED RESPONSE

Figure 6 Experimental and Predicted Stress-Strain Response for History A

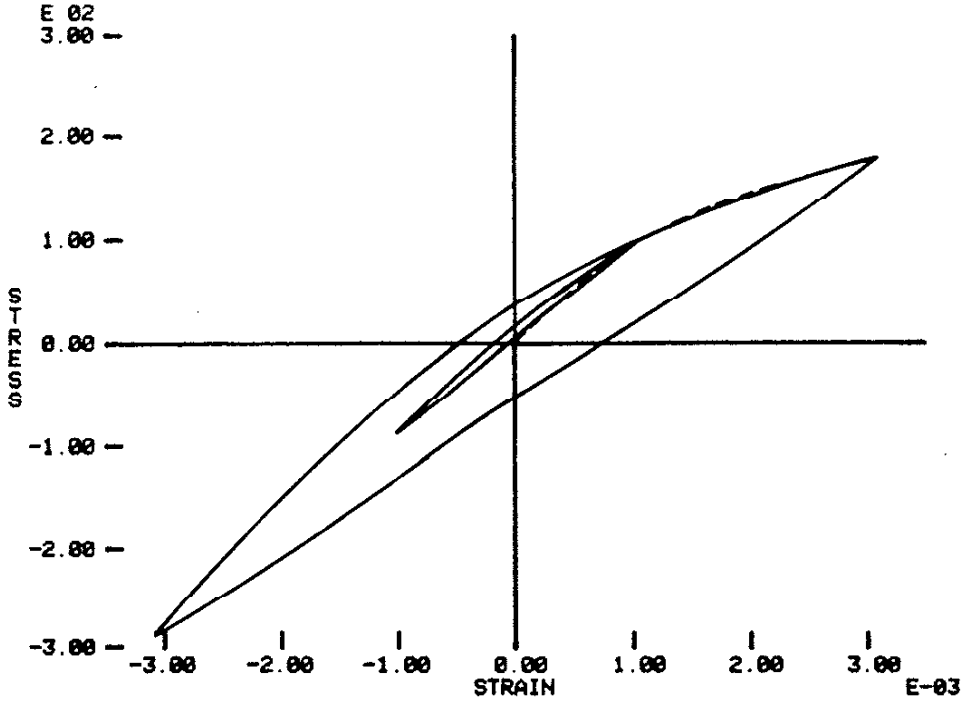

ACTUAL RESPONSE

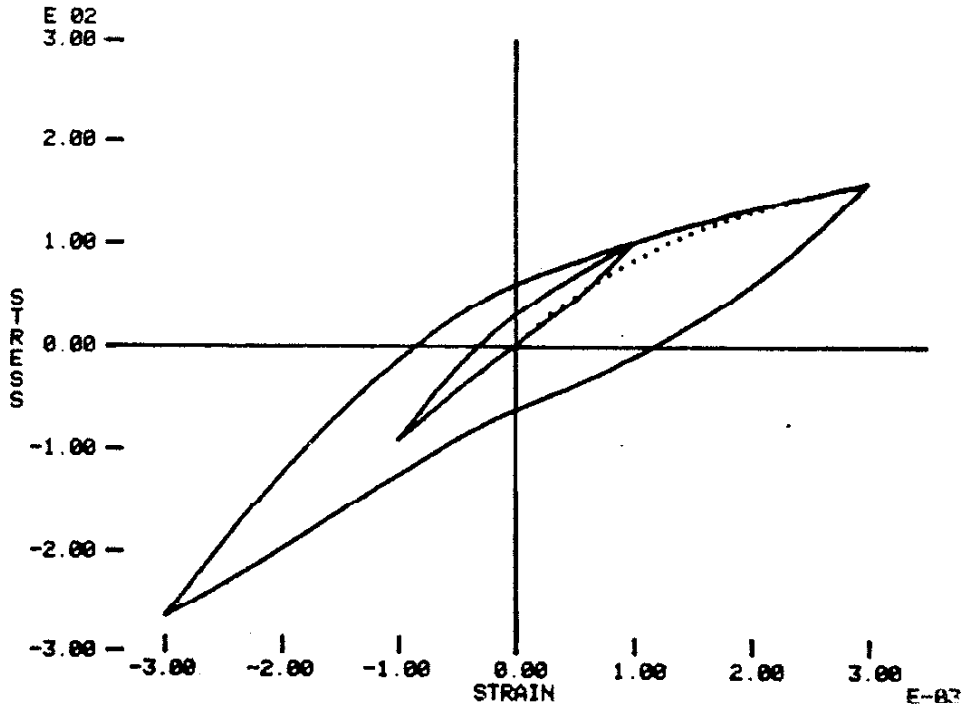

PREDICTED RESPONSE

Figure 7 Experimental and Predicted Stress-Strain Response for History B

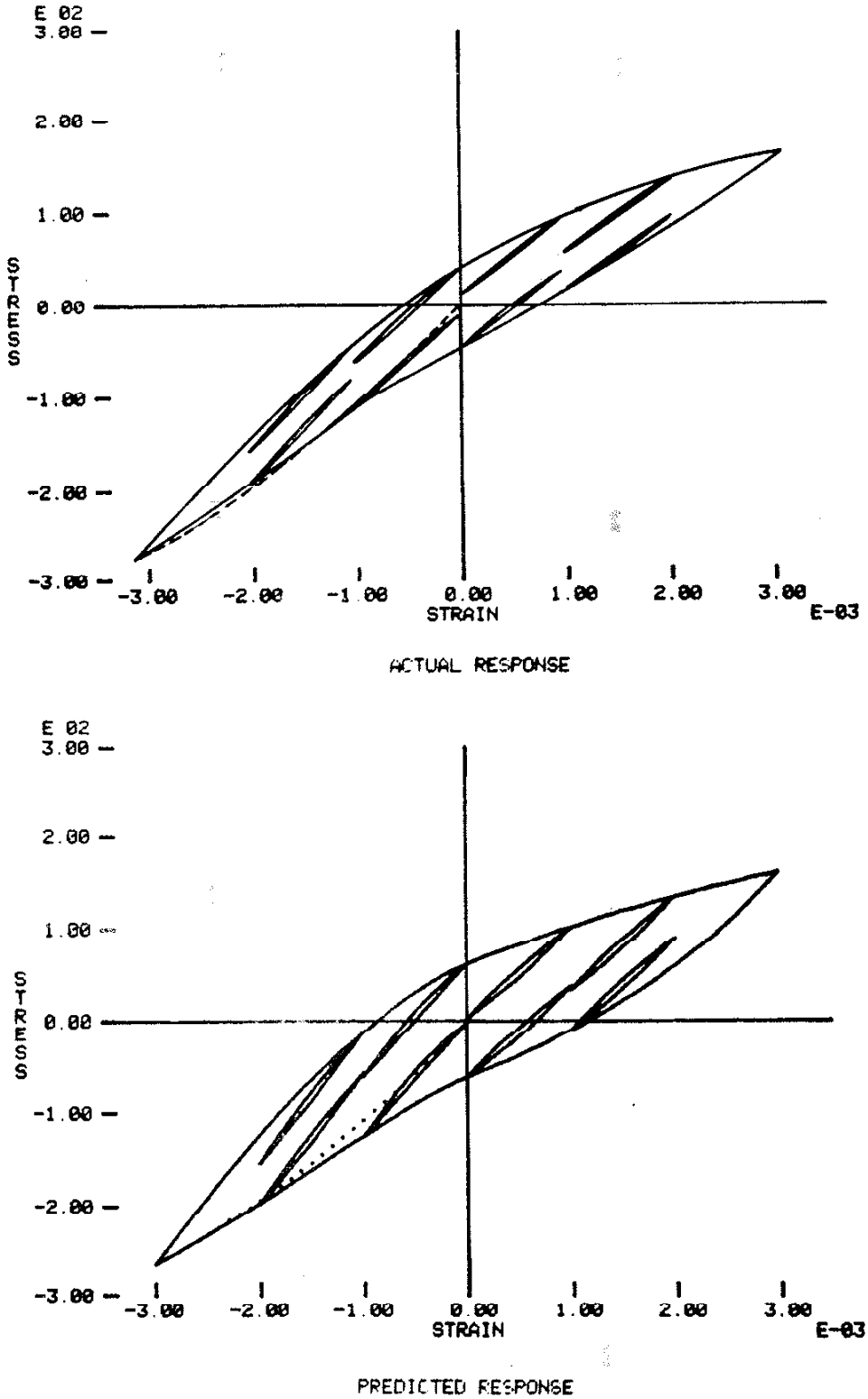

Figure 8 Experimental and Predicted Stress-Strain Response for History C

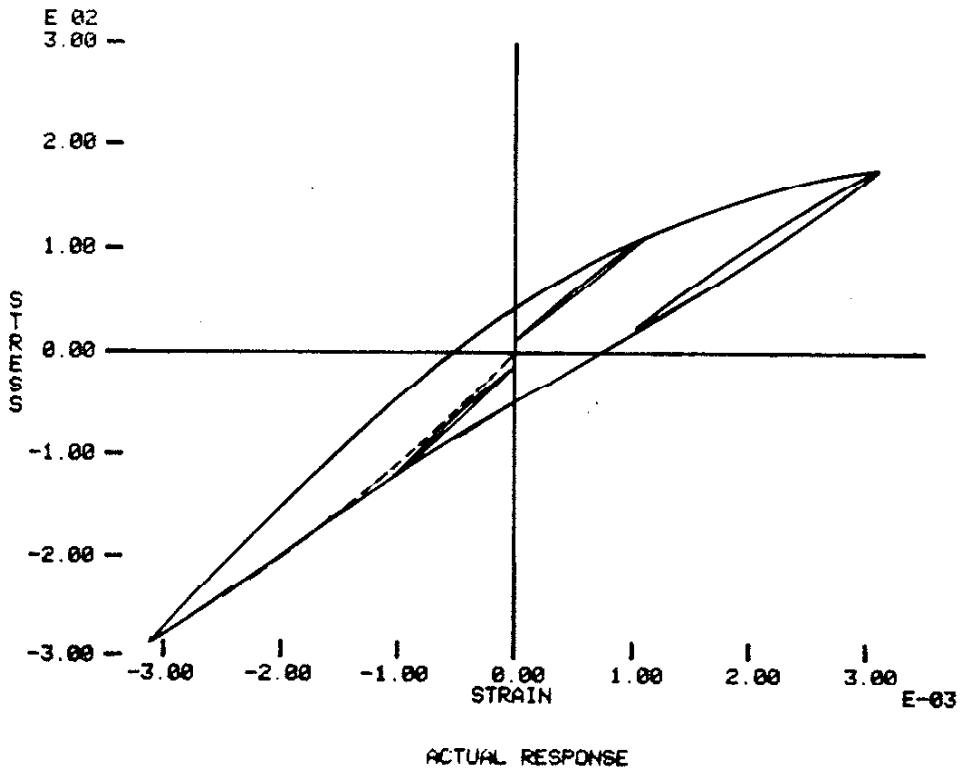

Figure 9 Experimental and Predicted Stress-Strain Response for History D

APPENDIX--SAMPLE CALCULATIONS

Strain History A (Fig. 5) will be used in the sample calculations which follow.

Initial Loading (OA) - The initial loading path for this history must be the monotonic tension curve which is defined by the unbroken elements since the broken elements cannot transmit tensile stress. Therefore, the stress in the unbroken elements at point A is given by:

$$(\sigma_u)_A = \frac{E\varepsilon_A}{1 + 1\,t\,\varepsilon_A}$$

$$= 161 \text{ MPa}$$

for the broken elements at point A

$$(\sigma_b)_A = 0$$

hence

$$\sigma_A = (\sigma_u)_A + (\sigma_b)_A$$

$$= 161 \text{ MPa.}$$

Unloading (AB)-The strain range between points A and B is

$$\Delta\varepsilon = |\varepsilon_B - \varepsilon_A|$$

$$= 0.0041$$

The unbroken elements follow a loading path defined by the following equations

$$\Delta\sigma_u = \frac{E\Delta\varepsilon}{1 + \frac{t\Delta\varepsilon}{2}} \cdot s \qquad (s = -1, \text{ unloading})$$

$= -263$ MPa

The stress on the unbroken at point B elements is

$$(\sigma_u)_B = (\sigma_u)_A + \Delta\sigma_u$$

$$= 161 - 263$$

$$= -102 \text{ MPa.}$$

The stress in the broken element at point B is

$$(\sigma_b)_B = \frac{E\varepsilon_B}{1-c\varepsilon_B} - \frac{E\varepsilon_B}{1-t\varepsilon_B} \quad (\varepsilon_B < 0)$$

$$= -23 \text{ MPa.}$$

Therefore,

$$\sigma_B = (\sigma_u)_B + (\sigma_b)_B$$

$$= -102 - 23$$

$$= -125 \text{ MPa.}$$

Loading (BC)

The strain range is for loading BC is

$$\Delta\varepsilon = |\varepsilon_C - \varepsilon_B)$$

$$= 0.002$$

The corresponding stress range of the unbroken elements is

$$\Delta\sigma_u = \frac{E\Delta\varepsilon}{1 + \frac{t\Delta\varepsilon}{2}} \cdot s \qquad (s = 1, \text{ loading})$$

168 MPa.

Thus, at point C

$$(\sigma_u)_C = (\sigma_u)_B + \Delta\sigma_u$$
$$= 66 \text{ MPa.}$$

For the broken elements

$$(\sigma_b)_C = 0 \qquad (\varepsilon_C > 0).$$

The total stress at point C is given by

$$\sigma_D = (\sigma_u)_D + (\sigma_b)_C$$
$$= 66 + 0$$
$$= 66 \text{ MPa.}$$

Unloading (CD)--As mentioned previously, the unbroken elements obey the same rules for material memory as any wrought material. Thus, a closed hysteresis loop would be found between points B and C. The stress and strain at point D would then be referenced to point A not point C. Therefore the strain range is defined as

$$\Delta\varepsilon = |\varepsilon_D - \varepsilon_A|$$
$$= 0.0062.$$

The unbroken element stress range is

$$\Delta\sigma_u = \frac{E\varepsilon\varepsilon}{1 + \frac{t\Delta\varepsilon}{2}} \cdot s \qquad (s = -1, \text{ unloading})$$

$= -321$ MPa.

And at point D

$$(\sigma_u)_D = (\sigma_u)_A + \Delta\sigma$$
$$= 161 - 321$$
$$= -160 \text{ MPa.}$$

Since the strain at point D is negative, the broken element stress is given by

$$(\sigma_b)_D = \frac{E\varepsilon_D}{1 - c\varepsilon_D} - \frac{E\varepsilon_D}{1 - t\varepsilon_D} \quad (\varepsilon_D < 0)$$

$$= -111 \text{ MPa.}$$

This gives a total stress

$$\sigma_D = (\sigma_u)_D + (\sigma_b)_D$$
$$= 160 - 111$$
$$= -271 \text{ MPa.}$$

Loading (DE)-The strain range is defined as follows

$$\Delta\varepsilon = |\varepsilon_E - \varepsilon_D|$$
$$= 0.0062.$$

The unbroken element stress range is

$$\Delta\sigma_u = \frac{E\Delta\varepsilon}{1 + \frac{t\Delta\varepsilon}{2}} \cdot s \quad (s = 1, \text{ loading})$$

$$= 321 \text{ MPa.}$$

$$(\sigma_u)_E = (\sigma_u)_D + \Delta\sigma_u$$
$$= -160 + 321$$
$$= 161$$

And

$$\sigma_b = 0$$
$$\sigma_E = (\sigma_u)_E + (\sigma_b)_E$$
$$= 161 + 0$$
$$= 161 \text{ MPa}$$

Part IV: FATIGUE BEHAVIOUR OF AS-CAST AND HEAT TREATED GRAY IRON

D. F. Socie

Department of Mechanical and Industrial Engineering
University of Illinois at Urbana-Champaign
Urbana, IL 61801

ABSTRACT

Fatigue behavior of gray iron in the as-cast and heat-treated condition was investigated. Hardened specimens exhibit better fatigue resistance in both stress and strain controlled testing. The Smith-Watson Topper parameter $\sigma_{max}(\Delta\varepsilon/2)$ provided a good correlation for both load and strain controlled tests.

INTRODUCTION

Mitchell [1] investigated the effects of matrix microstructure and the size and shape of the free graphite on fatigue resistance of cast irons. Decreasing the notch severity of the free graphite phase improved the fatigue behavior. In gray iron, this is accomplished by decreasing the graphite flake size. Fatigue data reported by Mitchell (see Fig. 1) shows the effects of changing matrix microstructure and hardness. These data suggest that increasing the matrix hardness will show some improvement in strain controlled fatigue resistance. Tucker and Olberts [2] show that increased strength improves fatigue resistance during stress controlled testing.

The purpose of this investigation is to compare as-cast and hardened gray iron and quantify the effect of heat treating. No attempt is made to achieve the optimum heat treatment.

Material

Materials tested in this investigation were provided by Deere and Company. Test bars, 36 mm in diameter and 200 mm long, were cast in green sand molds to produce pearlitic gray iron. The chemistry is given in Table 1.

Twenty-five test bars were heat treated by austenized at 850°C for one hour and quenched into hot oil at 200°C. They were then tempered for 8 hours at 200°C. This procedure was used to prevent matrix cracking during quenching.

Metallographic examination was performed by Deere and Company. A summary of the microstructural data is shown in Table 2. Details of the microstructure are shown in Figs. 2, 3, and 4.

Tensile and compression tests were performed on each material. Stress-strain curves are shown in Figs. 5 and 6 and the mechanical properties summarized in Table 3.

Fatigue tests were performed in both stress and strain control using the specimen shown in Fig. 7. The heat treatment was done before the specimens were machined.

Results and Discussion

The strain life behavior of both as-cast and hardened gray iron are shown in Fig. 8. The fatigue life has been improved by a factor of 10. Similar behavior is also obtained for stress controlled testing, Fig. 9.

The data have also been correlated in terms of the Smith-Watson type parameter, $\sigma_{max}(\Delta\varepsilon/2)$, for both irons (see Fig. 10). This parameter correlates both stress and strain controlled tests. It provides a better method of comparison between the two materials than either stress or strain alone. In notched members, the product of stress and strain is the controlling parameter. The as-cast iron data can be fitted with the following relationship;

$$\sigma_{max}\,\frac{\Delta\varepsilon}{2} = 2.74\ (N_f)^{-.225}$$

and the hardened iron data to

$$\sigma_{max}\,\frac{\Delta\varepsilon}{2} = 3.48\ (n_f)^{-.342}.$$

Data for two heats of similar composition and structure are shown in Fig. 12. Data from heat A are obtained from Ref. [3]. Heat B is from this investigation.

SUMMARY

Considerable increases in the fatigue properties of gray iron can be obtained by heat treating. The Smith-Watson type parameter provides a method for correlating both stress and strain controlled testing.

ACKNOWLEDGEMENT

The testing was performed by Ms. Calhoun and Mr. Furman.

REFERENCES

1. Mitchell, M. R., "Effects of Graphite Morphology, Matrix Hardness and Structure on the Fatigue Resistance of Gray Cast Iron," Society of Automotive Engineers, Inc., Report No. 750198 (1975).

2. Tucker, L. E., and Olberts, D. R., "Fatigue Properties of Gray Cast Iron," Society of Automotive Engineers, Inc., Report No. 690471 (1969).

3. Fash, J. W., and D. C. Socie, "Mean Stress Effects in Gray Iron,"

LIST OF TABLES

1. Chemical Composition

2. Microstructural Data

3. Mechanical Properties

Table I Chemical Composition

Element	No.1	No.2	No.7C	No.5C
C	3.20	3.20	3.19	3.28
Si	2.01	2.05	2.13	2.09
P	.014	.013	.010	.015
S	.023	.022	.018	.023
Mn	.48	.47	.49	.49
Ni	.10	.10	.09	.10
Cr	.07	.07	.07	.07
Mo	.007	.006	.004	.008
Cu	.15	.15	.15	.16
Al	.005	.005	.007	.005
Sn	.012	.012	.010	.012
Ti	.013	.012	.013	.013
Pb*	Nil	Nil	.003	Nil
Te*	Nil	Nil	Nil	Nil
V	.002	.002	.003	.002
Mg	Nil	Nil	.001	Nil
N, parts/million	95	108	87	104

*Marginal confidence in data.

Table 2 Hardness and Microstructure Data

Test Bar No.	Hardened?	Composite Hardness* Brinell Tests, BHN	Composite Hardness* Rockwell B&C Tests, Equiv. BHN	Matrix Hardness Equiv. Rockwell**	Microstructure Graphite Type	Graphite Size	Matrix
7C	No	159	153-156	B93-C27 (Ten tests averaging B97.5)	90-95% A 5-10% D	3,4 7	Moderately coarse to very coarse lamellar pearlite with 5-7% free ferrite
15C	No	183	165-171	B92-C28 (Ten tests averaging B98)	90-95% A 5-10% D	3,4 7	Moderately coarse to very coarse lamellar pearlite with 5-7% free ferrite
1	Yes	311	290-297	Martensite: C58.5-61.5 Pearlite and ferrite: C40-41.5 (three tests on each structure)	95% 5% D	3,4 7	14-50% lightly tempered, or untempered martensite; balance fine pearlite with grain boundary ferrite (most martensite near surface)
2	Yes	375	332-342	Martensite: C59.5-61.5 Martensite, pearlite and ferrite: C44.5-46.5 (Three tests on each structure)	90% A 10% D	3,4 7	40-60% lightly tempered, or untempered martensite; balance a mixture of martensite, fine pearlite and ferrite (structure is patchy but no apparent gradient)

*Brinell test made on ground flat on larger diameter of bar. Rockwell tests made on cut end in, or near, gauge length.

**Converted from 100 gram Knoop tests.

Table 3 Mechancial Properties

	AS-CAST		HEAT TREATED
Elastic Modules	103 Gpa		94 GPa
Yield Strength	180 Mpa		240 MPa
Ultimate Strength	230 Mpa		370 MPa
Fracture Strain	0.0088		0.0082
Bernell Hardness	180	400	

LIST OF FIGURES

1. Effect of Matrix Microstructure and Hardness of the Fatigue of Gray Irons
2. Microstructure of As-Cast Iron
3. Microstructure of Heat Treated Iron, Bar 1
4. Microstructure of Heat Treated Iron, Bar 2
5. Stress-Strain Curve for As-Cast Iron
6. Stress-Strain Curve for Heat Treated Iron
7. Fatigue Test Specimen
8. Strain Life Data for As-Cast and Heat Treated Irons
9. Stress Life Data for As-Cast and Heat Treated Irons
10. Smith-Watson-Topper parameter for As-Cast and Heat Treated Irons
11. Strain-Life Data for Two Heats of As-Cast Iron

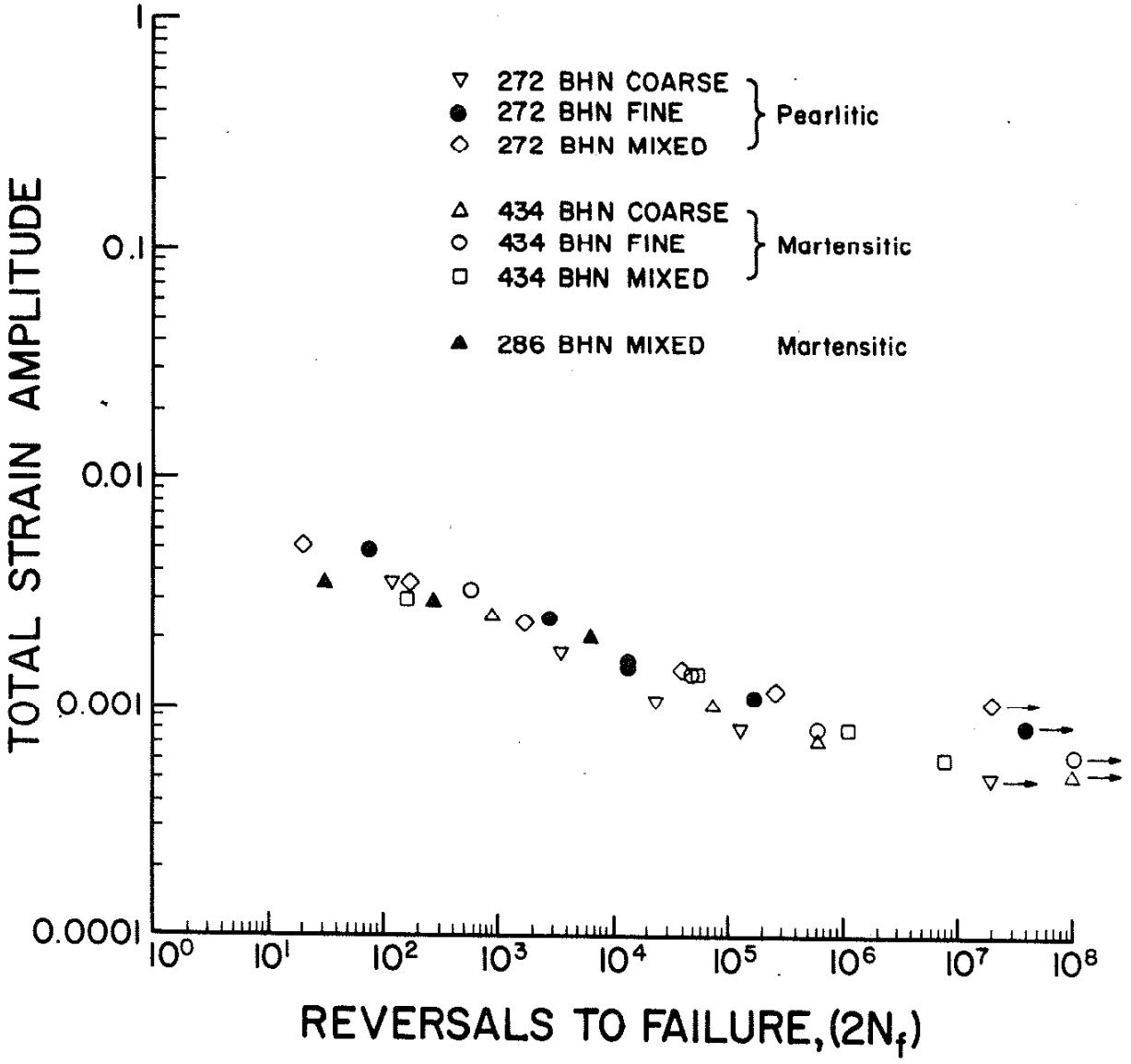

1. Effect of Matrix Microstructure and Hardness of the Fatigue of Gray Irons

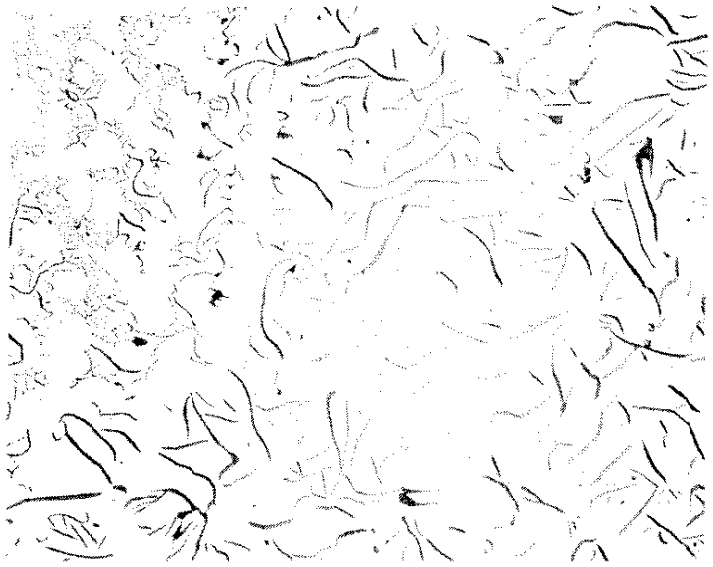

BAR 7C; NOT HARDENED; 100X; UNETCHED

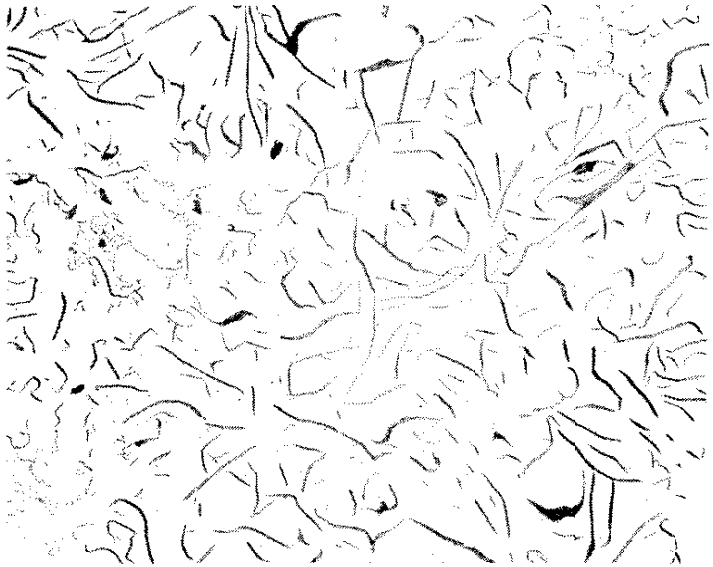

BAR 15C; NOT HARDENED; 100X; UNETCHED

BAR 7C; NOT HARDENED; 200X; PICRAL ETCH

BAR 15C; HARDENED; 200X; PICRAL ETCH

2. Microstructure of As-Cast Iron

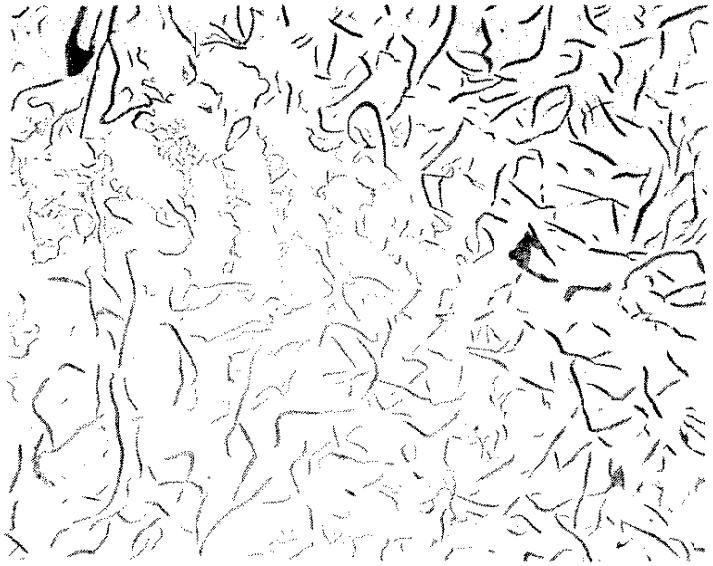

100X; UNETCHED

Bar No. 1; Hardened

The light gray areas below are martensite having a hardness of approximately Rockwell C60 and the darker areas are a mixture of fine pearlite and ferrite having a hardness of approximately Rockwell C40 (see data).

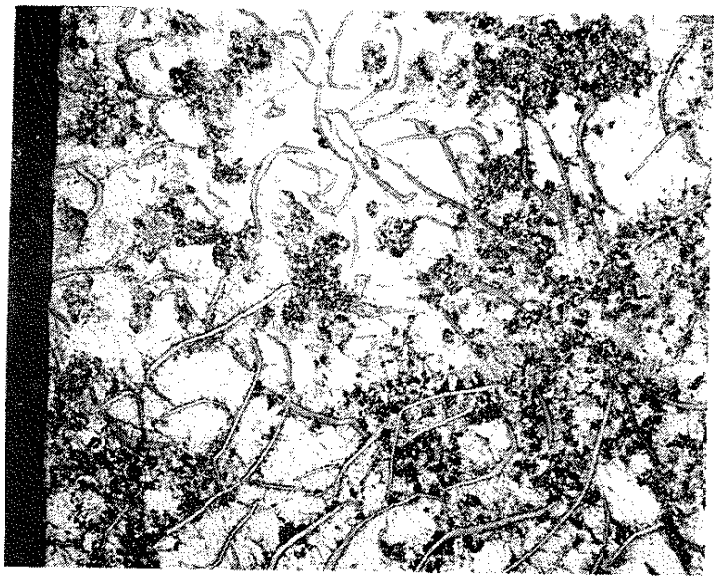

GAGE LENGTH SURFACE; 200X; PICRAL ETCH

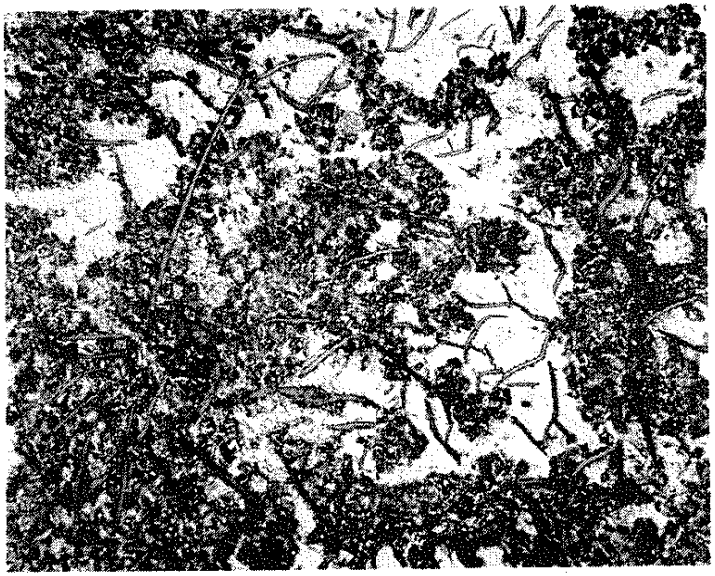

NEAR CENTER OF SECTION; 200X; PICRAL ETCH

3. Microstructure of Heat Treated Iron, Bar 1

100X; UNETCHED

Bar No. 2; Hardened

The light gray areas below are martensite having a hardness of approximately Rockwell C60. The darker gray areas are a mixture of martensite and ferrite and also a small amount of fine pearlite (darkest areas) near the center of the section. Hardness of these areas is approximately Rockwell C45 (see data).

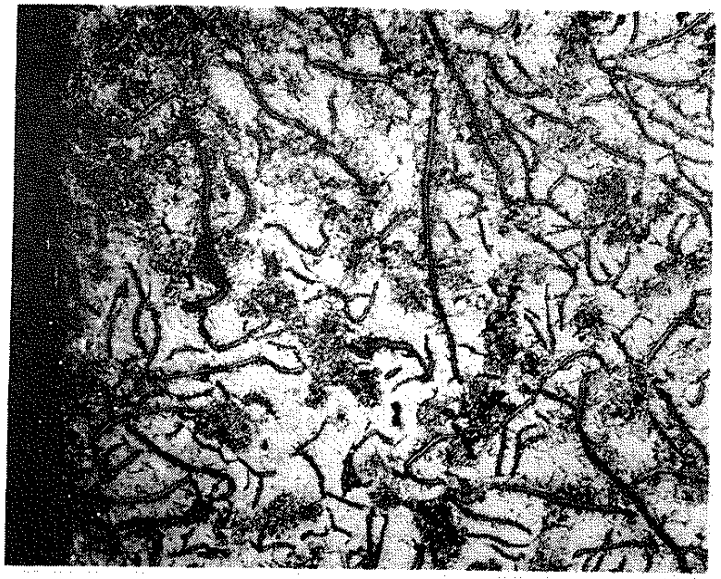

GAGE LENGTH SURFACE; 200X; PICRAL ETCH

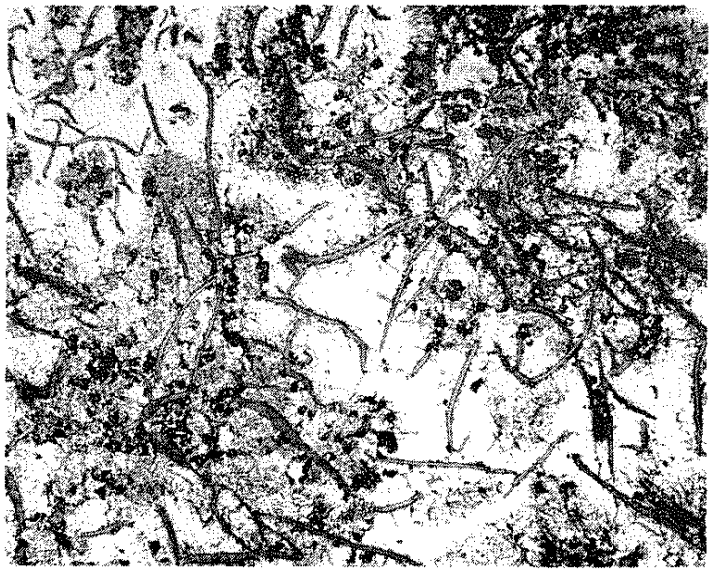

NEAR CENTER OF SECTION; 200X; PICRAL ETCH

4. Microstructure of Heat Treated Iron, Bar 2

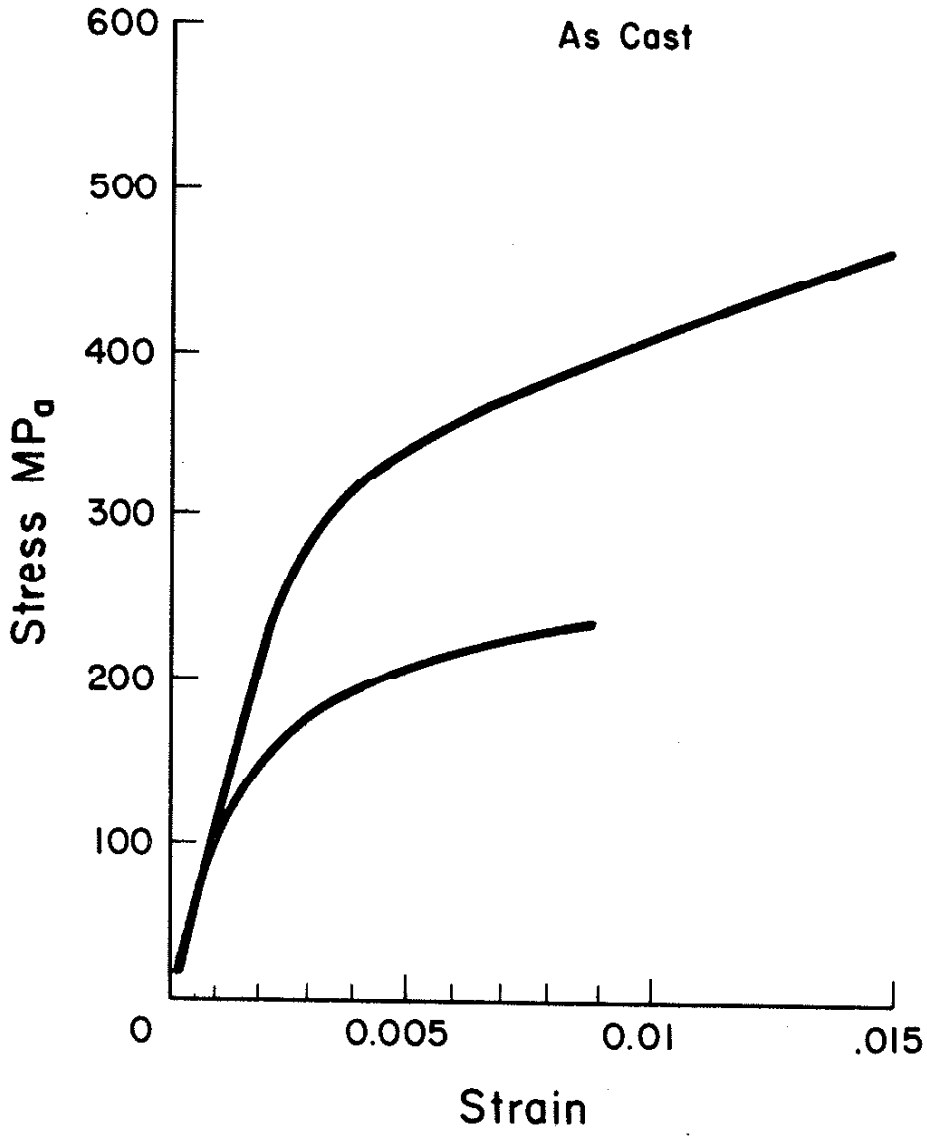

5. Stress-Strain Curve for As-Cast Iron

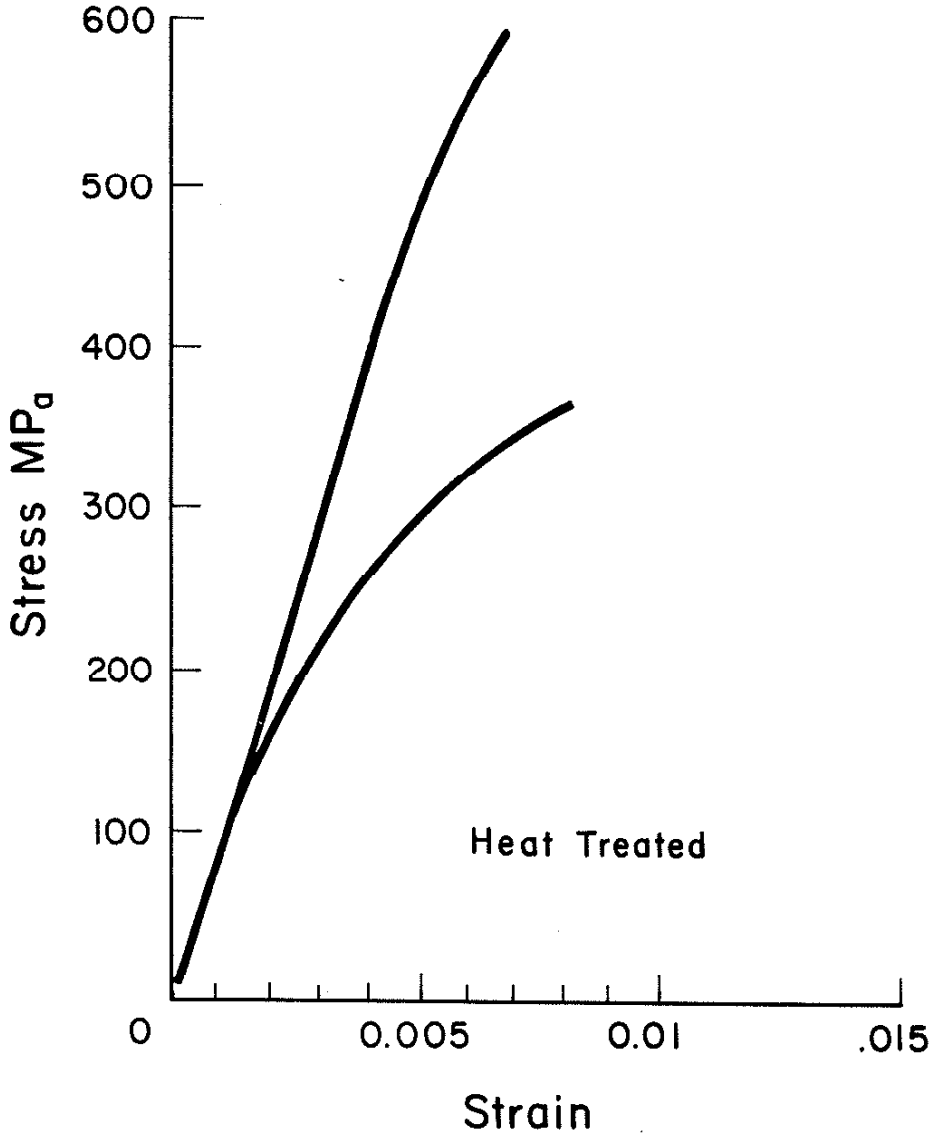

6. Stress-Strain Curve for Heat Treated Iron

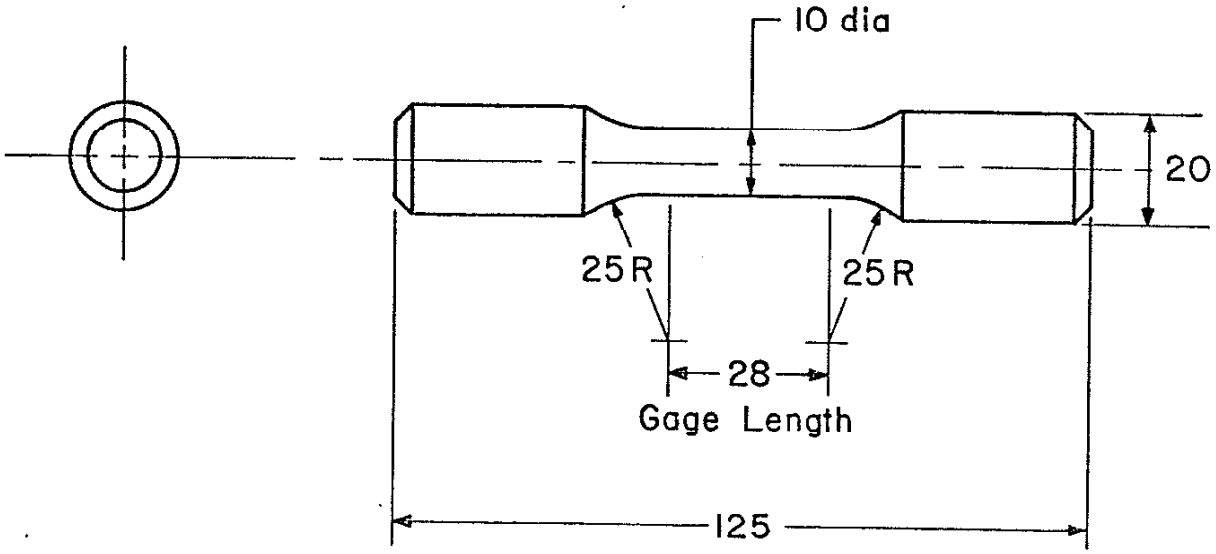

7. Fatigue Test Specimen

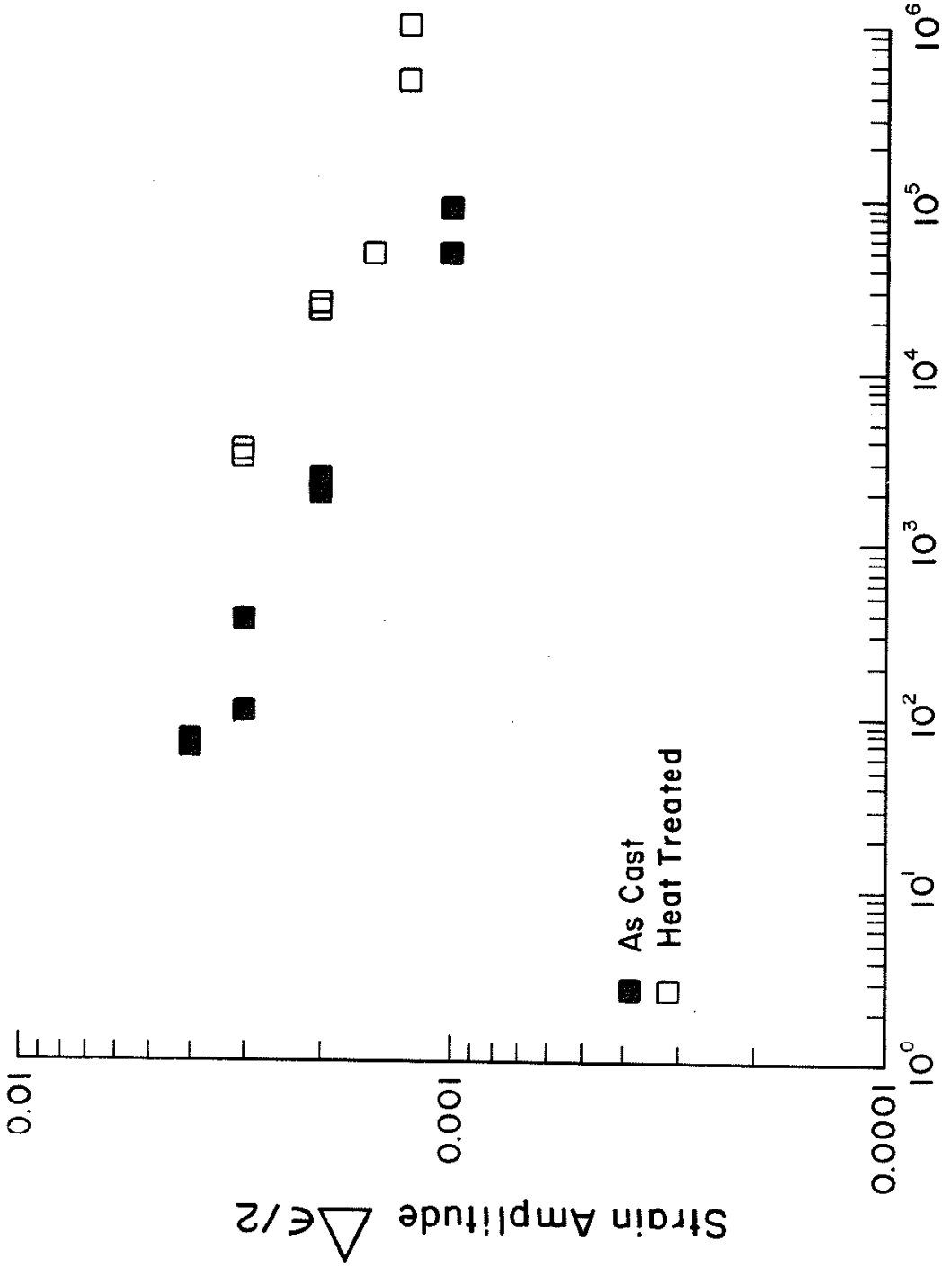

8. Strain Life Data for As-Cast and Heat Treated Irons

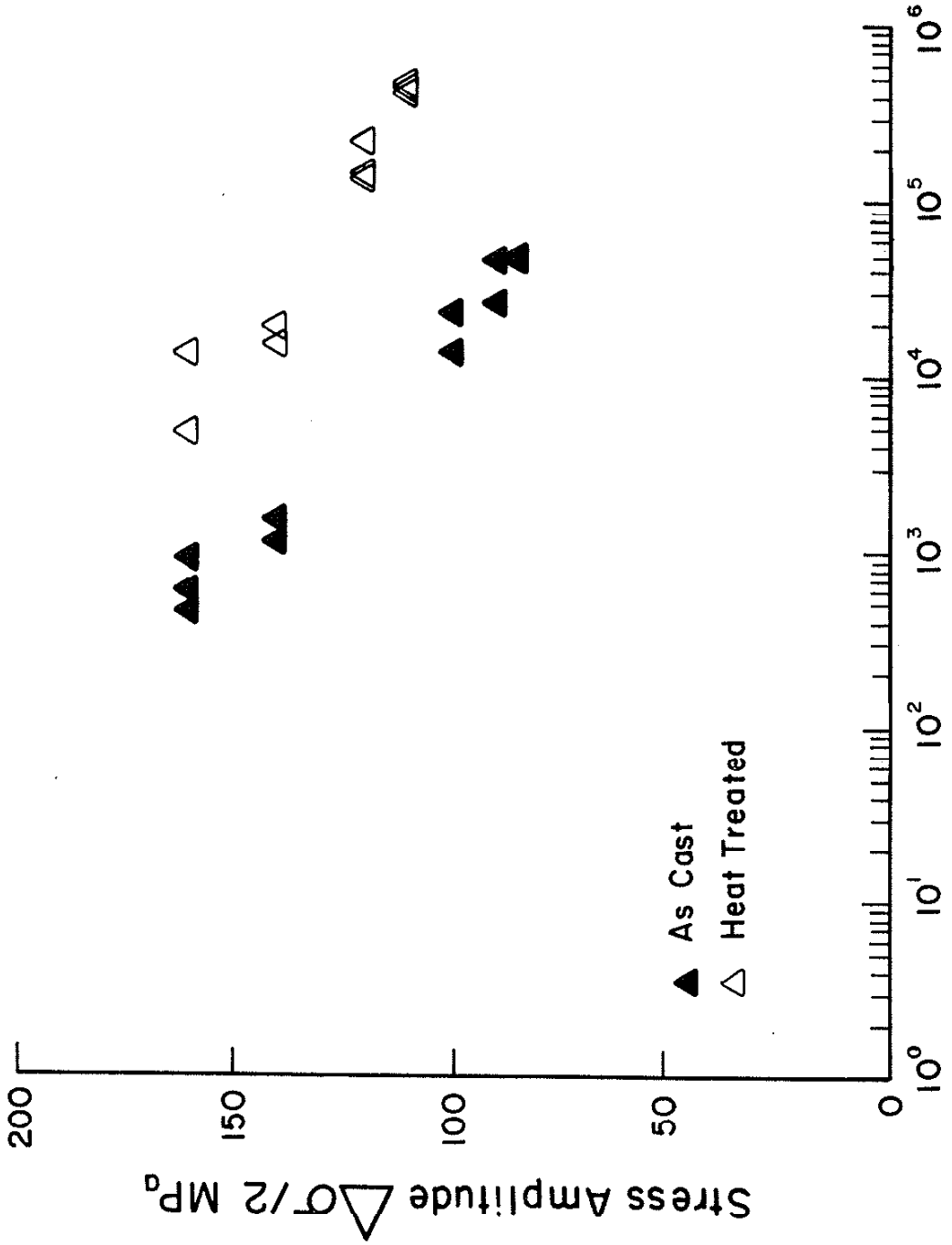

9. Stress Life Data for As-Cast and Heat Treated Irons

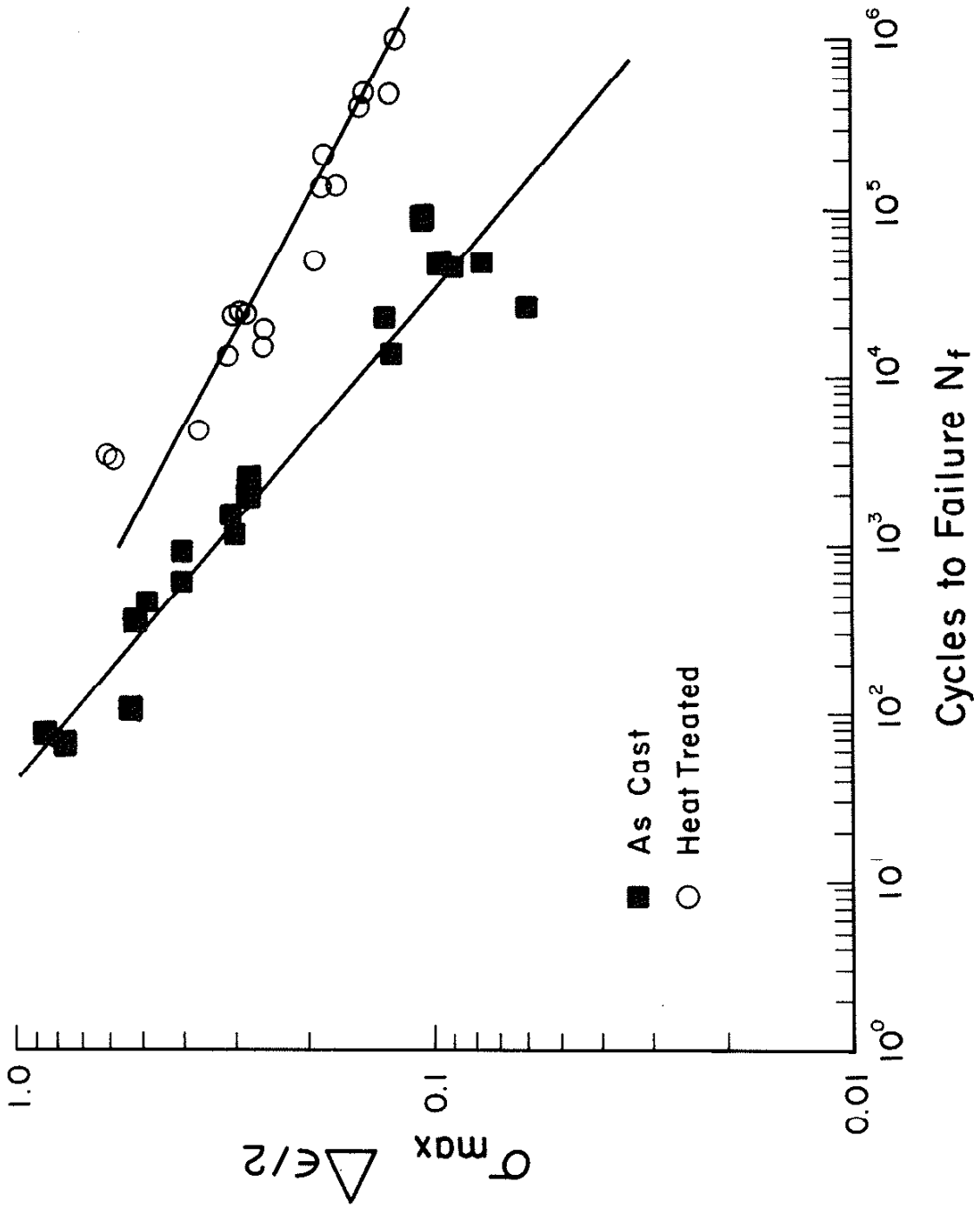

10. Smith-Watson-Topper parameter for As-Cast and Heat Treated Irons

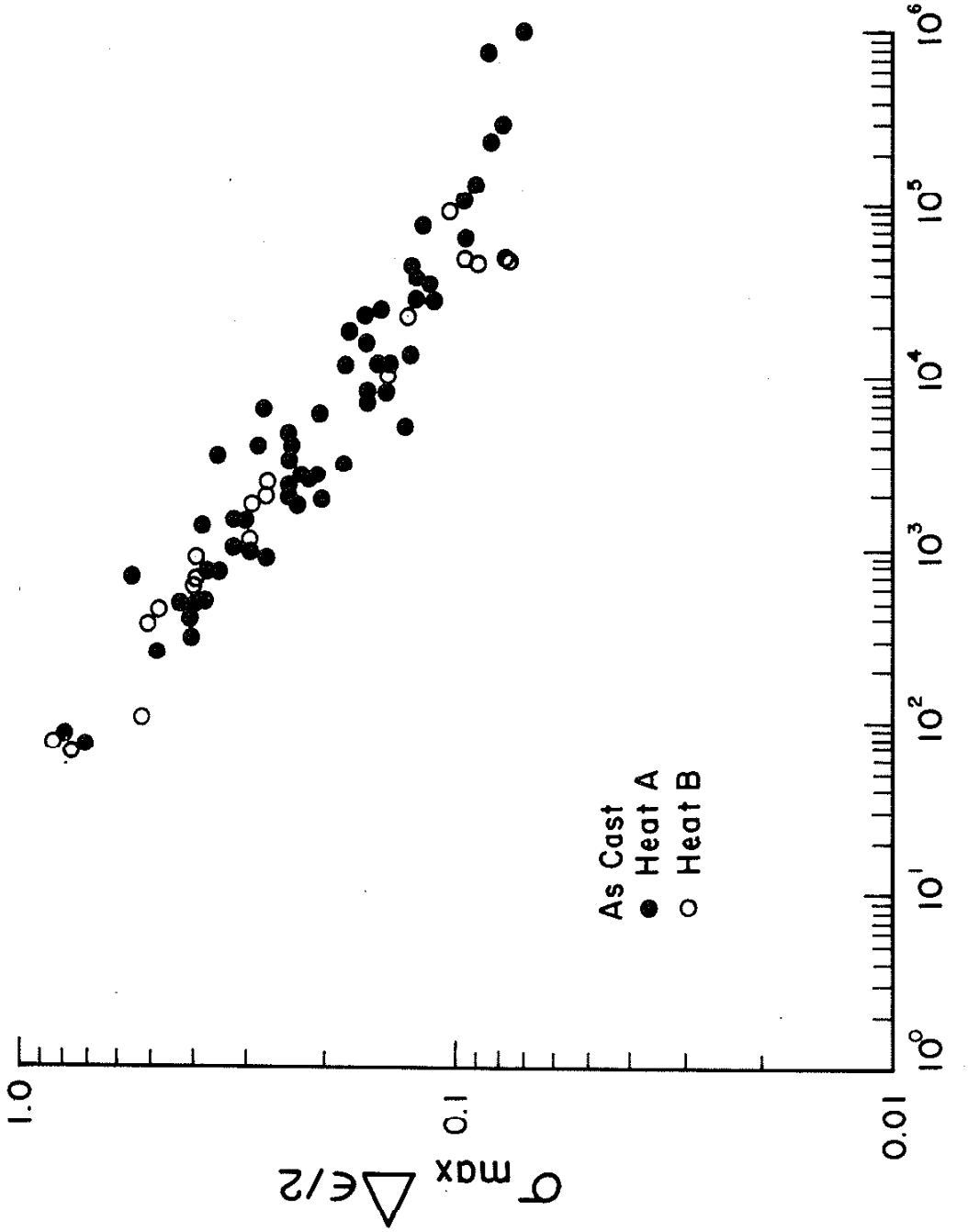

11. Strain-Life Data for Two Heats of As-Cast Iron